

Universiteit
Leiden
The Netherlands

Study of a new member of the Myelin Protein Zero Family

Racz, P.I.

Citation
Racz, P. I. (2010, June 30). *Study of a new member of the Myelin Protein Zero Family*. Retrieved from https://hdl.handle.net/1887/15748

Version:	Corrected Publisher's Version
License:	Licence agreement concerning inclusion of doctoral thesis in the Institutional Repository of the University of Leiden
Downloaded from:	https://hdl.handle.net/1887/15748

Note: To cite this publication please use the final published version (if applicable).

Study of a New Member of the Myelin Protein Zero Family

Proefschrift
ter verkrijging van
de graad van Doctor aan de Universiteit Leiden
op gezag van Rector Magnificus prof. mr. P.F. van der Heijden
volgens besluit van het College voor Promoties
te verdedigen op woensdag 30 juni 2010
klokke 11:15 uur

door

Peter Imre Racz

geboren te Budapest, Hungary
in 1979

Promotiecommissie

Promotor:	Prof. dr. H.P. Spaink
Co-promotor:	Dr. A.H. Meijer
Overige leden:	Prof dr. C.J. ten Cate
	Prof. dr. P.C.W. Hoogendoorn
	Prof. dr. A.J. Durston
	Prof. dr. N.S. Foulkes (University of Heidelberg)
	Prof. dr. K. Csiszar (University of Hawaii)
	Dr. M. Mink (University of Szeged)

ISBN: 978-90-8570-580-2

Printed by Wöhrmann Print Service, Zutphen

Contents

Chapter 1 5
General introduction

Chapter 2 13
Mutation in *Mpzl3*, a Novel Gene Encoding a Predicted Adhesion Protein, in the "rough coat" (*rc*) Mice with Severe Skin and Hair Abnormalities

Chapter 3 33
The human orthologue of murine *Mpzl3* with predicted adhesive and immune functions is a potential candidate gene for immune-related hereditary hair loss

Chapter 4 39
Functional analysis of the *mpzl3* gene in zebrafish

Chapter 5 59
Summary and General discussion

Bibliography 65

Samenvatting 69

Összefoglaló 75

Curriculum vitae 79

List of publications 80

Supplementary tables 81

Chapter 1

General Introduction

General introduction

The study of genomes and genetic defects that underlie complex diseases is an active research area that raises much public interest. The complete DNA sequence of the human genome was published in 2003 and this milestone led to many expectations. With the knowledge of the human genetic sequence it is anticipated that we will gain better understanding of the molecular mechanisms behind development and disease and that we will be able to advance medicine by discovering new targets for drugs to combat today's incurable diseases like many types of cancer. Since the sequencing of the human genome, numerous other genome projects were started and today we have sequence information and map data of over 1000 organisms (NCBI database). However, the function of approximately half of all genes in human and other vertebrate species is still unknown. Therefore, the functional annotation of genome sequences is now the major challenge. Functional annotation of the human genome can be supported by loss-of-function (knock-out or knock-down) studies in model organisms and by the analysis of mutations (polymorphisms) that associate with human disorders.

This thesis is focused on the investigation of the *Mpzl3*, a novel gene with unknown function that was identified through mapping of the rough coat mutation in mice. The *Mpzl3* gene is a member of the myelin protein zero family that consists of proteins containing immunoglobulin domains and with suggested roles related to immune function and cell adhesion. Functional studies of the *Mpzl3* gene in two model organisms, mouse and zebrafish, and investigations of the human orthologue by *in silico* techniques, suggested that the product of this gene plays a role in the immune system and is a potential candidate gene for immune-related hereditary hair loss diseases in human.

The rough coat mutation

The rough coat (*rc*) is a spontaneous recessive mutation in the inbred C57BL/6J mouse strain. The mutation was first observed at the Jackson laboratory in 1966 (Dickie, 1966). Homozygous *rc* mice (*rc*/*rc*) are indistinguishable from there littermates in the first two weeks, but from that time they start to develop a complex phenotype with several characteristic features. The most prominent peculiarity that the *rc*/*rc* mice develop is a cyclic and progressive hair loss starting from the first telogen phase in the hair cycle. In addition, they frequently develop spontaneous ulcerated wounds in the ventral region of the neck (Cao et al., 2007; Hayashi et al., 2004; Racz et al., 2009) (Figure 1). Histopathological examination of the homozygous mutant mice showed reduced amounts of extracellular matrix components, enlarged sebaceous glands in the skin and follicular atrophy in the ulcerated areas (Hayashi et al., 2004). The melanocyte pigments in the hair follicles change in color from black to light brown. Locally, extensive granulated tissue formations were noted with neu-

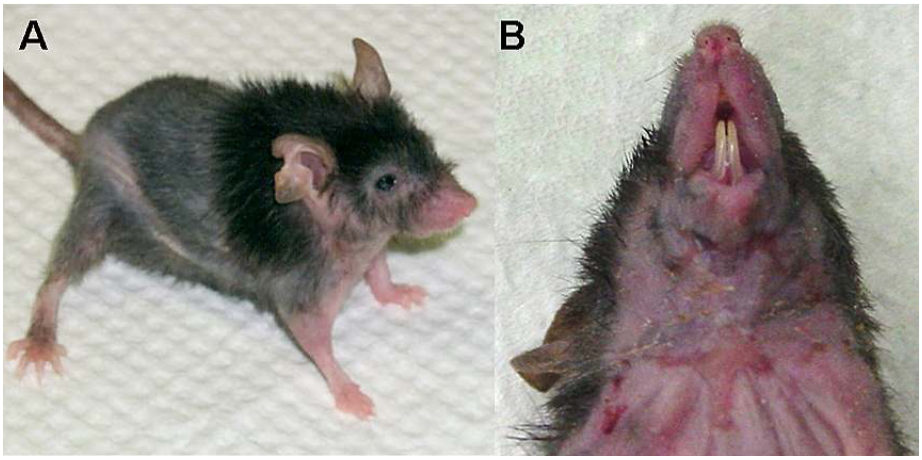


Figure 1 The "rough coat" phenotype in the C57BL/6J mouse strain. **(A)** Hair loss phenotype of an adult *rc/rc* mouse, **(B)** Ulcerated skin wounds in the neck of rc/*rc* mouse

trophilic, mastocytic and lymphoplasmacytic dermatitis (Hayashi et al., 2004). In addition to the diversified skin phenotypes, the adult *rc/rc* mice also show growth retardation, abnormal bone structure and lower body weight than controls, with differences increasing progressively with age (Hayashi et al., 2004). In the femur of the *rc/rc* mice, lack of Ca^{2+}-derived basophilic material was observed, which might correlate with the elevated level of calcium in the blood (Hayashi et al., 2004). Histopathological study of different organs pointed to several immune system malfunctions. For example, in the hepatic sinusoids numerous erythrocytes, lymphocytes, polymorphonuclear leukocytes and enlarged Kupffer cells were detected, and in the trabeculae of the spleen, numerous macrophages were observed loaded with hemosiderin granules (Hayashi et al., 2004). The heart is also affected by this mutation. The cardiac muscle fibers are disoriented, and multifocal myocardial degeneration is also observed. In addition, the pups from homozygotes parents have lower survival rates compared with the litter from heterozygous parents. This phenomenon is probably due to abnormal maternality behavior of the *rc*/rc female mice (Hayashi et al., 2004).

By positional cloning the mutation in the rough coat mice was mapped to a 246-kb interval on chromosome 9 (Cao et al., 2007; Chapter 2). A missense mutation in this area was identified within a novel open reading frame, predicted to encode a protein with a conserved immunoglobulin-like V-type domain. The predicted protein showed strong homology to myelin protein zero (MPZ) and myelin protein zero-like 2 (MPZL2, also called epithelial V-like antigen) and was therefore named MPZL3 (myelin protein zero-like 3) (Cao et al., 2007; Chapter 2). The mutation in the *rc/rc* mice occurred at a highly conserved arginine residue within the conserved immunoglobulin domain, thus likely altering the MPZL3 protein function.

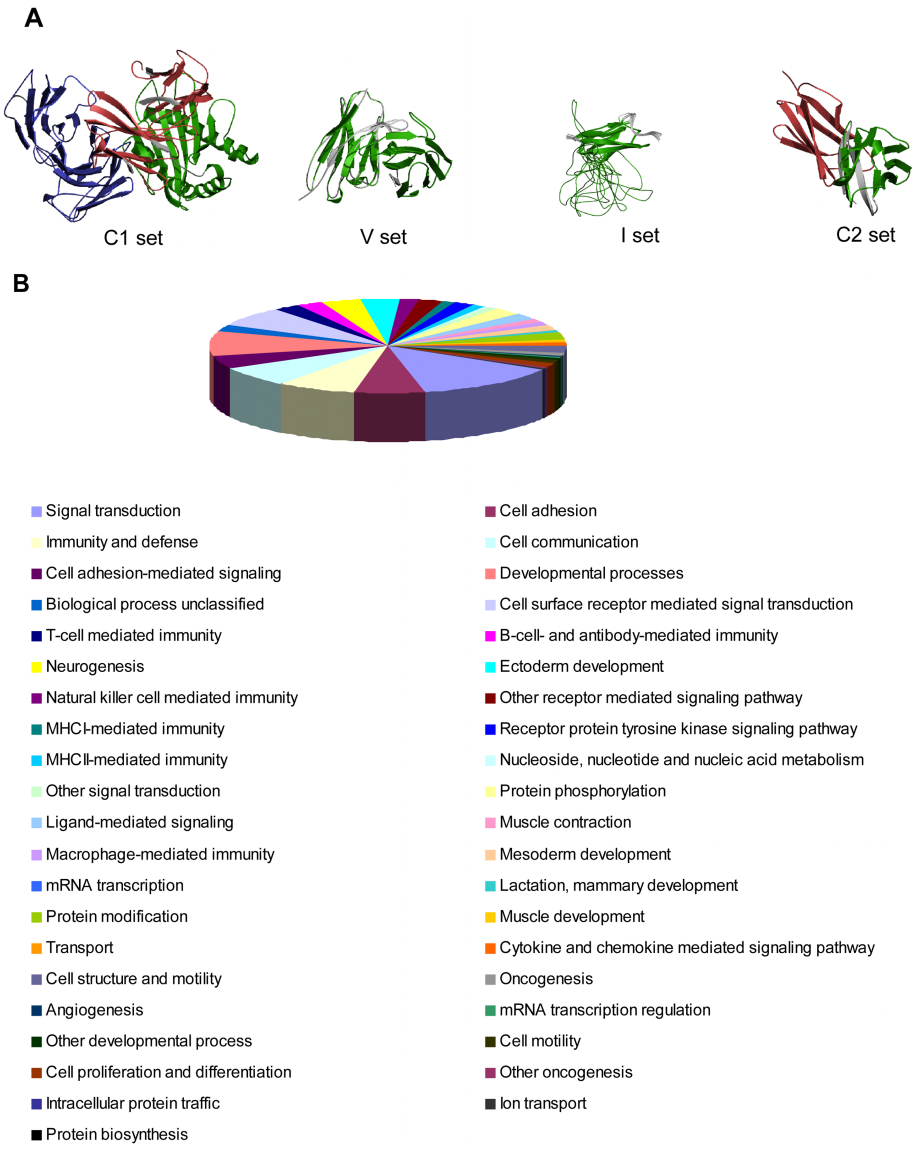


Figure 2. Structure and functions of IgSF proteins. **(A)** Structural models of proteins belonging to the different Ig sets. *C1-set*: complex of the human MHC class I glycoprotein hla-a2 and the T-cell coreceptor cd8 (PDB entry 1akj); *V-set*: fv fragment of mouse monoclonal antibody d1.3 (balb/c, igg1, k) variant chain I glu81->asp and chain H LEU312->VAL (PDB entry 1a7n) ; *I set*: central domain of cardiac myosin binding protein C (PDB entry 1gxe); *C2 set*: structures of an HIV and MHC binding fragment from human CD4 as refined in two crystal lattices (PDB entry 1cdh). Structures were imported from the Pfam database. **(B)** Gene ontology (GO) classification of the Ig domain containing proteins. The dataset was downloaded using BioMart service based on the Ensembl 56 database,

Homo sapiens genes dataset. GO classification was performed using Panther (Protein ANalysis THrough Evolutionary Relationships).

The Immunoglobulin domain superfamily

Immunoglobulin domain containing proteins belong to one of the largest and most diverse protein superfamilies based on domain classification. The immunoglobulin domain appeared more than 500 million years ago and the structure can be recognized already in primitive organisms like members of the poriferan phylum, where it is found in cell-surface-receptor proteins (Buljan and Bateman, 2009). The domain structure was first identified as a sequence similarity of approximately 100 amino acids, repeated in antibody proteins. The number of proteins in the immunoglobulin superfamily (IgSF) extended with the evolution from invertebrates to vertebrates, in parallel with the evolution of the adaptive immune system (Barclay, 2003). Later it was discovered that immunoglobulin-like sequences are not unique only for antibody proteins, but can be found in an wide variety of proteins that plays diverse roles, for example in the immune system, and in neural and muscular processes (Buljan and Bateman, 2009).

Immunoglobulin superfamily domains contain relatively few highly conserved residues and their amino acid sequences are highly diverged, therefore it is possible that most algorithms underestimate their frequency (Barclay, 2003). The basic structure of the domain was identified more than 30 years ago (Davies et al., 1971; Poljak et al., 1973). The IgSF domains comprise a β-sandwich structure with seven or more antiparallel strands in two sheets (Barclay, 2003; Hutchinson and Thornton, 1993; Richardson, 1981) (Figure 2A). The average length of a protein domain is approximately 120 amino acids (Buljan and Bateman, 2009). Based on the amino acid sequence, two different types of immunoglobulin (Ig) domains can be distinguished. The first is the constant domain, or C-domain (IgC), which is shorter (seven strands) and contains several characteristics invariable residues, and the second is the variable-domain or V-domain (IgV), raging from eight, to ten strands. When more proteins were sequenced and shown to be Ig-related, the structures of these proteins were reminiscent of the V-domains and were termed V-set. This term does not indicate sequence variability as in the antibodies, just sequence similarity to the overall V-set sequences (Barclay, 2003). Later many IgSF domains were found with sequence patterns more similar to V-domains but more similar in size to C-domains. These were called C2-set and the original C-domains were named C1-set (Barclay, 2003). Another important set variation that is distinguished among the Ig domains is called the Intermediate or I-set domain. The I-set domain has sequence features of the V-set, but also has some structural features that were previously found only in the constant domains (Harpaz and Chothia, 1994). The different Ig sets have varying numbers of strands in each of the β-sheets that form the sandwich (Smith and Xue,

Table 1. The Myelin P0 protein fingerprint containing proteins in the human genome

Ensembl Gene ID	Chromosome Name	Gene Start (bp)	Gene End (bp)	Strand	PRINTS ID	Associated Gene Name
ENSG00000158887	1	161274525	161279762	-1	PR00213	MPZ
ENSG00000197965	1	167690429	167761156	1	PR00213	MPZL1
ENSG00000144847	3	118619404	118864915	-1	PR00213	IGSF11
ENSG00000182985	11	115044346	115375112	-1	PR00213	CADM1
ENSG00000149575	11	118036187	118047241	-1	PR00213	SCN2B
ENSG00000160593	11	118064442	118095809	-1	PR00213	AMICA1
ENSG00000160588	11	118097409	118123035	-1	PR00213	MPZL3
ENSG00000149573	11	118124137	118135009	-1	PR00213	MPZL2
ENSG00000166257	11	123499897	123525315	-1	PR00213	SCN3B
ENSG00000079385	19	43009500	43032661	-1	PR00213	CEACAM1
ENSG00000105767	19	44126522	44143991	-1	PR00213	CADM4
ENSG00000105711	19	35521534	35531352	1	PR00213	SCN1B
ENSG00000167633	19	55327923	55378662	1	PR00213	KIR3DL1
ENSG00000243772	19	55235964	55279336	1	PR00213	KIR2DL3
ENSG00000198910	X	153126969	153174677	-1	PR00213	L1CAM
ENSG00000101842	X	107288201	107322327	1	PR00213	VSIG1

The list was harvested from the Ensembl release 56 Sept. 2009 database using BioMart service.

1997). Ig domains are often characterized by a conserved disulphide bond that links the two beta sheets, however this boundary is not essential for the structure of the domain, as an active antibody and many other immunoglobulin domain-contain proteins lacking this disulphide have been reported (Barclay, 2003).

The functions of the IgSF proteins vary as much as their sequences (Figure 2B). First it was suggested that the proteins with Ig domains play a role in the immune system, however later more and more proteins were discovered with different attributes. Generally the function of the Ig-like domains is to allow binding reactions, however the specific interactions mediated by these domains vary widely (Fraser et al., 2006). They can bind small molecules, hormones, or large protein complexes, like muscle proteins through homo- or heterophilic interactions (Halaby and Mornon, 1998). The binding sites on these domains are located on the surfaces of the sheets or in the loops that connect the strands (Fraser et al., 2006). IgSF domains are mostly found in association with other IgSF domains on membrane proteins. However, they can also be associated with other domain types such as fibronectin type III, C-type lectin complement control protein, cytokine receptor domains and rarely EGF domains (Barclay, 2003; Korhonen et al., 1992; Letunic et al., 2002). Investigations of the evolution of Ig domains point also to an association with kinase domains in poriferans, which might suggest that the ancestral function of the Ig is also related to signaling (Buljan and Bateman, 2009).

Proteins with a Myelin Protein Zero Domain

The Myelin Protein Zero Family is a small protein family in the Protein

Table 2. GO term classification of the human Myelin P0 domain containing proteins

Biological Process	# Genes	Genes
Cell adhesion	7	MPZ, IGSF11, MPZL1, L1CAM, CEACAM1, MPZL2, VSIG1
Signal transduction	5	KIR3DL1, KIR2DL3, AMICA1, L1CAM, CEACAM1
Cell communication	5	KIR3DL1, KIR2DL3, AMICA1, L1CAM, CEACAM1
Cation transport	3	SCN1B, SCN2B, SCN3B
Ion transport	3	SCN1B, SCN2B, SCN3B
Transport	3	SCN1B, SCN2B, SCN3B
Cell adhesion-mediated signaling	3	AMICA1, L1CAM, CEACAM1
Developmental processes	2	L1CAM, CEACAM1
Synaptic transmission	2	SCN1B, SCN3B
Neuronal activities	2	SCN1B, SCN3B
Cell structure	2	MPZ, MPZL1
Cell structure and motility	2	MPZ, MPZL1
Ligand-mediated signaling	2	KIR3DL1, KIR2DL3
Cell surface receptor mediated signal transduction	1	KIR3DL1
Ectoderm development	1	L1CAM
Neurogenesis	1	L1CAM
Other developmental process	1	CEACAM1
Natural killer cell mediated immunity	1	KIR3DL1
Immunity and defense	1	KIR3DL1

GO classification was performed using the Panther (Protein ANalysis THrough Evolutionary Relationships) server. The number of Myelin Protein o domain related genes that are associated to the GO term is indicated, together with the gene symbols. Data are based on the Ensembl release 56 Sept 2009 database.

Knowledgebase (UniProtKB) database. The common features are that all members of this family have an Ig V-set domain and possess at least three elements out of the characteristic six-element fingerprint of the Myelin Po protein (S-[KR]-S-x-K-[AG]-x-[SA]-E-K-K-[STA]-K.) (Entry: PS00568). Currently, four proteins have been assigned to this family: Myelin Protein Zero (MPZ), Myelin protein Zero Like 1 (MPZL1), Myelin protein Zero Like 2 (MPZL2), and Myelin protein Zero Like 3 (MPZL3). However, when we investigated the Ensembl release 56 Sept. 2009 *Homo sapiens* database we found altogether 16 proteins that have the Myelin Po protein fingerprint (Table 1). Investigation of the chromosomal localization of the family shows that one gene is located on the chromosome 3, two genes are on chromosome 1 and on the X chromosome, and the rest of the genes are spread over chromosomes 11 and 19 (Table 1). The predicted functions of the members of the family, based on the Panther (Protein ANalysis THrough Evolutionary Relationships) classification system, are mainly linked to cell adhesion , but several of these proteins are also linked to cell signaling, immune system processes, and ectoderm development (Table 2.). The classification of proteins according to GO terms allow for fast analyses based on experts knowledge of the biological data (Stevens et al., 2000), but such automated *in silico* analysis obviously has limitations, since not all published data are reflected in GO term annotations. For example, MPZL2 (EVA1) is annotated as an adhesion mol-

ecule, but it was reported that MPZL2 also plays a role in T cell and thymus development (DeMonte et al., 2007). Similarly, AMICA1 is associated with the general GO term signal transduction, but deeper investigation shows that this signaling function might affect the transmigration of leukocytes through epithelial and endothelial tissue (Moog-Lutz et al., 2003), suggesting that this myelin Po protein might play a role in the immune system too.

Outline of the thesis

The goal of this thesis is the functional characterization of a novel member of the myelin Po protein family, *Mpzl3*, which is mutated in mice with the rough coat phenotype. To gain understanding of the molecular mechanisms behind the complex rough coat phenotype, the defects caused by the mutation and the expression pattern of the affected *Mpzl3* gene were studied in detail. In addition, knock-down and overexpression studies of the zebrafish homolog of *Mpzl3* were performed.

Chapter 1 gives a general introduction about the rough coat mutation, a short description of the phenotype, and introduces the protein family of the mutated gene.

Chapter 2 describes the microsatellite marker based mapping strategy used to identify the rough coat mutation. It shows that the mutation is mapped to a conserved residue in the Ig domain of the *Mpzl3* gene. Furthermore, it describes the expression pattern of the *Mpzl3* gene in mouse tissues and the localization of the MPZL3 protein in skin sections.

Chapter 3 presents the results of *in silico* and histopathological analyses of the *MPZL3* gene in human and points out that this gene is a potential candidate for immune-related hereditary hair loss.

Chapter 4 describes the functional analysis of the Mpzl3 protein in zebrafish by means of overexpression and morpholino knock-down experiments in embryos. The knock-down effect was further investigated at the transcriptome level by microarray analysis.

Chapter 5 summarizes and discusses the work of this study.

Chapter 2

Mutation in *Mpzl3*, a Novel Gene Encoding a Predicted Adhesion Protein, in the rough coat (*rc*) Mice with Severe Skin and Hair Abnormalities

This chapter is based on:
Cao T, Racz P, Szauter KM, Groma G, Nakamatsu GY, Fogelgren B, Pankotai E, He QP, Csiszar K.. (2007) J Invest Dermatol.;127(6):1375-86.

Abstract

The rough coat (*rc*), is an autosomal recessive mutation, arose spontaneously in C57BL/6J mice. Homozygous *rc* mice develop severe skin and hair abnormalities, including cyclic and progressive hair loss and sebaceous gland hypertrophy. The *rc* locus was previously mapped to Chromosome 9. To elucidate the genetic basis underlying the *rc* phenotype development, we carried out positional cloning and mapped the *rc* locus to a 246-kb interval. We identified a missense mutation within a novel open reading frame in the *rc/rc* mice, which is predicted to encode a cell adhesion molecule with the highest homology to Myelin Protein Zero (MPZ) and Myelin Protein Zero-like 2 (MPZL2, also called Epithelial V-like Antigen). We therefore named this gene *Mpzl3* (Myelin Protein Zero-like 3). The mutation in the *rc/rc* mice occurred at a highly conserved residue within the conserved immunoglobulin V-type domain, thus likely altering the MPZL3 protein function. Reverse transcriptase-PCR and Western blot analysis revealed expression of the *Mpzl3* gene in various adult organs, including the skin. Using indirect immunofluorescence, we detected MPZL3 protein in the keratinocytes and sebocytes in the skin. Results from this study identified a novel gene encoding a predicted adhesion protein whose mutation in the *rc* mice likely caused the *rc* phenotype.

Introduction

The rough coat (*rc*) mutation arose spontaneously in the C57BL/6J (B6/J) inbred mouse strain at the Jackson Laboratory in 1966 (Dickie, 1966). The *rc* mutation is autosomal recessive. Homozygous *rc* mice are born with no apparent abnormalities, but display unkempt looking hair coats by weaning age, and develop cyclic and progressive hair loss thereafter (Figure 1) (Hayashi et al., 2004). In addition, histological analysis of skin sections revealed sebaceous gland hypertrophy in the *rc/rc* mice (Figure 2) (Hayashi et al., 2004; Ruvinsky et al., 2002). Both male and female homozygous *rc* mice are fertile (Dickie, 1966), although only about a quarter of the pups born to *rc*/*rc* females survive (Hayashi et al., 2004). Linkage analysis with DNA markers assigned the *rc* locus to 32.0 centimorgan on Chromosome 9, close to the *Mpi1* gene (2 recombinants among 107 backcross offspring) (Eicher EM, 1977) at 57.57 megabase (Mb) (Ensembl Mouse Genome Database v38, released in April 2006, www.ensembl.org/Mus_musculus), but the gene mutation remained unknown.

The appearance of rough hair coats in *rc/rc* mice is similar to matted (*ma*) mice, another strain with a spontaneous mutation (Searle AG, 1957). However, tests for allelism through breeding experiments with *ma* and several other mutant strains such as ichthyosis (*ic*), plucked (*pk*), fuzzy (*fz*) and rough (*ro*) (Dickie, 1966), abnormal feet and tail (*aft*) (Ruvinsky et al., 2002) have all been negative. Interestingly, mice homozygous for rough fur (*ruf*), another spontaneous mutation mapped to Chromosome 9, demonstrated similar skin abnormalities with the *rc/rc* mice, such

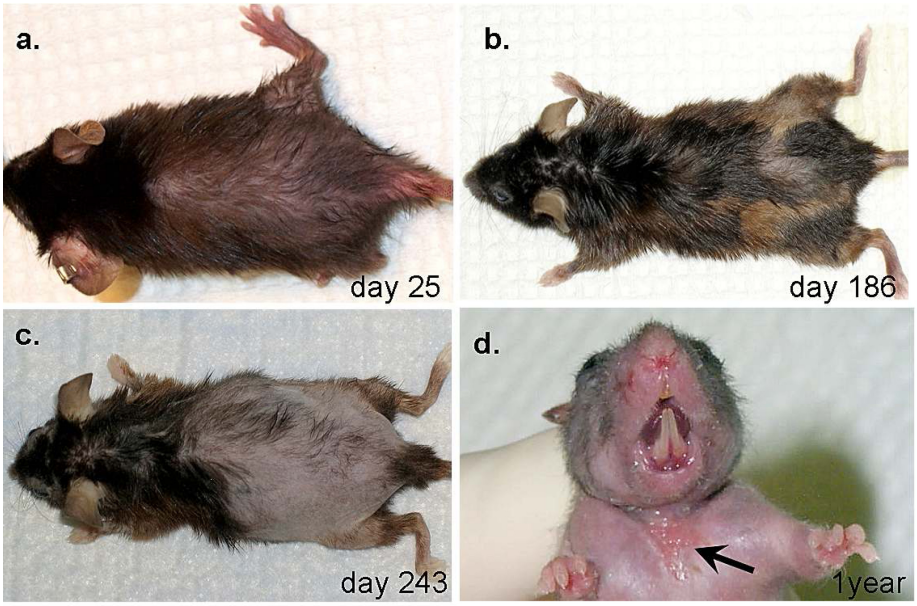


Figure 1. Gross phenotype of the *rc/rc* mice **(a)** Hair loss is apparent on the dorsal trunk of an rc/rc mouse on day 25 after birth. **(b)** New hair coat retains the rough coat phenotype, sometimes with reduced pigmentation. **(c)** Hair loss is progressive in older rc/rc mice. **(d)** In more than 50% of *rc/rc* mice older than 1 year, ulcerated wounds develop spontaneously in the ventral neck region (arrow).

as the "unkempt" and "wet" appearance and sebaceous gland hypertrophy (Park et al., 2001; Sweet HO, 1990). However, allelism has not been tested for *rc* and *ruf*, and the mutation in *ruf* mice has not been identified.

A previous study of the rough coat mutation (Hayashi et al., 2004) showed linkage of the *rc* locus with two microsatellite markers, *D9Mit162* at 49.954 Mb (one recombinant among 129 backcross offspring) and *D9Mit104* at 65.953 Mb (three recombinants among 129 backcross offspring). In this study, to elucidate the genetic basis and to better understand the molecular mechanisms of *rc* phenotype development, we carried out positional cloning in backcross mice.

Results

Cyclic and progressive hair loss and sebaceous hypertrophy in the *rc/rc* mice:

Homozygous *rc* pups were born with no apparent abnormalities, and developed normal hair coats that became plush 7 days after birth, suggesting that the initial hair growth (follicular neogenesis) in *rc/rc* pups was normal. However, by day 14 after

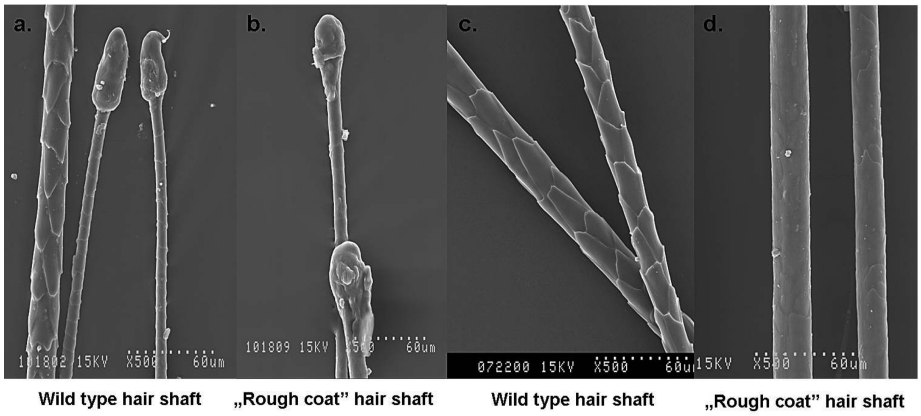


Figure 2. Ultrastructural analyses of hair shafts in *rc/rc* mice. Scanning electron microscopy images are shown of pelage hair from a 24 day old *rc/rc* mouse **(b, d)** and a wild type mouse **(a, c)**. Notice the smooth hair shaft **(d)** and abnormal hair bulb **(b)** from the *rc/rc* mouse. The presence of the hair bulb in **(b)** suggests that the hair loss in *rc/rc* mice is not due to breakage of hair. The smooth hair shafts of *rc/rc* mice **(d)** may result from the elevated level of sebum in the sebaceous glands.

birth, the *rc/rc* pups started to show unkempt-looking hair coats ("rough" coat) and a loss of glossiness. By day 18, hair loss became apparent on the dorsal, ventral, and lateral trunk. At the next anagen, the dorsal skin became dark and thickened, and the new hair coats retained the "rough coat" phenotype. Thereafter, the *rc/rc* mice underwent cyclic hair loss, and hair growth, sometimes showing reduced pigmentation in the new hair coat (Figure 1). Hair loss was progressive and some older *rc/rc* mice became nearly bald. In addition to hair loss, we observed a high incidence of spontaneous and persistent ulcerated lesions on the ventral skin of the neck in *rc/rc* mice over 1 year of age (17 of 27, 63%) (Figure 1d). Histological analysis of such lesions revealed typical features of chronic wounds, including inflammation in the wound bed and hyperplasia of the epidermal keratinocytes at the wound edge (Data not shown)

Scanning electron microscopy showed that *rc/rc* mice have smooth hair shafts compared to wild type mice (Figure 2a and 2b). No breakage of the hair shaft was observed in the *rc*/*rc* mice by scanning electron microscopy (Figure 2c and 2d), which supports that the hair loss phenotype is the consequence of deattachment of the hair bulbs and not due to loss of structural integrity of the hair shafts

We observed severe hypertrophy of the sebaceous glands in the skin sections from *rc*/*rc* mice at day 16 (Figure 3a and 3b). This observation was confirmed by oil red O staining of lipids in the cells of differentiated sebocytes (Figure 3c and 3d). Similar observations were made in *rc/rc* skin and at days 24, 34, and 76 (data not shown). Sebaceous gland hypertrophy was a result of sebocytes hyperplasia: there were twice as many sebocytes per sebaceous gland in *rc*/*rc* mice as in +/*rc* mice (14.9±2.8 vs.

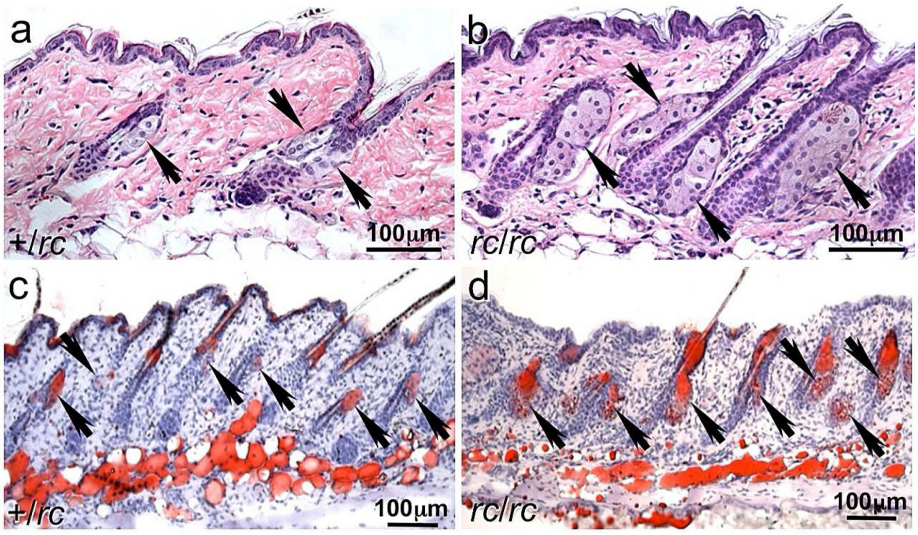


Figure 3. Sebaceous gland hypertrophy in the *rc/rc* mice. **(a, b)** Hematoxylin and eosin staining and **(c, d)** oil red O staining of lipids in back skin sections from **(a, c)** a +/rc and **(b, d)** an *rc/rc* mouse. Arrowheads point to the sebaceous glands. **(b, d)** Notice the hypertrophic sebaceous glands in the *rc/rc* mouse. The sebocytes **(d)** in the *rc/rc* mouse are functional lipid-secreting cells as **(c)** in the normal mouse. Bar = 100 mm

6.2±2.5 in the day 76 samples examined (P<<0.01). The smooth hair shafts observed in *rc/rc* mice (Figure 2) likely are the consequence of increased sebum production by the enlarged sebaceous glands.

High-resolution linkage analysis:

Before this study, no mapping interval was defined for the *rc* locus, even though it had been mapped close to the *Mpi1* gene (Eicher EM, 1977) and two microsatellite markers, *D9Mit162* and *D9Mit104* (Hayashi et al., 2004). To define a mapping interval for the *rc* locus, we outcrossed B6/J-*rc*/*rc* mice with both CAST/Ei mice and BALB/cJ mice to obtain F_1 hybrids (+/*rc*) on two mixed strain backgrounds to avoid a potential low rate of recombination within the *rc* region (Fernandez-Gonzalez et al., 2002). Female F_1 hybrids were backcrossed with male B6/J-*rc*/*rc* mice to obtain F_2 hybrids.

We monitored F_2 hybrids daily from birth for the *rc* phenotype development. F_2 hybrids that showed unkempt hair coats by day 16, hair loss by day 24, ensuing hair growth, and subsequent hair loss were considered phenotypic and homozygous for the *rc* mutation (*rc*/*rc*). F_2 hybrids that never showed hair abnormality at these stages were considered non-phenotypic and heterozygous for the *rc* mutation (+/*rc*). Penetrance of the *rc* phenotype was 100% in both F_2 hybrid backgrounds.

Table 1. Summary of linkage analysis of five microsatellite marker and the rc locus in 200 C57BL/6J-BALB/cJ F2 offspring. p<<0.0001 for all markers.

Marker	Position (Mb)	Number of Recombination	Number of Mice Analyzed	Distance (cM)	LOD score
D9Mit67	36.961	11	200	5.5	41.7
D9Mit328	41.822	6	200	3	48.5
rc					
D9Mit191	46.647	4	200	2	51.7
D9Mit162	49.954	6	200	3	48.5
D9Mit73	71.609	25	200	12.5	27.5

Mb: megabase. The Mb positions are based on the Ensembl Mouse Genome Database (http://www.ensembl.org/Mus_musculus), v38 (released in April 2006), based on the NCBI m35 assembly (released in December 2005). cM: centimorgan.

We analyzed linkage between the *rc* locus and five microsatellite markers in 200 B6/J-BALB/cJ F_2 hybrids (Table 1). Linkage was shown between the *rc* locus and all five microsatellite markers ($p<<0.0001$). All four recombinants with *D9Mit191* also showed recombination with *D9Mit162* and *D9Mit73*, and none of them showed recombination with *D9Mit67* or *D9Mit328*. All six recombinants with *D9Mit328* also showed recombination with *D9Mit67*, and none of them showed recombination with *D9Mit73*, *D9Mit162* or *D9Mit191*. These recombinations defined the *rc* interval between *D9Mit328* and *D9Mit191*.

Using a similar approach, we analyzed linkage between the *rc* locus and the published polymorphic microsatellites shown in Figure 4a in 361 B6/J-CAST/Ei F_2 hybrids. We were able to reduce the *rc* interval to 1.560 Mb, between *D9Mit228* and *D9Mit192*. We then identified eight novel microsatellite polymorphisms within the *D9Mit228~D9Mit192* interval between B6/J and CAST/Ei strains (Figure 4a). The chromosomal locations and primer sequences of these novel polymorphisms are shown in Table 2. Haplotype analysis of F_2 hybrids B292, B329 and B359 revealed that the *rc* locus lay within a 246-kb interval, between 44.8334 Mb (microsatellite # 9) and 45.0796 Mb (microsatellite #25) (Figure 4b).

Mutation detection:

Within this 246-kb interval, there are 10 candidate genes, including nine known genes and one novel gene (Figure 4c). Using reverse transcriptase (RT)-PCR analyses, we detected expression of nine of the 10 candidate genes in normal as a well as *rc/rc* skin (data not shown). As we could not pinpoint a most likely "functional" candidate gene, such as one whose expression in the rc/rc skin was drastically down-regulated, we carried out sequence analyses of all the coding sequences and flanking splice sites of all 10 candidate genes. There are total of 71 exons among these genes, 68 of which contain coding sequences, according to the Ensembl Mouse Genome Database (www.ensembl.org/Mus_musculus). These numbers included all exons predicted from different transcripts in the Ensembl database (www.ensembl.org/

Table 2. Summary of linkage analysis of novel microsatellite polymorphisms we identified between B6/J and CAST/Ei strains and the rc locus in 361 C57BL/6J-CAST/Ei F2 hybrids.

Marker	Chromosomal Position (Mb)	Number of Recombinants	Primer Sequences
# 3	44.4246	1	F: CTGGCTCTACAGGCGTGTAC R: TGCTAAGTAAGGAGAGAGGG
# 5	44.4827	1	F: TGATCTCCTGGTCCCATGAG R: GGATCCACTTGTAAATGTGC
# 14	44.6485	1	F: CTCTGCTCTCCACACTCATC R: TGCACACGCTTGTGACCATG
# 7	44.8185	1	F: TCAATGGGAGAGTGCTTGCC R: GAATCTCTCTCAGTGCCTCC
# 9	44.8334	1	F: GGAGAGTGAGAAAGCAGGAC R: CCCTAGCCTATGAGATCTCC
# 10	44.8827	0	F: AGGTTTTGTAGAATCCAGGC R: CTGACCTCCACACTACACTC
# 25	45.0796	1	F: TCACAGACATGGCAGGAGTC R: CCTCTGCTTCTGGTTGCTAC
# 26	45.1235	1	F: GGCTAATTCAGCGTACACAC R: CTCAGGTCATTTGGCACCAG

Mb: megabase. The Mb positions are based on the Ensembl Mouse Genome Database (http://www.ensembl.org/Mus_musculus), v38 (released in April 2006), based on the NCBI m35 assembly (released in December 2005).

Mus_musculus, NCBI m35 assembly released in December 2005, with reference to NCBI m36 assembly released in April 2006). We did not identify any mutation in the known genes in the *rc/rc* DNA.

However, we identified a point mutation in the open reading frame within the novel gene ENSMUSG00000070305, located at 44.989~45.009 Mb (Figure 5, Table 3). This novel gene consists of six exons, and encodes a polypeptide, ENSMUSP00000091378, of 230 amino acids. A closer examination revealed that the coding sequence did not start with an ATG nor ended with a STOP codon. We therefore considered it incomplete. This novel gene has a human homologue ENSG00000160588 at 117,602,619 ~ 117,628,245 bp on Chromosome 11, and a rat homologue ENSRNOESTG00000015598 at 48,004,303 ~ 48,024,405 bp on Chromosome 8. The human homologue and rat homologue encode polypeptides of 235 (ENSP00000278949) and 236 (ENSRNOESTP00000021062) amino acids, respectively. By comparison with the human and rat homologues and analyses of the mouse genomic sequence and expressed sequence tags (ESTs), we predicted additional four amino acids at the amino and carboxyl termini of the encoded mouse polypeptide. There are additional four amino acids at the amino terminus, starting with a methionine encoded by ATG. We also identified an in-frame STOP codon 36 bp upstream from this ATG within the 5' flanking sequence. Furthermore we predicted an additional three amino acids at the carboxyl terminus, followed by a STOP

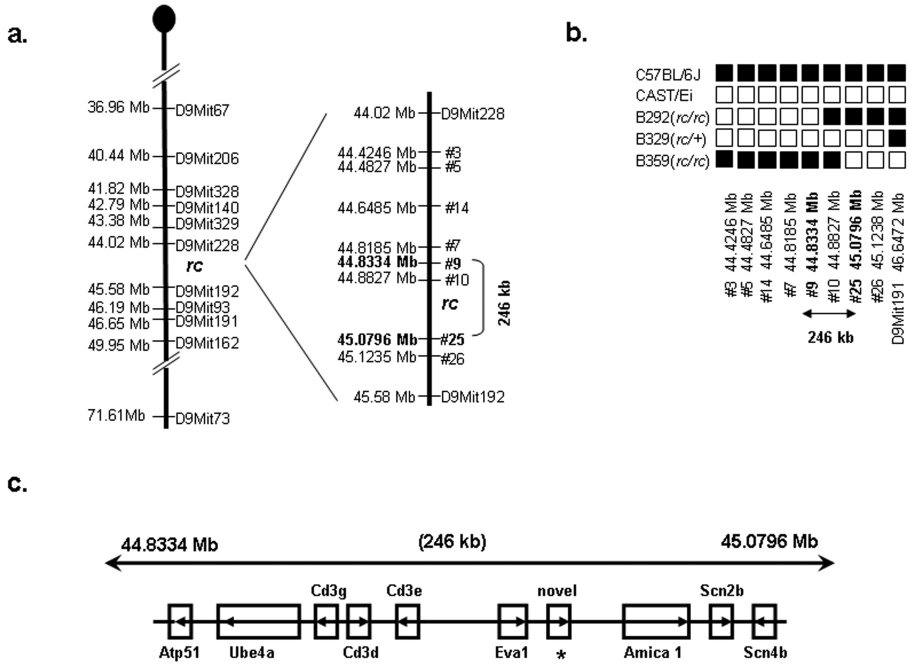
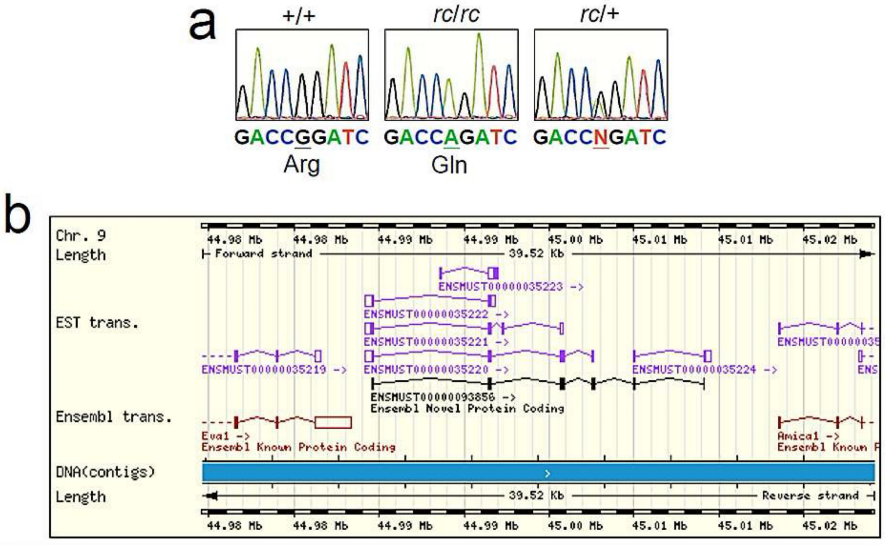


Figure 4. High-resolution genetic map of the *rc* interval and the candidate genes. **(a)** High-resolution genetic map of the *rc* interval based on linkage analysis in 200 C57BL/6J-BALB/cJ and 361 C57BL/6J-CAST/Ei F2 hybrid offspring. Microsatellite markers in the Ensembl Mouse Genome Database (http://www.ensembl.org/Mus_musculus) are shown on the left with their chromosomal locations in megabases (Mb). Novel microsatellite polymorphisms between the C57BL/6 and CAST/Ei strains identified in this study are shown on the right. Marker #10 was concordant with *rc* in all the F2 hybrids we analyzed, and its location relative to the *rc* locus could not be determined in our linkage analysis. **(b)** Haplotype analysis of the three recombinants with D9Mit191 or marker #3 among the 361 C57BL/6J-CAST/Ei F2 hybrid offspring. These results show that the rc locus lies within a 246-kb interval. **(c)** Candidate genes in the 246 kb mapping interval for the *rc* locus (Ensembl Mouse Genome Database, www.ensembl.org/Mus_musculus).

codon. Thus, we predicted a polypeptide of 237 amino acids encoded by the mouse gene ENSMUSG00000070305. We have submitted this novel gene/mRNA sequence to GenBank (GenBank accession number EF102773).

The mutation we identified in the *rc/rc* DNA is a G→A transition in exon 3 of this gene, resulting in an, Arg100→Gln substitution, in the predicted 237-amino acid polypeptide (Figure 5). This mutation was confirmed in multiple *rc/rc* mice of different parents and in *rc*/+ mice, as well as in C57BL/6J-*rc* genomic DNA purchased from the Jackson Laboratory (Bar Harbor, ME).

To determine whether this mutation could be a polymorphism, we carried out



Exons	Exon Size (bp)	5' Splice Donor Sequence	Intron Size (bp)	3' Splice Acceptor Sequence
1	Noncoding + 76	TCCAGG**gt**gagt	6,722	cattag**GTGCGC**
2	167	GAGTCT**gt**gagt	4,131	tcttag**ATTTTT**
2'	215 + noncoding	-	-	-
3	211	AAAGGG**gt**aagc	1,657	ctacag**GGTTCG**
4	166	CGATGA**gt**aagt	2,283	ccacag**CACTGA**
5	64	TGTCTG**gt**aagt	4,034	ctctag**GATTCA**
6	30 + noncoding			

Figure 5. Gene structure and mutation analysis of a novel gene in which a mutation was identified in the *rc/rc* DNA. **(a)** Sequence analysis identified a point mutation in a predicted open reading frame in the *rc/rc* genomic DNA, which was confirmed in *rc*/+ genomic DNA and *rc/rc* cDNA. We have named this gene "*Mpzl3*" based on the similarity of the predicted domain structure of its encoded protein to Myelin Protein Zero (MPZ) and Myelin Protein Zero-like 2 (MPZL2, also called EVA1). **(b)** The *Mpzl3* gene (ENSMUSG00000070305), predicted on the basis of multiple Ensembl transcripts based on ESTs, in its genomic context. *Eva1* (*Mpzl2)* gene is upstream, and *Amica1* gene is downstream. **(c)** Our prediction of the murine *Mpzl3* gene that is homologous to the human gene ENSG00000160588 and rat gene ENSRNOESTG00000015598. Exon and EST information was based on the Ensembl Genome Database (www.ensembl.org) and our prediction by sequence

comparison between species. Numbers underneath each exon indicate the length of the coding sequence in that exon (shaded portion). Exon 2 has 167 bp of coding sequence, and exon 2′ has 215 bp of coding sequence (48 bp longer than exon 2) as well as a 3′ UTR. Block arrow points to the splice site in exon 2′ used to generate the 6-exon transcript. The arrows denote primers 2F, 2R, 4F and 4R used for RT-PCR analysis in Figure 6. The asterisk (*) denotes the position of the mutation detected in *rc/rc* DNA. **(d)** Exon-intron information of the predicted murine *Mpzl3* gene.

sequence analysis of this gene in multiple mouse strains. This mutation was absent in wild type Balb/c, CAST/Ei, B6C3F1 (F1 hybrid of C57BL/6NCr and C3H/HeN MTV-), B6D2F1 (F1 hybrid of C57BL/6NCr and DBA/2NCr), CD1, and SwissGP mice.

The protein encoded by the mutated gene:

According to our prediction based on homology to human and rat counterparts, the full length polypeptide encoded by the murine ENSMUSG00000070305 gene consists of 237 amino acid residues, and has a predicted molecular weight of 26,058 Dalton and isoelectric point of 7.73. It is predicted to be a type I transmembrane protein, with a signal peptide at the amino terminus (amino acids 1~32), an immunoglobulin (Ig)-like V-type domain at amino acids 33~149, and a transmembrane domain at amino acids 160~182 (Figure 6). The Ig-like V-type domain is predicted to be extracellular upon cleavage of the signal peptide, and the carboxyl terminus is predicted to be cytoplasmic. The conserved cysteines in the Ig-like domain are at amino acids 53 and 129, and there is a putative N-glycosylation site (NXS/T) at amino acid 124. Arg100 is a highly conserved residue within the Ig domain.

Among known murine proteins, the highest sequence homology to this 237-amino acid protein was identified in the Myelin Protein Zero (MPZ) and Myelin Protein Zero-like 2 (MPZL2, also called Epithelial V-like Antigen, (EVA1)) (Figure 6). We therefore registered this novel gene as *Mpzl3* (Myelin Protein Zero-like 3) with the International Committee on Standardized Genetic Nomenclature for Mice and the Mouse Genomic Nomenclature Committee (MGNC) through the Mouse Genome Informatics (MGI) Resource (The Jackson Laboratory, Bar Harbor, ME). Both MPZ and MPZL2 (EVA1) proteins have been implicated in cell-cell adhesion (Guttinger et al., 1998), and the Ig-like domains in a number of other proteins have been shown to mediate homophilic cell-cell adhesion. Hence, it is likely that the MPZL3 protein is also involved in cell adhesion through its immunoglobulin V-type domain, and that substitution of the highly conserved Arg100 alters its function.

The coding sequence of the six-exon murine *Mpzl3* transcript shares an 84.5% nucleotide identity with its human homologue, and the murine and human MPZL3 proteins share an 86.8% identity and 93.2% similarity. However, within the conserved Ig-like V-type domain, the murine and human MPZL3 proteins share a 93.3% identity and 96.6% similarity. The coding sequence of the six-exon murine *Mpzl3* transcript shares a 93.3% nucleotide identity with its rat homologue, and the murine and rat MPZL3 proteins share a 96.6% identity and 97.9% similarity. Interestingly, EST evi-

Table 3. Sequences of primers used to PCR amplify the six exons of the novel mouse gene ENSMUSG00000070305 (later named Mpzl3) for sequence analysis.

Exons	Forward Primer	Reverse Primer	Amplicon (bp)
Exon 1	ATCAGATCCTCCTGAGAGTC	TCAAGTCTCACAAGGTGGTC	518
Exon 2/2'	TGAAGCATCTCTCATGTTCAC	AAACTTGCACAGCAGGTGAC	433
Exon 3	ACAGCCAAGGGAAGAGAAGC	ACCTTGACACAGTGATCCTC	422
Exon 4	CTTTTACGAACATGCGTCCTG	TCAGCAGTGGACCAAACGTC	441
Exon 5	GCTCCGATATGTGCTTCACG	GTTCATACGTTCCTGTGCTG	307
Exon 6	GAGCATAGGTGTGCTCTCAG	GATCTTCTGTCACTGCTGTC	267

The reverse primer for exon 2/2' was also used to PCR amplify the two-exon Mpzl3 cDNA (primer 2R in Figure 5c).

dence also suggests a two-exon *Mpzl3* transcript in mice (ENSMUST00000035222) and rats (ENSRNOT00000032837), encoding a polypeptide of 96 amino acids. The 96-amino acid mouse and rat polypeptides are highly homologous, with 90.6% identity and 95.8% similarity.

A search of the available genome databases showed MPZL3 homologues in human, chimpanzee, rhesus monkey, rat, mouse, bovine, dog, and opossum. In all of these organisms, Arg100 is highly conserved. However, the function of the MPZL3 protein is not known in any of these organisms.

The murine *Mpzl3* gene:

The murine *Mpzl3* gene consists of six exons, spanning over 19 kb on mouse Chromosome 9 (44.989 ~ 45.010 Mb) (Ensembl v38; Vega release 18, May 08, 2006) (Figure 5b). According to our prediction based on homology to human and rat counterparts, the coding sequences in the murine *Mpzl3* exons varied from 30 bp (exon 6) to 215 bp (exon 2'), and the introns varied from 1,657 bp (intron 3) to 6,722 bp (intron 1) (Figure 5c, 5d). EST analysis provided evidence for at least two transcripts through alternative splicing, both containing coding sequences flanked by a 5' UTR that included an in-frame STOP codon and a 3' UTR. One transcript consisted of two exons encoding a polypeptide of 96 amino acids. EST evidence suggested a 5' UTR of at least 53 bp and a 3' UTR of at least 3,160 bp for this transcript. This transcript, however, does not contain a mutation. Interestingly, there is a consensus splice donor site within the coding sequence of exon 2' (Figure 5d). When this site is used, a transcript containing six exons would result from the *Mpzl3* gene, encoding a protein of 237 amino acids. EST evidence suggested a 5' UTR of at least 57 bp and a 3' UTR of at least 261 bp for this transcript. In the *rc/rc* mice, the G→A missense mutation we identified in exon 3 would result in Arg100→Gln substitution.



Figure 6. Sequence comparison of the human, murine, and rat MPZL3 protein and murine MPZ and MPZL2 (EVA1). The signal peptides and trans-membrane domains are underlined, flanking the immunoglobulin (Ig)-like V-type domains, with conserved residues highlighted. "N" over grey background: N-linked glycosylation site; "C" over grey background: conserved "signature" Cysteines for disulfide bond formation in the Ig-like domain. The Arginine (R) 100→glutamine (Q) substitution caused by the G→A mutation in the *rc/rc* mice is highlighted over grey background

Expression of the *Mpzl3* mRNA:

We carried out RT-PCR analysis to determine the tissue distribution of the *Mpzl3* transcripts in normal adult mice. Primers were designed to amplify the complete coding sequences from both the six-exon (845 bp amplicon using primers 2F and 4R) (Figure 5c) and two-exon (457 bp amplicon using primers 2F and 2R) (Figure 5c) transcripts based on EST predictions. As shown in Figure 7a, the two *Mpzl3* transcripts were detected in a variety of organs examined, with high levels of expression in the brain, heart, liver, and skin. The tissue distribution patterns of the two-exon and six-exon transcripts were similar.

RT-PCR analysis also showed *Mpzl3* transcripts expression in the *rc/rc* mouse skin (Figure 7b). We sequenced the RT-PCR products from both normal and *rc/rc* skin complementary DNA (cDNA), and confirmed the G→A mutation in exon 3 of *Mpzl3* in the *rc/rc* cDNA derived from the 6-exon transcripts.

To detect the MPZL3 protein, we generated affinity purified rabbit polyclonal antibodies against a peptide (DKLTIDWTYRPPSSSRT) in the predicted extracellular domain of the murine MPZL3 protein. To test the specificity of these antibodies,

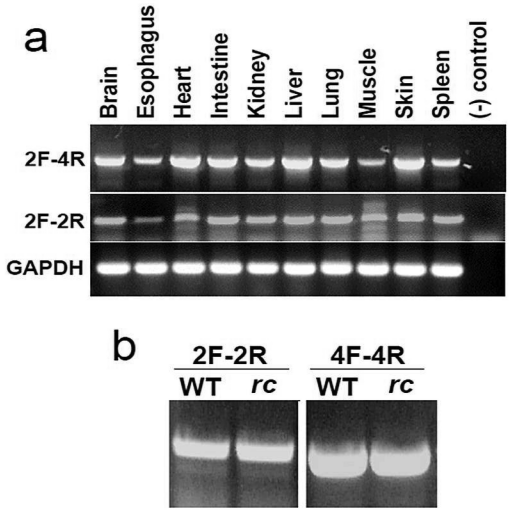


Figure 7. RT-PCR analysis of *Mpzl3* gene expression. **(a)** Expression of the 6-exon *Mpzl3* transcripts (2F-4R) and the 2-exon *Mpzl3* transcripts (2F-2R) in normal adult mouse organs. The two transcripts had similar tissue distribution. **(b)** Expression of the 6-exon *Mpzl3* transcripts (4F-4R to amplify exons 3~6) and the 2-exon *Mpzl3* transcripts (2F-2R) in wild type (WT) and *rc/rc* mouse skin.

we transfected NIH/3T3 cells with an expression vector encoding a fusion protein between the murine MPZL3 and Myc epitope tag. We analyzed total cell extracts by western blot analyses using the anti-MPZL3 antibodies, detecting two bands at approximately 27 and 29 kDa (Figure 8a). These bands were also recognized by the anti-Myc antibody (Figure 8b). The size difference may be due to different post transcriptional modifications. when the anti-MPZL3 antibodies were preabsorbed with the DKLTIDWTYRPPSSSRT peptide at a 1:3, 1:10, or 1:32 molar ratio, binding to the fusion protein became much weaker at 1:3 molar ratio (Figure 7c; very faint band s at 27 and 29 kDa were visible with much longer exposure, data not shown) and could not be detected at a 1:10 (Figure 8d) or 1:32 molar ratio (data not shown). These result suggest that the anti MPZL3 antibodies specific for the antigen. The anti MPZL3 antibodies also detected 27 and 29 kDa bands in NIH/3T3 cells transfected with a plasmid encoding the *rc* mutant MPZL3 protein fused to the Myc tag (data not shown) as expected. In addition, using the anti-MPZL3 antibodies, we detected bands that were of much higher molecular weight (~80 and ~110kDa), which were not detected with preabsorbed anti-MPZL3 antibodies or the anti-Myc antibody (Figure 8a-d). These bands could be endogenous MPZL3 with different post-transcriptional modifications or from different transcripts.

In all the adult mouse organs analyzed by Western blot, we detected a single band at approximately 70 kDa (Figure 8e) When we used preabsorbed antibodies to analyze skin and kidney extracts, we detected no signal (data not shown) suggesting the antibody binding was specific. The band detected is much larger than the size predicted from the amino-acid sequence (237 amino acids before the cleavage of predicted signal peptide), which may result of post-transitional modification, such glycosylation or dimerization or from translation of different transcripts. Interestingly, the bands detected in NIH/3T3 cells (~80 and ~110 kDa) were not detected in any

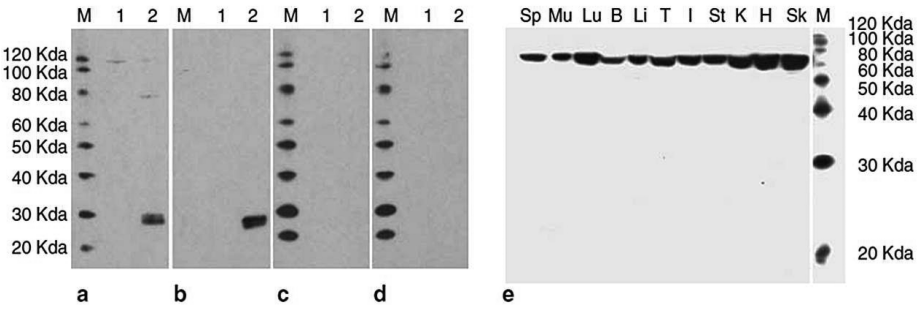


Figure 8. Characterization of the anti-MPZL3 antibodies and expression of MPZL3 in adult mouse organs. **(a–d)** Western blot analysis of total cell extracts from control NIH/3T3 cells **(lane 1)** and NIH/3T3 cells transfected with pEF/myc/cyto containing wild-type murine Mpzl3 cDNA **(lane 2)**. The primary antibodies used were: **(a)** rabbit anti-MPZL3 peptide DKLTIDWTYRPPSSSRT affinity-purified antibodies**, (b)** mouse anti-Myc tag antibody, rabbit anti-MPZL3 affinity-purified antibodies preabsorbed with **(c)** 1:3 or **(d)** 1:10 molar ratio of peptide DKLTIDWTYRPPSSSRT. Blot c showed very faint bands of 27 and 29 kDa after a much longer exposure (data not shown). **(e)** Western blot analysis of total protein extracts from adult mouse organs detected by rabbit anti-MPZL3 affinity-purified antibodies. Sp: spleen; Mu: muscle; Lu: lung; B: brain; Li: liver; T: testis; I: intestine; St: stomach; K: kidney; H: heart; Sk: skin. M: MagicMark XP.

mouse organs analyzed, suggesting they may unique for cultured NIH/3T3 cells.

We were interested to determine MPZL3 protein expression and localization in the skin, therefore we carried out indirect immunofluorescence of adult mouse skin sections. We detected MPZL3 expression in keratinocytes of the epidermis and hair follicles (Figure 9). By examining staining at high magnifications, it was clear that the staining was strong around the plasma membrane (Figure 9e and f), consistent with the prediction of a transmembrane protein involved in cell adhesion. We also detected staining in the cytoplasm, but not in the nuclei. We did not detect differences in the MPZL3 protein distribution pattern between normal and *rc/rc* mouse skin. Using *rc/rc* skin sections with hypertrophic sebaceous glands, we also detected MPZL3 expression in the sebocytes (Figure 9c, d, and g). As a negative control, indirect immunofluorescence using normal goat serum instead of anti-MPZL3 antibodies did not show any specific staining (data not shown).

Sequence analysis of the *Mpzl3* gene in *ruf/ruf* mice:

The *ruf/ruf* mice develop skin abnormalities similar to the *rc/rc* mice, such as "unkempt" and "wet" looking hair coats and sebaceous gland hypertrophy (Park et al., 2001), and the locus has been mapped to Chromosome 9 (Sweet HO, 1990). Although allelism between these two spontaneous mutations has not been tested directly, it is possible that they are caused by mutations in the same gene. However, our sequence analysis of the *Mpzl3* gene coding sequences did not detect any differ-

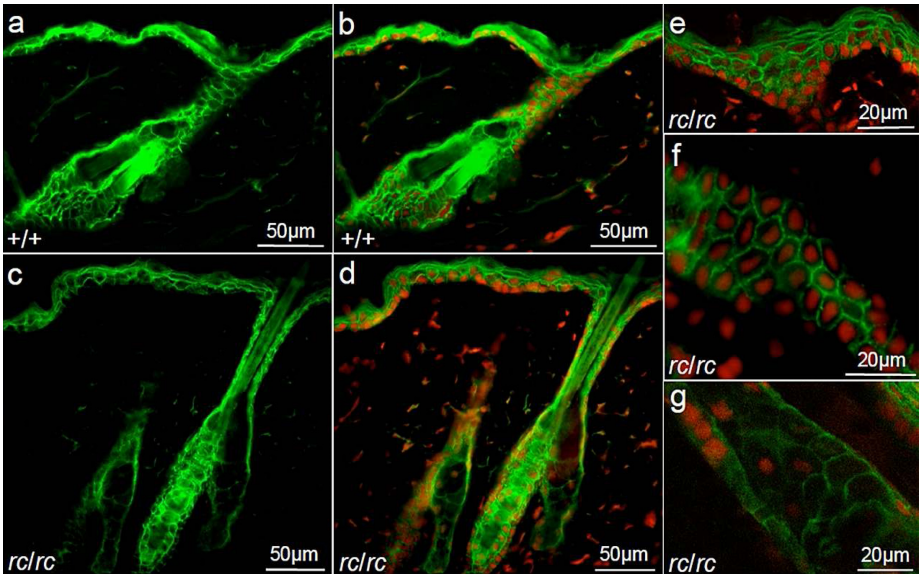


Figure 9. Expression of MPZL3 in mouse skin sections detected by indirect immunofluorescence. **(a–f)** MPZL3 (green) was detected in the keratinocytes of the epidermis and hair follicles as well as **(a–d, g)** the sebocytes. **(b, d–g)** Sections were counterstained with propidium iodide (red). **(a, b)**: +/+ skin; (c–g): *rc/rc* skin. Bar¼50 mm in **(a–d)**, 20 mm in **(e–g)**.

ence between the parental C3H/HeJ and *ruf/ruf* genomic DNA purchased from the Jackson Laboratory (Bar Harbor, ME). Therefore, our results suggest that *ruf* and *rc* are likely not allelic.

Discussion

In this study, we carried out positional cloning of the gene mutated in the *rc* mice. We mapped the *rc* locus to a 246-kb interval by high-resolution linkage analysis, and identified a missense mutation which resulted in an Arg100→Gln substitution in a novel open reading frame within this interval. Based on the predicted domain structure of the encoded protein, we named this novel gene *Mpzl3* encoding a full-length MPZL3 polypeptide of 237 amino acids. Arg100 is a highly conserved residue within the conserved Ig-like V-type domain. Therefore, substitution of Arg100 is highly likely to alter the MPZL3 protein function in the *rc/rc* mice.

The MPZL3 protein:

Through BLAST search, the highest levels of sequence homology with the MPZL3 protein were identified in the Myelin Protein Zero (MPZ) and MPZL2 (Myelin Protein Zero-like 2, also called EVA1) proteins (Figure 6). Within the Ig-like V-type

domain, however, the MPZL3 protein shares a 40.0% identity and 54.2% similarity at the amino acid level with MPZ, and a 36.1% identity and 60.5% similarity at the amino acid level with EVA1. All the consensus residues within the Ig V-type domain, such as the cysteines and the N-glycosylation site, as well as the Arg corresponding to Arg100 in the MPZL3 protein, are conserved between these three proteins. Interestingly, the *Mpzl3* gene is located approximately 1 kb 3' to the *Eva1* gene, and the sizes of exons 2 and 3 are identical (167 bp and 211 bp, respectively). It is possible that these two genes arose through tandem duplication.

Whereas the *Mpzl3* gene encodes a short peptide of 96 amino acids through an alternatively spliced transcript in both mice and rats, there is no EST evidence that such a transcript exists in humans. Both the mouse and rat 96-amino acid polypeptides possess a signal peptide but have only a portion of the Ig-like domain, and lack a transmembrane domain downstream. In addition, EST evidence suggests the existence of other forms of *Mpzl3* transcripts (Figure 5b). It is not known whether such transcripts are expressed at significant levels in mice and rats, and the subcellular location and possible functions of the encoded polypeptides remain to be determined.

The *rc* mutation:

The *rc* mutation arose spontaneously without mutagens in 1966, and all the allele has been maintained in cryopreserved embryos during most of the past four decades. Hence we expected a "simple" mutation without gross chromosomal rearrangement (such as those induced by X-ray irradiation). It is therefore not surprising that we detect a single nucleotide transition, which resulted in an amino –acid substitution. The mutated *Mpzl3* transcripts and protein were detected at significant levels in the skin of *rc/rc* mice, suggesting that the effect of the mutation is likely posttransitional. Substitution of the highly conserved Arg100 in the conserved Ig-like domain required for adhesion may result in decreased cell adhesion. Shedding of hair at the telogen phase in the *rc/rc* mice may be one of the effects of such reduced adhesion.

In this study, we did not detect any mutations/polymorphisms in the *Mpzl3* gene in other mouse strains we analyzed. However, there are at least five documented variations in the mouse *Mpzl3* gene between mouse strains: four of them being synonymous, and one being non-synonymous. This non-synonymous polymorphism results in an Ala27→Val substitution within the signal peptide in the 129X1/SvJ strain, and likely has no functional consequence on the mature protein, as the mice appear normal.

The abnormalities in the *rc/rc* mice are not limited to the skin (Hayashi et al., 2004), and the mutated gene likely plays a role in the normal functioning of multiple organ systems. Not surprisingly, the *Mpzl3* transcripts were detected in a variety of organs. However, no other alleles of the *Mpzl3* mutation have been described. It is possible that the mutation we identified in the *rc/rc* mice is a "hypomorph". A more drastic change in the *Mpzl3* gene, such as a large deletion or early frame-shift muta-

tion, may lead to much more severe abnormalities in other organ systems and result in a lethal phenotype, and would therefore have never been documented as a natural mutation. Future functional analyses such as knock-out or knock-down experiments will be able to address such a possibility.

Mutations in adhesion molecules:

Mutations in a number of genes involved in cell adhesion, particularly components of the desmosomes, both transmembrane and intracellular, have been associated with defects of the skin and heart, where there are high levels of mechanical stress (McMillan and Shimizu, 2001). The *Mpzl3* gene expression was detected at high levels in the skin and heart, where the *rc/rc* mice develop severe abnormalities (Hayashi et al., 2004), and the MPZL3 protein is localized to the plasma membrane, consistent with the assumption that the MPZL3 protein may be involved in cell adhesion. Whereas there have been no reports of mutations in the *MPZL2* (*EVA1*) gene in human diseases, substitutions of conserved residues such as Thr124→Met in the Ig domain in the MPZ protein have been identified in patients with Charcot-Marie-Tooth disease (Chapon et al., 1999; De Jonghe et al., 1999; Misu et al., 2000). Similarly, substitution of the highly conserved Arg100 with Gln in the Ig domain of the MPZL3 protein likely results in alteration of the protein function in the *rc/rc* mice.

Interestingly, transgenic mice over-expressing c-*myc* in the keratinocyte stem cells also show sebaceous hypertrophy, hair loss, and spontaneous wounds (Arnold and Watt, 2001; Frye et al., 2003; Waikel et al., 2001) , though not as severe. In addition, while the effects of over-expressing c-*myc* were dominant, the effects of *rc* mutation were recessive. Over-expression of c-*myc* has been shown to drive the KSCs out of the stem cell compartment (Arnold and Watt, 2001; Waikel et al., 2001), and gene expression profiling has revealed that 40% of all down-regulated genes in the c-*myc* transgenic mice encoded cell adhesion molecules or cytoskeleton proteins, resulting in the reduced adhesive interactions of KSCs with the local microenvironment or niche. In addition, the failure of hair differentiation of the c-*myc* transgenic mice may reflect an inability of keratinocytes to migrate along the outer root sheath to receive hair inductive stimuli (Frye et al., 2003). It is therefore possible that the *Mpzl3* leads to similarly compromised interactions of the keratinocytes with their microenvironment and manifestation of the *rc* phenotype.

Materials and methods

Mice:

All animal procedures were approved by the University of Hawaii Institutional Animal Care and Use Committee (IACUC). Mice were maintained in a temperature-, humidity-, and light cycle (12:12) controlled vivarium under specific pathogen-free conditions. One male and three female heterozygous rough coat (+/*rc*) mice in the C57BL/6J (B6/J) strain background were purchased from the Jackson Laboratory

(Bar Harbor, ME) to establish our own rough coat mouse colony. Female BALB/cJ and CAST/Ei mice were also purchased from the Jackson Laboratory for backcross studies.

Histological analysis:

The dorsal skin of euthanized B6/J-*rc*/*rc* and age- and sex-matched B6/J-+/*rc* mice was shaved, and skin biopsies were collected. They were embedded in OCT or fixed in phosphate-buffered formalin and dehydrated and cleared in xylene before being embedded in paraffin. The cryosections were stained with oil red O for lipids, and the paraffin sections were stained with hematoxylin and eosin. Ultrastructural analyses were made using a Hitachi S-4800 Field Emission Scanning Electron Microscope with Oxford INCA X-Act EDS System.

Backcross:

B6/J-*rc*/*rc* mice were outcrossed with both female BALB/cJ and CAST/Ei mice to obtain F_1 hybrids (+/*rc*). Because female *rc*/*rc* mice do not breed well (Hayashi et al., 2004), we used male B6/J-*rc*/*rc* mice and F_1 females for our backcross experiment to obtain F_2 hybrids for linkage analysis.

Genotyping:

Genomic DNA of F_2 hybrids was extracted from tail tip biopsy at the time of weaning using Proteinase K (Invitrogen Corporation, Carlsbad, CA) digestion and ethanol precipitation. PCR reactions were carried out to amplify microsatellites polymorphic between the parental strains, and the amplified DNA fragments (amplicons) were analyzed using 4% Metaphor agarose (Cambrex, Rockland, ME) gel electrophoresis. In cases when there were no more published microsatellite polymorphisms between the parental strains in the Mouse Genome Informatics "Strains and Polymorphisms" database (www.informatics.jax.org) or the Ensembl Mouse Genome Database (www.ensembl.org/Mus_musculus), we designed primers to detect novel polymorphisms between B6/J and BALB/cJ or between B6/J and CAST/Ei. Microsatellites with at least 15 CA or TG repeats based on sequence information in the Ensembl Mouse Genome Database (C57BL/6 strain) were amplified by PCR from these strains and the amplicons were analyzed by agarose gel electrophoresis. Those with detectable polymorphisms (at least 8 bp on a 4% Metaphor agarose gel) were used for linkage analysis.

Linkage analysis:

Backcross offspring were scored for recombination events that segregate the microsatellite markers contributed by the two parental alleles and the *rc* locus (indicated by the phenotype). The distances between the loci and the LOD scores were calculated using the QTXb20 software(Manly et al., 2001) .

Mutation detection:

Primers for sequence analysis were designed based on the C57BL/6 genomic sequence and exon structure in the Ensembl Mouse Genome Database (www.ensembl.org/Mus_musculus). Primers were located in the introns, 5' and 3' UTRs or 5' and 3' flanking sequences so that mutations in the exon sequence as well as the splice donor, acceptor, and branch sites could be detected. Primers were synthesized at Integrated DNA Technologies (Coralville, IA), and PCR reactions were carried out using both wild type B6/J and B6/J-*rc*/*rc* mouse genomic DNA as templates. The amplicons were analyzed by agarose gel electrophoresis, and the DNA was recovered from the gel using GeneClean Spin Kit (Q-Biogene, Carlsbad, CA). Sequences from both strands were obtained BigDye sequencing kit and an ABI PRISM 3100 Genetic Analyzer (Applied Biosystems, Foster City, CA) at sequencing core facilities (MBSR, CGPBRI, and GMBF) at University of Hawaii at Manoa. Once a mutation was identified, it was confirmed in four more mice each of both +/+ and *rc*/*rc* genotypes from different parents, and in heterozygous (+/*rc*) mice. We also confirmed the mutation in B6/J-*rc* genomic DNA purchased from the Jackson Laboratory (Bar Harbor, ME) and in PCR-amplified cDNA generated from *rc*/*rc* mouse skin RNA. Sequence analysis of the mutated gene was also carried out on genomic DNA extracted from BALB/cJ, CAST/Ei, C3H/HeJ mice (The Jackson Laboratory, Bar Harbor, ME), B6C3F1, B6D2F1, CD1, and SwissGP mice (NCI-Frederick Animal Production Area, Frederick, MD), and C3H/HeJ-*ruf* genomic DNA purchased from the Jackson Laboratory (Bar Harbor, ME).

RNA extraction and RT-PCR analysis:

The dorsal skin of euthanized B6/J-*rc*/*rc* and age- and sex-matched B6/J-+/+ mice was shaved, and skin biopsies as well as the internal organs were collected. Samples were frozen immediately in liquid nitrogen or immersed in RNA*later* (Qiagen, Valencia, CA). Total RNA was extracted using TriReagent (Molecular Research Center, Inc., Cincinnati, OH) following manufacturer's manual. Total RNA was reverse transcribed using the SuperScript III Reverse Transcriptase Kit (Invitrogen Corp., Carlsbad, CA). The first strand cDNA was used as templates for PCR amplification. The quality of the cDNA was confirmed by PCR amplification of glyceraldehyde-3-phosphate dehidrogenase cDNA analyzed by agarose gel electrophoresis.

Antibody generation

Two rabbits were immunized with synthesized peptide DKLTIDWTYRPPSSSRT (amino acids 63~79, in the predicted extracellular domain of the murine MPZL3 protein), and the serum was affinity purified for antibodies against the peptide (Bethyl Laboratories, Montgomery, TX).

Western blot analysis and indirect immunofluorscence

The full coding sequences of the wild type murine Mpzl3 cDNA, as well as

Mpzl3 cDNA harboring the rc mutation, were subcloned into the Pst I/Not I sites of pEF/myc/cyto (Invitrogen Corp., Carlsbad, CA), so that the Myc tag was at the carboxyl terminus of the fusion protein. The resulting plasmids were transfected into NIH/3T3 cells (ATCC, Manassas, VA) using LipofectAmine 2000 (Invitrogen Corp.), and the total cellular proteins were extracted using modified RIPA buffer (50mM Tris-Cl, pH7.4, 1mM each of EDTA, PMSF, Na_3VO_4 and NaF, 1% NP-40, 62.5mM each of ALLN and N-Etylmaleimide, and 1:15 diluted Protease Inhibitor cocktail). Biopsies of adult mouse skin were homogenized and the proteins extracted as described (He et al., 2002). Protein extracts were analyzed by gradient (Invitrogen Corp.) or non-gradient SDS-PAGE and blotted onto Immobilon transfer membrane (Millipore Corporation, Billerica, MA) for Western blot analysis following standard protocols. The molecular weight marker used was MagicMark XP (Invitrogen Corp.). The rabbit anti-MPZL3 antibodies were diluted 1:400 and mouse anti-Myc tag antibody (Covance Research Products, Princeton, NJ) was diluted 1:200. For antibody preabsorption, the rabbit anti-MPZL3 antibodies were incubated with excess peptide DKLTIDWTYRPPSSSRT at 1:3, 1:10, or 1:32 molar ratio for 1 hour before being added to the blot. Antibody binding was detected with ECL Western Blot Detection Reagents (GE Healthcare Bio-Sciences Corp., Piscataway, NJ) and BioMax film (Eastman Kodak Company, Rochester, NY). Cryosections of back skin biopsies of normal and rc/rc mice were incubated with 1:200 dilutions of rabbit anti-MPZL3 antibodies or normal goat serum. Antibody binding was detected with goat anti-rabbit IgG conjugated with FITC, and the slides were mounted in VectorShield with propidium iodide (Vector Laboratories, Burlingame, CA). The sections were examined and photographed on a Zeiss AxioSkop 2 Plus fluorescent microscope or a Zeiss 5 PASCAL LSM confocal microscope (Carl Zeiss MicroImaging, Inc., Thornwood, NY).

Acknowledgments

This work was supported by grants AR047713 (KC) and AR050487 (TC) from NIH/NIAMS and G12RR003061 (KC, TC) from NIH/NCRR (RCMI program), and the Ingeborg v.F. McKee Fund from the Hawai'i Community Foundation (20040450 and 20050401 to TC). The authors would like to thank Scott Lozanoff, Charles D. Boyd, Yusuke Marikawa, Olivier Le Saux, Athula Wikramanayake's laboratory, Yvonne Tatsumura, Keith S. Fong, Xiao-Jing Wang's laboratory (Oregon Health and Science University), Dennis R. Roop and Paul A. Overbeek (Baylor College of Medicine) for helpful suggestions, Shannon Bennett and Durrell Kapan for help in linkage analysis, and Darlene Ramones and Marisa Tricas for technical assistance. Sequencing analyses were carried out at the CGPBRI, GMBF, and MBSR Sequencing Core Facilities at UHM, and microscopic images were captured and analyzed at the RCMI Imaging Core Facility. The GenBank accession number for murine Mpzl3 gene/mRNA is EF102773.

Chapter 3

The human orthologue of murine *Mpzl3* with predicted adhesive and immune functions is a potential candidate gene for immune-related hereditary hair loss

This chapter is based on:
Racz P, Mink M, Ordas A, Cao T, Szalma S, Szauter KM, Csiszar K.
Exp Dermatol. 2009 Mar;18(3):261-3. Epub 2008 Oct 22

Abstract

We have recently reported a mutation within the conserved immunoglobulin V-type domain of the predicted adhesion protein MPZL3 (MIM 611707) in rough coat (*rc*) mice with severe skin abnormalities and cyclic and progressive hair loss. In this study, we analyzed the human orthologue gene MPZL3 on chromosome 11q23.3, to test the hypothesis that mutated MPZL3 might be a candidate for similar symptoms in humans. Data were integrated from the Ensembl, NCBI and USCS genome informatics databases, protein structure modeling was carried out using THMM and EBI Inter Pro Scan softwares, domain structure and potential posttranslational modification sites were identified with CBS servers and 3D structure was generated with the Swiss-Model server. Results show that the predicted MPZL3 protein is highly conserved in mammals, has two transmembrane motifs flanking an extracellular Ig-like domain and is expressed in immune cells among others. The R100Q mutation identified in *rc* mice is within the Ig-domain recognition loop known for functions in T-cell receptors and cell adhesion. Further support for an immune related role is that the homologous Myelin Protein Zero and EVA1 function in cell adhesion and immune response. Based on the results of the *rc* mouse study, 3D structure, homology predictions, comprehensive NCBI Entrez database analyses of multiple polymorphisms and mutations within the human MPZL3 gene, and its cell and tissue expression pattern, we postulate that homologous or compound heterozygous mutations of MPZL3 might be involved in immune mediated human hereditary disorders presenting with hair loss.

Introduction

The rough coat (*rc*) mutation arose spontaneously (Dickie, 1966) and homozygous *rc* mice show in both sexes growth retardation, cyclic and progressive hair loss, and sebaceous gland hypertrophy due to sebocyte hyperplasia which results in increased lipid synthesis and clumped hair (rough coat) (Hayashi et al., 2004). In the hepatic sinusoids of the liver of *rc* mice, we noted increased numbers of erythrocytes, lymphocytes, polymorphonuclear leukocytes (neutrophils) and enlarged Kupffer cells compared to normal controls. By one year of age, 60% of the *rc* mice develop spontaneous and persistent ulcerated lesions on the ventral skin of the neck (Cao et al., 2007). At the ulcer sites, localized extensive granulation tissue formations were present with neutrophilic, mastocytic and lymphoplasmacytic dermatitis (Hayashi et al., 2004). The *rc* locus was previously mapped to 32.0 cM on mouse chromosome 9 (Eicher EM, 1977). Subsequently, we defined and reduced the mapping interval for this locus to 246kb, which contains 11 candidate genes. Using DNA sequence analysis of all coding exons and flanking splice sites within this region, we identified a single missense mutation in the Myelin Protein Zero Like 3 (*Mpzl3*) gene (MIM 611707) that resulted in an R100Q substitution within the conserved immunoglobulin (Ig)

```
Hs  MQQ-RGAAGSRGCALFPLLGVLFFQGVYIVFSLEIRADAHVRGYVGEKIKLKCTFKSTSDVTD
Pt  MQQ-RGAAGSRGCALFPLLGVLFFQGVYIVFSLEIHADAHVRGYVGEKIKLKCTFKSTSDVTD
Mm  MQLARGTVGGRGCALFPLLSILVVQGARIVLSLEISADAHVRGYVGEKIKLKCTFKSSSDVTD
Md                  VFKYFGFLYL-GLYAVLSMEIKADAHVRGYIGESIKLKCTFRSSSPVSD
Gg   LSGAGAAGMRGGEVVAYLGWLLPSGICGALSLDIKTSPEVRGYVGEQIVLKCSFKSSFPITE
Dr        MMDVNRSAFKGLLWCVFFTSGLC---MSVWSPAEVSVVSGSAVSLSCSFSSSSRVTS

Hs  KLTIDWTYRPPSSSHTVSIFHYQSFQYPTTAGTFRDRISWVGNVYKGDASISISNPTIKDNGT
Pt  KLTIDWTYRPPSSSRTVSIFHYQSFQYPTTAGTFRDRISWVGNVYKGDASISISNPTIKDNGT
Mm  KLTIDWTYRPPSSSRTESIFHYQSFQYPTTAGTFRDRISWAGNVYKGDASISISNPTLKDNGT
Md  KLTIDWTYRQPTSSRIEPIFHYQSFQYPTTAGTFRDRISWVGDVYRGDASISISNPTMRDNGT
Gg  SLTIDWTYRPLTGGLMETVFHYQSVAYPASVGRFKDRISWVGNAAKGDASIAIQSPSVSDNGT
Dr  LMSVDWKFKPQSGGPAKLFFHFSSVAYPVEDERFRGRVKWTGSPSGGDASIQLLNATQNDNGT

Hs  FSCAVKNPPDVHHNIPMTELTVTERGFGTMLSSVALLSILVFVPSAVVVALLLVRMGRKAAGL
Pt  FSCAVKNPPDVHHNIPMTELTVTERGFGTMLSSVALLSILVFVPSAVVVALLLVRMGRKAAGL
Mm  FSCAVKNPPDVYHNIPLTELTVTERGFGTMLSSVALLSILVFVPSAVVVILLLVRMGRKATGV
Md  FSCSVKNPPDVHHNIPMTELVVTERGFAIQLSSAALLSILVFIPSAVVVTLLLVRMGRKSAGL
Gg  FICSVKNPPDVYHNIPQTVLIVTERGFSFQLTSVTLLSIVVFIPSTVVVVLMLVRMGRKSGVI
Dr  FSCSVRNPPDIQGNTAQTVLTVTPKRVSLTLTDVGVLLVCVVGPSAVVTLLLLSRICCCSEGP

Hs  KKRSRSGYKKSSIEVSDDTDQEEEEACMARLCVRCAECLDSDYEE-TY
Pt  KKRSRSGYKKSSIEVSDDTDQEEEEACMARLCVRCAECLDSDYEE-TY
Mm  QKRSRSGYKKSSIEVSDETDQEDSNDCMTRLCVRCAECLDSDYEEEAY
Md  KKKSKSGYKKSSIEVSDDTDQGEDEDCMRRFCTRCAECLDSDYEE-AY
Gg  KEKKRPSCKKSSVE---ESESEYTDNCMGRLKTWCLNCVDTDEED-PY
Dr  PALQHHSPIEVIAGEEYFYTQTQHKHSACCCYFKDSEYDEDEYMADKLHEHTITESQC
```

Compare	Identities	Positives	Gaps
Hs-Pt	233/235 (99%)	233/235 (99%)	0/235 (0%)
Hs-Mm	205/237 (86%)	214/237 (90%)	2/237 (1%)
Hs-Md	175/221 (79%)	195/221 (88%)	1/221 (0%)
Hs-Gg	127/232 (55%)	163/232 (70%)	3/232 (1%)
Hs-Dr	71/238 (30%)	102/238 (43%)	4/238 (2%)

Figure 1. Different level of MPZL3 amino acid sequence homologies in mammals and lower vertebrates. The identical residues (identities) are highlighted with yellow background, the conservative substitutions (positives) are highlighted with blue background. Dashes (-) indicate deletions. Bold letters show the conserved Immunoglobulin V-type domain. The red highlighted R indicates the R100Q mutation found in *rc* mice. Hs: *Homo sapiens*, Pt: *Pan troglodytes*, Mm: *Mus musculus*, Md: *Monodelphis domestica*, Gg: *Gallus gallus*, Dr: *Danio rerio*.

V-type domain of the predicted MPZL3 protein (Cao et al., 2007) (Chapter 2). In this study, towards understanding the normal and pathological function of human MPZL3, we analyzed its gene structure along with polymorphisms and mutations, tissue expression pattern and functional domains using genome database information, homology modeling and protein structure predictions.

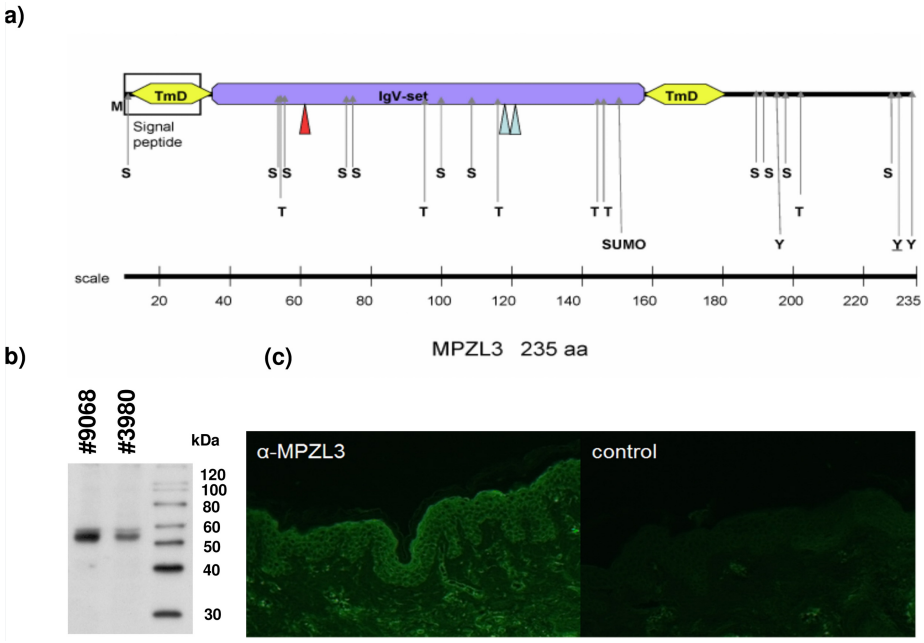


Figure 2. (**a**) MPZL3 domain structure and potential posttranslational modification sites. Empty rectangle: signal peptide, yellow hexagons: transmembrane (TmD) domains; purple hexagon: immunoglobulin V-type domain; blue triangles: potential N-glycosylation sites; red triangle: potential O-glycosylation site; purple arrow, predicted sumoylation site; grey arrows, potential phosphorylation sites; S: Ser; T: Thr; Y: Tyr. The underlined Y is a predicted sulphated tyrosine. **(b)** Western blot analysis of cultured primary human fibroblasts (donors #9068 and #3980) using affinity-purified anti-MPZL3 antibodies (1:500). **(c)** Immunofluorescent detection of MPZL3 (1:100) in human skin. Controls were incubated with normal goat serum instead of anti-MPZL3.

Results

Ensembl database analysis identified orthologues of the MPZL3 protein in mammals with 88–99% similarity that declined in non-mammalian vertebrates (Figure 1). The R100Q substitution we identified in *rc* mice lies within the conserved Ig V-type domain of MPZL3 and affects a residue conserved in all vertebrate species.

The human gene *MPZL3* at chromosome band 11q23.3 is highly homologous to the mouse *Mpzl3* gene including genomic context, exon/intron organization, nucleotide and predicted amino acid sequences. Analysis of the predicted 235 amino acid MPZL3 protein using TMHMM (Krogh et al., 2001; TMHMM) and EBI InterProScan software revealed two transmembrane motifs at amino acid positions 12–34 and 159–181 that flank the extracellular Ig-like domain (position 31–148, Figure 2a). Structural modeling placed the R100Q mutation within the recognition loop of the Ig-like domain known for roles in T cell receptors, cell–cell recognition and cell

adhesion (Teichmann and Chothia, 2000). The Human Protein Reference Database biological process prediction suggested an immune response role for MPZL3 (Peri, 2003)

The NCBI Entrez SNP database contained numerous single nucleotide polymorphisms (SNPs) within the *MPZL3* gene. Two synonymous SNPs fall within the conserved Ig V-type domain at amino acid positions 63 and 137. A frame shift mutation outside the Ig V-type domain is at amino acid 150 -/A. Three non-synonymous mutations, M155V, V168G and V172M substitutions were in exon 4 and a D228V substitution in exon 6. As the mouse and human genes are orthologues with 84.5% identity at the nucleotide and 86.8% identity at the amino acid level that reaches 93.3% within the Ig V-type conserved domain (Cao et al., 2007), it is suggested that humans with mutations within the conserved Ig V-type domain may develop symptoms similar to the *rc* mouse.

Our RT-PCR studies detected *Mpzl3* expression in multiple mouse tissues and immunostaining localized MPZL3 in the epidermis and hair follicles (Cao et al., 2007). Based on EST counts in NCBI, Unigene database human *MPZL3* expression was similarly detected in brain, esophagus, heart, kidney, liver, lung, muscle, spleen, and in addition in blood, colon, eye, lymph node, mammary gland, mouth, ovary, parathyroid, pharynx, pituitary gland, prostate, stomach, testis, uterus and vascular tissues. EMBL-EBI Array Express microarray database analysis showed *MPZL3* expression in dendritic, CD4 and CD8 central memory and effector T cells.

Western blot analysis of MPZL3 detected a 54 kDa and a fainter 56 kDa band in cultured primary human dermal fibroblasts, which may result from dimerization and/or from posttranslational modifications of MPZL3 (predicted MW 25.98 kDa, Figure 2b). Using immunohistochemistry, we localized MPZL3 in similar regions of the human skin (Figure 2c) as in the mouse skin (Cao et al., 2007) including hair follicles (not shown).

Conclusion

This study demonstrated that the MPZL3 Ig V-type adhesive domain is extracellular flanked by transmembrane domains, a domain motif found in proteins with immune function. Expression of *MPZL3* in immune cells supports its potential immune-related role. Furthermore, the evolutionary closely related protein (Ensembl Gene Tree View analysis data) Epithelial V-like antigen 1 (EVA1) plays roles in cell adhesion and thymus and lymphocyte development (Guttinger et al., 1998). The results suggest that the MPZL3 protein may be involved in immune function and mutations within the conserved V-type domain may contribute to human disorders with immune-system deficiencies.

Significant association exists between mutations causing skin and hair follicle abnormalities and immunological defects (Hayashi et al., 2004; Yu et al., 2008). Hair follicles have properties of an immune privileged/protected site (Gilhar and

Kalish, 2006). Human hair loss disorders including alopecia areata, represent a breakdown in immune privilege with subsequent destruction of the hair follicle by T lymphocytes (Gilhar et al., 2005; Martinez-Mir et al., 2007). Ig-domain containing adhesion molecules play important roles in homing of lymphocytes to inflammation sites (Gilhar and Kalish, 2006). *PVRL1* located on the same chromosome as *MPZL3*, encodes a membrane adhesion protein with one V-like and two C-like extracellular Ig domains and is known to be associated with hereditary alopecia (Suzuki et al., 2000). Alopecia areata affects adults and children of both sexes with a lifetime risk of approximately 1.7%. While its exact molecular mechanism is not known, it is considered an autoimmune disease (Freyschmidt-Paul et al., 2001) and likely a polygenic disorder similar to other autoimmune diseases (McDonagh and Tazi-Ahnini, 2002). Based on our results, expression and mutational analysis of *MPZL3* in patients and families may provide valuable information towards understanding the involvement of MPZL3 in hereditary alopecia.

Methods

The NCBI (http://www.ncbi.nlm.nih.gov/), Ensembl (http://www.ensembl.org/index.html), and UCSC Genome Bioinformatics (http://genome.ucsc.edu/) databases were used for gene structure and sequence analyses. EST confirmed protein sequence was used to predict the protein structure with TMHMM (Krogh et al., 2001; TMHMM) (http://www.cbs.dtu.dk/services/TMHMM/) and EBI InterProScan softwares (http://www.ebi.ac.uk/InterProScan/). The template sequence that showed the highest sequence identity to MPZL3 was 1NEU (Myelin P0 protein precursor) and was selected for 3D homology modeling by the 3D jury consensus method (Ginalski et al., 2003) using the fold recognition server BioInfoBank Meta Server (Metaserver1) (http://bioinfo.pl/meta/). The 3D structure generation was carried out through the Swiss-Model server (Guex, 1997) (http://swissmodel.expasy.org//SWISS-MODEL.html) and visualization was performed using the Swiss-PDBViewer (Guex, 1997) program (http://expasy.org/spdbv/). MPZL3 domain structure and potential posttranslational modification sites identified with EBI-InterProScan (http://www.ebi.ac.uk/Tools/InterProScan/) and CBS servers (Blom et al., 1999; Gupta R, 2004; Julenius et al., 2005), SUMOplot™ Analysis Program (Xue et al., 2006).

Acknowledgments

This work was supported by NIH/NIAMS grants AR47662 to KC, and AR050487 to TC, and Ingeborg v. F. McKee Funds #20040636 and #20050401 from the Hawaii Community Foundation to TC.

Chapter 4

Functional analysis of the *mpzl3* gene in zebrafish

Racz P, Zakrzewska A, Csukonyi E, Ordas A, Spaink HP, Mink M, Meijer AH,
in preparation

Abstract

MPZL3 is a novel member of the myelin Po protein family. The gene was identified through a mutation in the rough coat mouse strain and is conserved in all vertebrates. Although *in silico* analyses suggest that the gene encodes an adhesion molecule with a possible immunological role, functional analyses have not yet been reported. In this study we investigated the zebrafish homolog of *mpzl3*. We determined the expression pattern of the gene during zebrafish embryo development by whole-mount *in situ* hybridization, and examined the effects of overexpression and morpholino knock-down regulation. Our results show that *mpzl3* has an important role in early developmental processes, and that its overexpression causes major defects in eye development and general retardation of larval development. Knock-down of *mpzl3* using morpholino antisense technology also resulted in several defects, including locomotion disorder, altered head morphology, edema in the eye and the heart, and other cardiovascular abnormalities. Microarray analysis of the effects of *mpzl3* knock-down during early embryogenesis revealed altered expression of genes involved in several developmental processes and suggested that *mpzl3* might be involved in Notch and Wnt signaling.

Introduction

MPZL3 is a novel member of the myelin Po family. The gene was identified at mouse chromosome 9 (Dickie, 1966), at 44, 86 Mb (Cao et al., 2007) through a spontaneous recessive point mutation in an inbred C57BL/6J mouse strain, called rough coat (*rc*) (Cao et al., 2007; Hayashi et al., 2004). The gene encodes a 237 amino acid long polypeptide with an Immunoglobulin V-type domain (IgV). The rough coat mutation causes a single nucleotide transition in the gene and an Arg-Gln substitution within a conserved residue of the functional IgV domain (Cao et al., 2007). RT-PCR analysis revealed that the gene is expressed in a variety of organs like brain, esophagus, heart, intestine, kidney, liver, lung, muscle, skin, and spleen (Cao et al., 2007). The mutated gene in mice causes numerous abnormalities, including growth retardation, severe skin abnormalities, myocardial degeneration, hypercalcaemia, liver inflammation and abnormal hemosiderin granules deposition in the spleen (Hayashi et al., 2004). Although *in silico* based annotation indicates that the protein might play a role in thymus and T cell development (Racz et al., 2009), *in vivo* functional analyses have not yet been achieved. Knock-out analysis in mice will be a useful approach to study the function of the gene. However, given that the rough coat point mutation in *Mpzl3* already has strongly effects, it is possible that the complete lack of *Mpzl3* function may lead to more drastic changes in the affected organ systems and result in a lethal phenotype. Considering the time investment and the possible outcome of the mouse knock-out experiment, we decided first to investigate the *Mpzl3* gene function in the zebrafish embryo model, in which rapid knock-down

studies are possible.

Zebrafish has become a widely used model organism in biology. In the last decade many studies have used zebrafish as a model to better understand human diseases or to investigate functions of genes conserved between fish and human. The zebrafish has several advantages, like easy maintenance, small space requirements, large brood size, and reasonably short life cycle (generation time is about 10 weeks). It is a convenient model organism to do large scale screenings because the females are able to produce 200–300 new progeny every week. As the embryos develop outside the mother and remain translucent for several days, it is possible to visually track every aspect of their development. The embryogenesis is rapid and most organ systems are fully developed by 5 days post-fertilization (dpf). The transparency of the embryos can be exploited to localize specific cell types and developing organs by whole mount *in situ* hybridization (WISH) in fixed embryos, or to monitor developmental processes in real time using fluorochrome tagged cells in living embryos. As the embryos are developing *ex vivo* in the aquarium medium, any soluble molecule can be readily applied and used for example to probe developmental signaling pathways or for testing of pharmacological activity. Furthermore, embryo development can be easily manipulated by micro-injection of messenger RNAs for overexpression studies or by injection of antisense morpholino oligonucleotides for transient gene knock-down. The zebrafish embryo model allows the phenotypic assessment of mutations that in mammals would cause very early embryonic lethality. For example, even drastic cardiovascular defects can be studied, as the embryos can gain sufficient oxygenation via diffusion through the skin during the first days of their development (Grillitsch et al., 2005; Pelster and Burggren, 1996).

Relevant to the study of *mpzl3*, is that the zebrafish immune system has proven to be remarkably similar to that of humans (Traver et al., 2003). Studies of hematopoiesis have revealed that most if not all cell types of the human immune system have zebrafish counterparts (Berman et al., 2003; Traver et al., 2003). Macrophages and neutrophils already develop during the first day of embryogenesis. T cell developmental genes show strong homologies to mammalian genes with similar expression and functional profiles. B cells also exist and express activation-induced cytidine deaminase but do not undergo class-switch recombination (Barreto et al., 2005) and somatic hypermutation is inefficient (Wakae et al., 2006). The thymus in zebrafish is similar to that of mammals with the main exception that the zebrafish thymus remains as two discrete bilateral structures (Meeker and Trede, 2008). T cells exit the thymus and populate various tissues including the kidney, pharynx, intestinal tract, nose, spleen, and skin. In adult fish the hematopoiesis occurs in the kidney which is equivalent to the human bone marrow (Al-Adhami MA, 1977). The zebrafish lymphatic system has also been identified (Kuchler et al., 2006; Yaniv et al., 2006), although they do not have lymphatic nodes, Peyer's patches or splenic germinal centers.

In this study we identified the evolutionary conserved counterpart of mamma-

lian *mplz3* in zebrafish and characterized the expression pattern of this gene during embryo development. We performed overexpression and morpholino knock-down experiments to investigate the function of the *mpzl3* gene. In addition to detailed phenotype analysis of the fish with enhanced or reduced *mpzl3* expression, we used microarrays to investigate the global gene expression changes induced by *mpzl3* knock-down.

Results

Characterisation of the *mpzl3* gene in zebrafish:

Based on the Ensembl database (Ensembl release 56 - Sept 2009 Zv8) the zebrafish *mpzl3* gene (ENSDARG00000079225) is located on chromosome 15 at 47 Mb on the forward strand. According to the NCBI Reference Sequence database (NM_213169.1) the coding sequence of the gene consists of 648 nucleotides and encodes a 215 amino acid long polypeptide. We analyzed the protein sequence using the InterProScan domain prediction program and identified Myelin Po motifs at amino acid positions 13-37, 62-89, and 91-120, and a conserved Immunoglobulin (Ig) V-set domain at amino acid positions 16-99

Phylogenetic analysis:

To determine the evolutionary relation between the myelin Po domain (MyPo) containing proteins of zebrafish we downloaded all proteins with a MyPo domain using the Ensembl 54 - Danio rerio Zv8 database. This dataset was uploaded into the ClustalW multiple sequence alignment program and a phylogenetic tree was made using the Neighbor Joining method, allowing the addition of gaps. The results (Figure 1) show that Mpzl3 (ENSDARP00000103451) is most closely related to Mpz (ENSDARP00000101478; ENSDARP00000056371), Mpzl1 (ENSDARP00000092425) and Mpzl2 (ENSDARP00000032601).

Expression of *mpzl3* in zebrafish:

To analyze *mpzl3* expression during zebrafish development first we carried out quantitative RT-PCR (qRT-PCR) analyses using total RNA. As shown in Figure 2A, the *mpzl3* mRNA levels were highest between the 4-cell and dome stages, probably reflecting maternal expression. Expression of *mpzl3* dropped to a much lower level at 80% epiboly, but remained detectable until at least 5 dpf. For more detailed analyses whole-mount *in situ* experiments were performed to analyze the spatial expression pattern of the *mpzl3* mRNA at different time points during embryo and larval development. We observed that in the early developmental stages (4 cell, 8 cell, and 30% epiboly) the mRNA was ubiquitously expressed (data not shown). At later time points *mpzl3* expression became gradually restricted. At 5 dpf, *mpzl3* expression was specifically detected in different areas of the head, including the anterior neuromasts and the branchial arches. We also recognized *mpzl3* expression in neuromasts of the

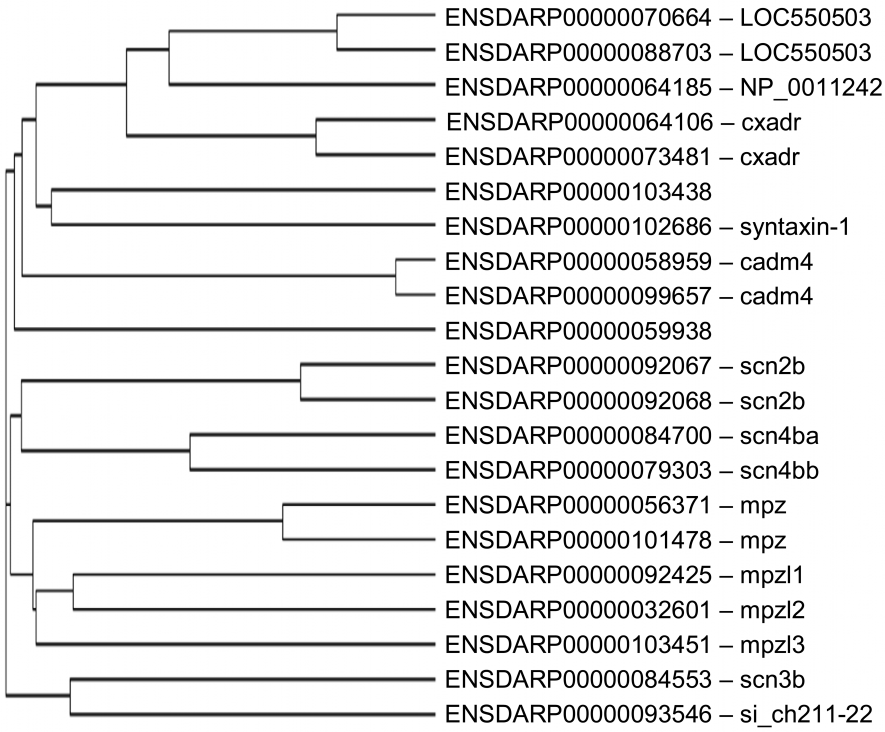


Figure 1. Evolutionary relations of the MyPo domain proteins of zebrafish. The cladogram was made by the ClustalW Neighbour Joining method.

posterior lateral line, in the swim bladder, and the cloaca (Figure 2A).

Overexpression analysis of *mpzl3*:

To investigate the role of *mpzl3* in zebrafish we cloned the *mpzl3* full length coding sequence into the pCS2+ plasmid and used SP6 polymerase to transcribe capped mRNA for micro-injection into embryos at the 1-2 cell stage. Injection of 5 pg mRNA did not induce phenotypic alterations, but injection of 10-75 pg mRNA caused a general retardation of development and edema of the heart cavity was sometimes observed as well as bent and shortened tails. However, the most remarkable and consistent phenotype was aberrant eye development, which was observed in 23% of the embryos injected with 10pg of mRNA and 42% of the embryos injected with the highest amount of mRNA. Embryos injected with the lowest concentration do not show phenotypic difference compare to the uninjected control embryos. Some embryos showed aberrant development of both eyes and others showed asymmetric development of the two eyes, with one developing normally and the other being highly abnormal or completely undeveloped (Figure3).

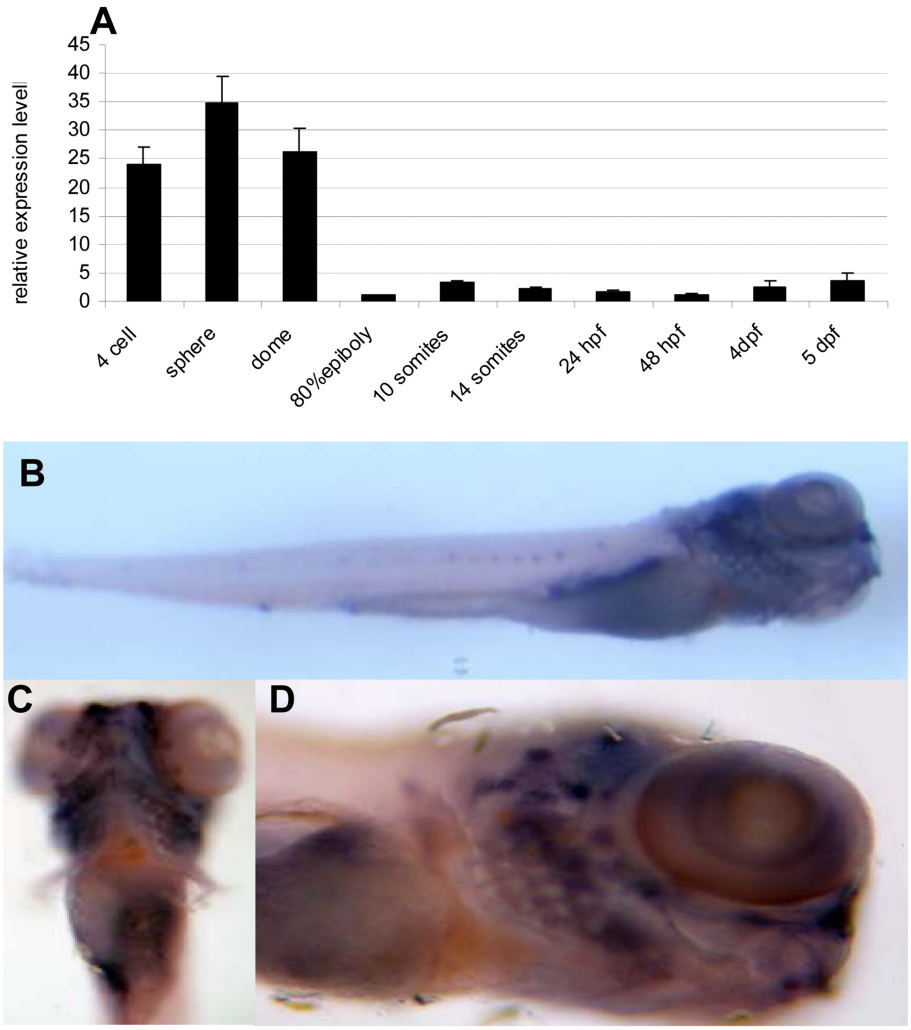


Figure 2. Expression of the *mpzl3* gene in zebrafish embryos. **(A.)** qRT-PCR analysis of *mpzl3* expression. Relative expression levels of *mpzl3* were determined at the indicated developmental stages between the 4-cell stage and 5 dpf. The expression at 80% epiboly is set to 1. Data were normalized to expression of peptidylprolyl isomerase A-like (*ppial*), which showed no changes over the mRNA samples used. **(B-D)**. Expression pattern of *mpzl3* investigated by whole-mount *in situ* hybridization at 5 dpf. *Mpzl3* is highly expressed in the head, including the anterior neuromasts and the branchial arches. Furthermore, *mplz3* expression was detected in the neuromasts of the posterior lateral line, the swim bladder, and the cloaca. Embryos in **(B)** and **(D)** are in lateral view, anterior to the right. A ventral view of the head is shown in **(C)**, anterior to the top.

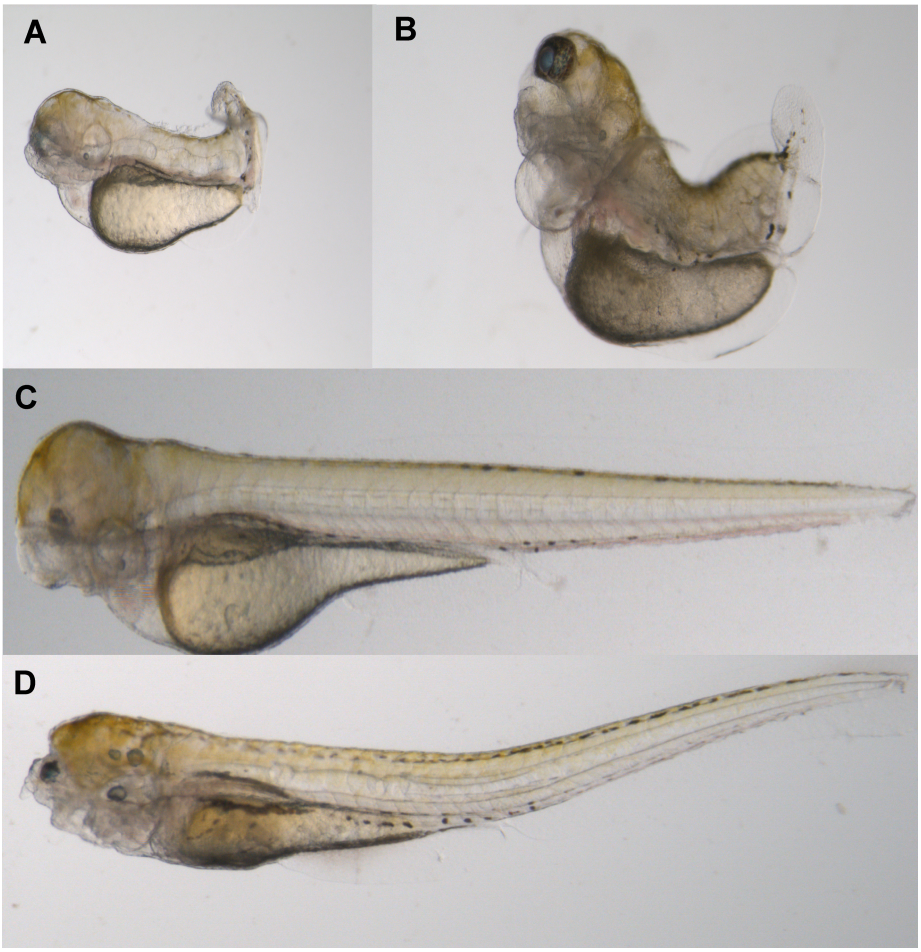


Figure 3. Overexpression analysis of *mpzl3*. Embryos were injected at the 1-2 cell stage with *mpzl3* capped mRNA. **(A)** 3 dpf embryo, injected with 10 pg *mpzl3* mRNA. The embryo shows cardiac edema, a bent tail and only the eye on the right side of the embryo is developed properly. **(B)** 5 dpf embryo, injected with 50pg of *mpzl3* mRNA, the embryo shows cardiac edema, a shortened tail, and only the eye on the left side of the embryo is developed. **(C)** 3 dpf embryo, injected with 10 pg of *mpzl3* mRNA. Here the embryo shows normal tail development, but neither of the eyes was developed. **(D)** 5dpf embryo, injected with 50 pg of *mpzl3* mRNA. Development of the head and both eyes was strongly affected.

Morpholino knock-down analysis of *mpzl3*:

A morpholino knock-down approach was used to block the translation of the *mpzl3* mRNA during zebrafish embryo development (Figure 4). As controls we used non-injected embryos and embryos injected with the standard control morpholino from Genetools. The most conspicuous phenotype that we observed was that injec-

tion of 0.25mM morpholino caused 55 % lethality in the injected population. It was also notable that after hatching a subset of the embryos (4% of 0.1mM morpholino injection, 28% of 0.25mM morpholino injection, and 33% of 0.5mM morpholino injection) lost the ability of movement. We punched these morphants with an acupuncture needle to force them to move in the liquid medium, but the morphants did not react to this treatment. We monitored the phenotype between 3 dpf and 7dpf and no changes were observed during this time (data not shown).

The *mpzl3* morphant fish also developed heart edema at 1 dpf. To further examine this phenotype we used the fli:EGFP transgenic line which expresses green fluorescent protein in the entire vasculatory system. As shown in Figure 4B and 4E-F, the structure of the caudal vasculature of the mpzl3 morphants was affected. A possible explanation for this observation might be that it is a result of the accumulation of erythrocytes in the caudal vasculature region of the morphant fish. We next tested whether the cardiovasculatory defects were associated with any alteration of the heart rate. Therefore, we investigated the heart rate of 10 *mpzl3* morphant fish versus 10 standard control morphants at 7dpf and calculated the average heart beat per minute (bpm). We found that the *mpzl3* morphant embryos had a lower heart rate compared to the controls (90 bpm vs. 155 bpm).

Since Mpzl3 proteins have proposed immune functions, we next tested the hypothesis that *mpzl3* knock-down might affect thymus and T cell development. To this extent we carried out *in situ* hybridization using the recombination activating gene-1 (*rag1*) thymus specific marker (Corripio-Miyar et al., 2007) and found that the *mpzl3* morphant fish do not express the *rag1* marker at 6 dpf, while *rag1* is already detectable in wild type zebrafish larvae at 4 dpf (Figure 4C (Willett et al., 1997).

To test the specificity of the morpholino effect, we designed another translation blocking morpholino (MO2) upstream of the first morpholino (MO1). Repeating all experiments with the second morpholino (MO2), we found that this morpholino (MO2) phenocopied the effects of the first morpholino (Figure 4C-D). In addition, we used the synthetic *mpzl3* mRNA to rescue the morpholino phenotypes by co-injection. We co-injected in the 1-2 cell stage 116 embryos with 10 pg of the *mpzl3* cRNA and 0.125 mM of the *mpzl3*-MO2. After the co-injection the survival rate was elevated from 45 to 84% at day 5. We investigated the ability of fish to move. After 3 days all fish were capable of free swimming and responded to needle punching by swimming away, while more than 20% of the surviving embryos injected with 0.125 mM of *mpzl3*-MO2 showed the motionless phenotype. We also observed that some of the embryos co-injected with *mpzl3* mRNA and morpholino showed undeveloped eye phenotypes (9%) of which more than half also showed heart edema. As eye defects and heart edema were also observed in the overexpression analysis, these phenotypes are probably due to the effect of increased *mpzl3* mRNA level, while the increased survival rate and normal motion of the embryos co-injected with *mpzl3* mRNA and morpholino indicates effective rescue of the morpholino knock-down phenotype.

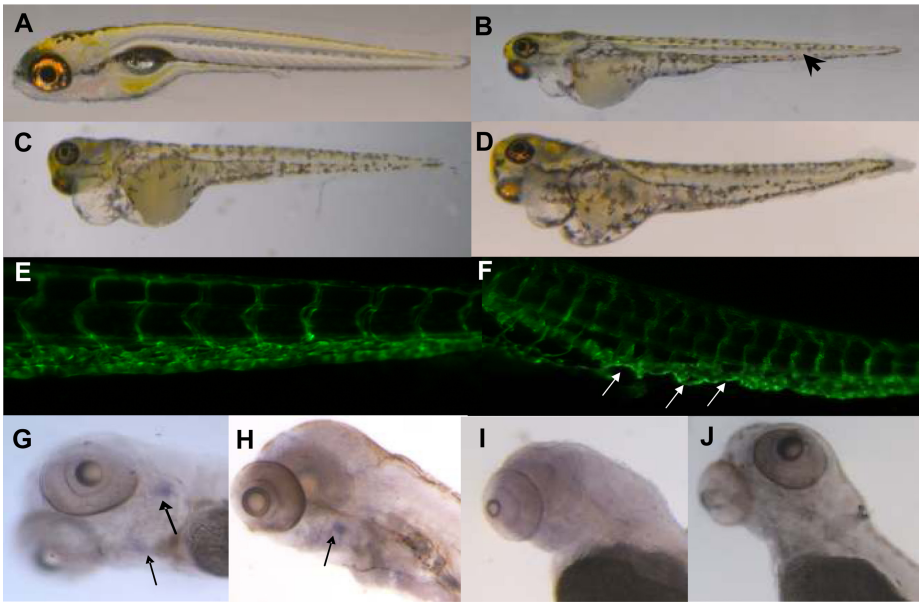


Figure 4. Phenotypes of *mpzl3* morphant fish. **(A-B)** 5 days old wild type **(A)** and embryo injected with 1 nl of 0,25 mM *mpzl3* morpholino (MO1) **(B)**. The morphant fish developed heart edema, and the erythrocytes often accumulated in the caudal region (black arrowhead). **(C,D)** Comparison the effect of the two translation blocking morpholinos MO1 **(C)** and MO2 **(D)**. 1 nl of 0.25 mM concentration was injected for both morpholinos. Embryos are shown at 5 dpf. **(E-F)** Fluorescent microscopy images of the caudal vasculature of wild type **(E)** and MO1 morphant **(F)** fli:EGFP fish. In the morphant fish it is recognizable that the vasculatory system in the caudal part was affected (white arrow) **(G-J)** whole mount *in situ* hybridization of wild type **(G)**, standard control morphant **(H)**, and *mpzl3* MO1 **(I)** and MO2 **(J)** morphants with recombination activating gene-1 (*rag1*) probe at 6 dpf. All images show lateral views, anterior to the left.

Microarray analysis of the *mpzl3* knock-down effect:

To analyze the global gene expression changes that underlie the altered phenotypes caused by *mpzl3* morpholino knock-down, we carried out 4x44k Agilent microarray chip analyses. We investigated the transcriptome level changes in both *mpzl3*-MO1, and *mpzl3*-MO2 morphant fish at 8 hpf, at which time-point phenotypical alterations between morphants and controls could not yet be observed. By choosing this early time-point for our analysis we aimed to gain insight into altered signaling pathways that might be responsible for the later phenotypic defects. As a control we used embryos injected with the standard control morpholino and we analyzed the samples in duplicate with a dye swap. Using the Rosetta Resolver pipeline for normalization and data analysis, we generated an overlapping dataset of the MO1 and MO2 effects versus the standard control. With the significance cut-off at $P \leq 10^{-4}$ level we found that 504 sequences associated with 464 genes were up-regulated

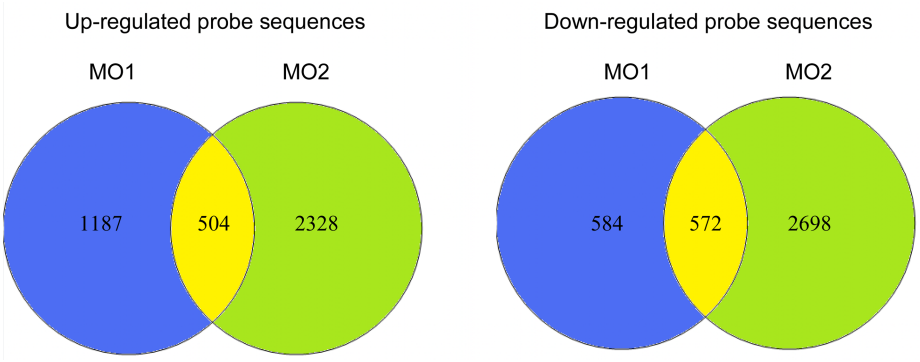


Figure 5. Microarray analysis of the *mpzl3* knock-down effect. **(A)** Venn diagram showing the overlap between the probe sequences up-regulated in embryos injected with *mpzl3* morpholinos MO1 and MO2. The 504 sequences overlapping between MO1 and MO2 corresponded to 464 different genes. **(B)** Venn diagram showing the overlap between the probe sequences down-regulated in embryos injected with *mpzl3* morpholinos MO1 and -MO2. The sequences overlapping between MO1 and MO2 corresponded to 445 different genes. The significance cut off level was $P \leq 10^{-4}$ in both cases.

(Figure 5A) and 572 sequences associated with 445 genes showed down-regulated expression (Figure 5B) with both morpholinos.

To achieve an unbiased functional annotation of the gene set affected by *mpzl3* morpholino knock-down we performed Gene Ontology (GO) analysis using eGOn (explore GeneOntology), a web-based tool for interpreting and statistical analysis of genomic data using GO terms (supplementary Table 1 and 2). The eGOn software classifies user input gene lists by GO criteria for biological process (GO:0008150), cellular components (GO:0005575) and molecular functions (GO:0003674) in a species-independent manner, and produces hierarchical trees of GO terms in these three categories. Among the up-regulated transcripts we observed gene groups associated with negative regulation. For example, we identified negative regulation of cellular processes like, negative regulation of cell cycle (GO:0045786), negative regulation of the signal transduction (GO:0030514, GO:0030178, GO:0040036, GO:0035023), negative regulation of endodermal cell fate specification (GO:0042664) and genes which play a role in the negative regulation of transcription (*her1*, *tp73l*). Genes associated with regulation of apoptosis were also identified by GO analysis. Possibly as the consequence of the enhanced expression of the negative regulation processes, a wide range of developmental processes were also affected, such as liver (GO:0001889), gut (GO:0048547), morphogenesis of the eyes (GO:0048048), skeletal (GO:0001501) and muscle development (GO:0007517). Six genes associated with the morphogenesis of the epithelium (GO:0002009) showed altered expression. Four out of these 6 genes, Bloody fingers (*blf*) Bone morphogenetic protein 2b (*bmp2b*), GLI-Kruppel family member GLI2a (*gli2a*), Nodal-related 2 (*ndr2*) showed upregulated expres-

sion and 2 genes Mix-type homeobox gene 2 (*mxtx2*) and Siaz-interacting nuclear protein (*sinup*) were down-regulated in the *mpzl3* morphants. We also identified several genes involved in development of the brain, where we identified specific *mpzl3* expression by RT-PCR and Western Blot analyses in mouse. Based on the array data the expression level of genes involved in forebrain (GO:0030900), hindbrain (GO:0030902) midbrain (GO:0030901) and diencephalon (GO:0021536) development was increased in *mzpl3* morphants. GO investigation of signal transduction pathways affected by *mpzl3* morpholino knock-down identified eight genes involved in Wnt signaling that showed up-regulated expression. These genes included frizzled homolog 8b (*fzd8b*), dapper homolog 1 (*dact1*), dickkopf 1 (*dkk*), and Sp5 transcription factor-like (*sp5l*) frizzled related protein (*frzb*), frizzled homolog 3 (*fzd3*), casein kinase 2 beta (*ck2b*) sizzled (*szl*), which all showed eleveted expression levels in *mpzl3* morphants. Furthermore, we also identified five signaling molecules that play a role in the Notch pathway. Four out of these five genes, DeltaD (*dld*), Hairy-related 6 (*her6*), Lunatic fringe homolog (*lfng*), and zgc136520,(*zgc136520*) showed up-regulated expression and one gene, disabled homolog 2 (*dab2*), showed down-regulation. In addition, molecules involved in BMP / transforming growth factor beta receptor signaling, MAD homolog 1 and 2 (*smad1* and *smad2*) and sizzled (*szl*), showed up-regulated expression.

Discussion

In this study we performed the first functional analysis of *mpzl3,* a newly identified myelin Po family member in zebrafish and the homolog of the gene mutated in mice with the rough coat phenotype. Overexpression studies showed that elevated levels of *mpzl3* mRNA strongly affected eye development of zebrafish embryos. Knock-down analysis of *mpzl3* using morpholinos resulted in lower survival rates, cardiovasculatory system defects, and affected locomotion of larvae after hatching. Furthermore, expression of the recombination activating gene product (*rag1*) in the thymus was absent in morphant larvae at 6 days postfertilisation. Microarray analysis of the expression pattern changes caused by morpholino knock-down suggested that the Wnt and Notch signaling pathways were affected in addition to the expression levels of several genes involved in developmental processes.

Evolutionary relationships:

Phylogenetic analysis showed that the closest evolutionary related proteins of Mpzl3 in zebrafish are Mpz (myelin protein zero), Mpzl1 (myelin protein zero like 1), and Mpzl2 (myelin protein zero 2) or Eva1 (epithelial V antigen). All three proteins have immunoglobulin V type and myelin Po domains. Comparing this result to data from human and mouse indicates that the members of the family are evolutionary conserved. It is known that EVA1 has the highest sequence homology to MPZL3 in mice (Cao et al., 2007) and plays a role in thymus and early T cell development

(DeMonte et al., 2007; Guttinger et al., 1998). We hypothesized in Chapter 3 that EVA1 and MPZL3 might interact with each other (Racz et al., 2009) and this hypothesis has been supported by a recent large-scale extracellular protein interaction study called AVEXIS (avidity-based extracellular interaction screening) (Bushell et al., 2008). In this study, a systematic screen for receptor-ligand pairs within the zebrafish immunoglobulin superfamily was performed. Two interacting proteins of Mpzl3 were identified, including Eva1 and Cssl:d179; however, the interaction strength between Mpzl3 and Cssl:d179 was one of the weakest measured in this study (Bushell et al., 2008). The other closely related protein, Mpz, is known as the major constituent of the myelin sheath in mammalians, and mutation of *Mpz* causes hereditary motor and sensory neuropathy, called type 1B Charcot-Marie-Tooth disease (CMT). CD8-positive T-lymphocytes were present in mpz mutant mice in the endoneurium (Schmid et al., 2000; Shy et al., 1997). The number of these immune cells increased with time and progression of demyelinating neuropathy, suggesting that the disease might be the consequence of autoimmune inflammation (Maurer et al., 2002).

Mpzl3 expression pattern:

We identified the expression pattern of *mpzl3* in zebrafish embryos and larvae by whole mount *in situ* analyses. Expression of *mpzl3* in embryos at 5 dpf was found to be localized in different areas of the head including the neuromast cells of the anterior lateral line and the branchial arches. We also identified specific expression in the neuromasts of the posterior lateral line, the swim bladder, and the cloaca. The expression in the cloaca is consistent with previous immunohistochemistry results of Bushell et al. (2008), who detected Mpzl3 protein in the pronephric duct of embryos at 53 hpf. Bushell et al. also detected Mpzl3 protein in the epidermis. We did not observe epidermal expression of *mpzl3* mRNA in our *in situ* analysis except for the expression in epidermal cells of the lateral line neuromasts. The lateral line is an organ with hair cells that are involved in reception of mechanical stimuli. It was hypothesized earlier that *mpzl3* plays a role during hair morphogenesis (Cao et al., 2007). The lateral line organ of zebrafish has been used as a model for hair cell loss and regeneration (Ma and Raible, 2009). It is possible that mutation of the protein caused abnormal differentiation not only of the hair-follicles cycling in the skin surface, but also might affect the sensory ability of the secondary sensory structure. The neuromasts are deposited by a migrating primordium that originates from the otic region. At the end of zebrafish embryogenesis, this line comprises 7–8 neuromasts regularly spaced between the ear and the tip of the tail (Gompel et al., 2001). Adhesion molecules like cadherins are required for normal lateral line development. For example, zebrafish embryos in which *cadherin-2 (cdh2)* expression had been knocked down did not develop an appropriate lateral line (Kerstetter et al., 2004) and *cadherin-4 (cdh4)* morphants developed shorter lateral line nerves and a reduced number of neuromasts, suggesting a disrupted migration of the lateral line primordium after the knock-down of adhesion molecules (Wilson et al., 2007). The signaling process

required for normal hair formation and secondary sensory structure involves the Notch and Wnt pathways (Hawkins et al., 2007; Ma and Raible, 2009), where we observed altered expression in our microarray analysis of *mpzl3* morphant fish. In addition, we observed that *mpzl3* morphant larvae were unable to respond to a touch stimulus. The possibility that this phenotype might be due to dysfunction of the lateral line sensory organ requires further investigation.

Overexpression analysis:

The phenotypes caused by overexpression of *mpzl3* were variable but the common phenotypic difference was that the fish developed anophthalmia. The phenotype varied between the formation of two very small and immature eyes and asymmetric eye development, where one eye developed correctly but the other one was missing. The processes involved in eye formation are conserved from the planaria to the vertebrates (Silver and Rebay, 2005) and require the function of several homeobox genes like *ey/pax6*, *toy*, *six3*, and *six6*. Mutation in these genes causes absence or ectopic formation of the eyes (Chow et al., 1999; Czerny et al., 1999; Loosli et al., 1999). In addition to the conservation of such genes involved in eye morphogenesis, several conserved signaling pathways, including the Wnt and Notch pathways that were affected upon *mplzl3* knock-down, also play a role in eye development (Cagan and Ready, 1989; Gage and Zacharias, 2009; Wehrli and Tomlinson, 1998).

Morpholino knock-down analysis:

Gene knock-down of *mpzl3* using two translation blocking morpholinos resulted in severe abnormalities in zebrafish embryos, including lower survival rate, immobility, cardiovascular system defects and expression deficiency of the *rag1* thymus marker. As discussed above, the immobility of *mpzl3* morphants in response to touch stimuli might be related to dysfunction of neuromast cells that showed *mpzl3* expression in wild type embryos. Two other mechanisms can be hypothesized to explain the motionless phenotype. First, as Mpzl3 is protein closely related to Mpz it might play a role in myelin sheet formation or have an effect on the transmission/processing of impulses propagated along the myelinated fiber. Second, as Mpzl3 has been proposed as an immune-related protein, mutation of the gene might lead to autoimmune-derived demyelination of the axons. However, this possibility is perhaps less likely since the adaptive immune system is not yet matured in zebrafish embryos. Interestingly, when mice heterozygously deficient in *mpz* were cross-bred with homozygous null mutants for the recombination activating gene 1 (*rag-1*) or cross-bred with mice deficient in T-cell receptor a-subunit genes (*tcra*) myelin degeneration and impairment of nerve conduction properties was less severe compared to the heterozygously *mpz*-deficient mice without immune cell deficiencies, suggesting that T cells are involved in the demyelinating process of hereditary neuropathy caused by the *mpz* mutation (Schmid et al., 2000). Another study demonstrated that macrophages are actively involved in demyelination in a model for MPZ-caused inher-

ited neuropathies (Carenini et al., 2001). In addition, CD8-positive T-lymphocytes were found in the endoneurium of *mpz* mutants (Shy et al., 1997). Taken together these data provide strong evidence that the immune system plays a role in neuropathies induced by *mpz* mutation. The possible involvement of *mpzl3* in neurodegenerative disorders needs to be further studied. In zebrafish a screen was performed for mutations that affect myelin gene expression in Schwann cells and oligodendrocytes. This screen identified the motionless mutation *(mot)*, associated with the absence of the myelin basic protein (Mbp) expression and vascular defects. The mutated fish died around 4 dpf probably due to vasculatory system malfunction (Kazakova et al., 2006). Another study in zebrafish shows that mutations affecting neurogenesis are often associated with cardiovascular defects, like in the *natter* (*nat*), *viper* (*vip*), *otter* (*ott*), *fullbrain (ful),* and *snakehead (snk)* mutants (Jiang et al., 1996). In our study of *mzpl3* morphants, in addition to the motility defect, heart edema was also observed, with vasculatory system structure alteration. To investigate the possible relation of *mpzl3* with the immune system we determined *rag1* expression in the morphant embryos. In morphants at 6 dpf obtained with two different *mpzl3* morpholinos, no *rag1* expression could be detected. It is very unlikely that the *rag1* deficiency was the consequence of a developmental delay, as the control fish showed *rag1* expression in the thymus at day 4, consistent with the reported *rag1* expression pattern (Willett et al., 1997). Therefore, the lack of *rag1* expression in *mpzl3* morphants might be the first direct experimental support that the vertebrate Mpzl3 proteins are involved in immune system processes. Based on these results, it would be of great interest to investigate *rag1* expression and T cell functions in the *rough coat* mutant mice.

Microarray analysis of the *mzpl3* knock-down effect:

We performed a preliminary microarray analysis to identify the gene expression pattern changes that may underlie the altered phenotypes caused by the *mpzl3* morpholino knock-down. To avoid secondary effects of the altered embryo morphology, the microarray analysis was performed at 8 hpf, prior to detectable phenotypical differences between morphants and controls. Gene ontology term based classification of the gene set showing altered expression with both *mzpl3* morpholino treatments showed that this set included genes involved in developmental processes that were affected in embryos with altered *mpzl3* expression and/or in the rough coat mice. For example, the rough coat mice show severe skin abnormalities and the morphant embryos showed up-regulated expression of genes associated with the morphogenesis of the epithelium, including *blf*, *bmp2b*, *gli2a,* and *ndr2*. In addition, *ndr2* mutation caused a cyclopia phenotype in zebrafish (Rebagliati et al., 1998), indicating an important role of this gene in eye developmental processes, which we found to be affected by *mzpl3* overexpression. In future work, it would be of interest to extend the overexpression study with microarray analysis for comparison with the results of morpholino knock-down. Another up-regulated gene linked with developmental processes altered in rough coat mice is fibulin 4 (*fbln4*). Based on Gene Ontology

FBLN4 associated with wound healing and plays a role in elastogenesis as it interacts with the propeptide of Lysyl oxidase (LOX), which efficiently promotes assembly of LOX onto tropoelastin (Horiguchi et al., 2009). In the *mpzl3* mutated rough coat mice Lysyl oxidase like molecule (LOXL) was expressed at reduced level (Hayashi et al., 2004). Finally, AP-2 alpha (tfap2a) involved in melanocyte differentiation was also up-regulated in the microarray analysis. In rough coat mice melanocyte color changes were observed in the hair follicles (Hayashi et al., 2004).

As we collected our RNA samples for microarray analysis at 8 hpf and the thymus developmental processes do not start before 60 hpf (Willett et al., 1999), not surprisingly we found only two differentially expressed genes associated with immune system gene ontology terms: sprouty4 (*spry4*) and interleukin enhancer binding factor 2 (*ilf2*), which were upregulated in the morphants. Sprouty 4 is an antagonist of Fgf and Ras/Map kinase signaling and has an important role in embryonic development (Furthauer et al., 2001). Interleukin enhancer binding factor 2, also known as nuclear factor of activated T-cells (NFAT), is one of the several transcription factors required for T-cell expression of the interleukin 2 (IL-2) gene. IL-2 is a key cytokine for T cell activation and its absence caused lethal autoimmunity in mice (Ma et al., 2006), while reduced levels of IL-2 protein caused autoimmune disorders (Crispin and Tsokos, 2008; Setoguchi et al., 2005). In zebrafish ilf2 expression was increased in regenerating fin tissue following amputation(Yoshinari et al., 2009), but its function in zebrafish is currently unknown.

Because the *mpzl3* morphant fish developed heart edema and the rough coat mice developed cardiac muscle fiber disorientation and multifocal myocardial degeneration (Hayashi et al., 2004), we hypothesized that the expression of genes involved in heart developmental processes might be changed in our microarray analysis. Our gene set contained four genes related to heart development: DAZ interacting protein 1 (*Dzip1*), bone morphogenetic protein 2b (*bmp2b*) floating head (*flh*) and nodal-related 2 (*ndr2*). Interestingly, bone morphogenetic protein plays a role in heart development but together with Hedgehog (Hh) also acts as a negative regulator of thymocyte development (Varas et al., 2003).

Finally, the mpzl3 morphant embryos also showed altered expression of genes involved in two conserved signaling pathways. Eight genes involved in Wnt signaling were down-regulated and five genes of the Notch pathway showed up-regulated (4 genes) or down-regulated (1 gene) expression. Both signaling pathways play a role in early embryonal development. Wnt genes encode a large family of secreted glycoproteins that are involved in a wide spectrum of cell activities (Miller, 2002). Wnt receptor binding is tightly modulated through association with diverse secreted proteins, like Dickkopf (Niehrs, 1999), Frzb-1 (Leyns et al., 1997; Wang et al., 1997) or Cerberus (Leyns et al., 1997), and through association with glycosaminoglycans. In addition to the essential role in embryonic patterning, the Wnt canonical pathway also plays a role in cell fate determination, and non-canonical Wnt signaling is required for regulation of planar cell polarity, cell adhesion, and motility (Katoh, 2008).

Wnt signaling also plays a role in T-cell development in the thymus. Using wnt1 and wnt4 double knock-out mice it was shown that after 15-16 days of gestation the number of the thymocytes was reduced by 50-70% (Mulroy et al., 2002). The Notch signaling pathway, which was also affected in mzpl3 morphants, plays multiple roles in the development of the central nervous system including the regulation of neural stem cell (NSC) proliferation, survival, self-renewal and differentiation (Gaiano and Fishell, 2002; Lathia et al., 2008). Notch signaling also regulates keratinocyte proliferation, and commitment and differentiation decisions in the skin (Blanpain et al., 2006; Lee et al., 2007), and contributes to maintenance of the follicular structure of the hair (Demehri and Kopan, 2009). Furthermore, Notch signaling also activates T lineage differentiation from hemopoietic progenitors (Tydell et al., 2007) and has an important role in autoimmune disease through a non-canonical signaling pathway (Talora et al., 2008). The possible link of *mpzl3* with Wnt and Notch signaling suggested by our microarray data is of great interest for further investigation.

Conclusion

In this study we investigated the function of *mpzl3* using overexpression and morpholino knock-down analysis in zebrafish embryos. Taken together, the experimental data suggested that *mpzl3* plays a role in developmental processes during early embryogenesis, which has not been previously reported in mammalians. The *mzpl3* mutation in rough coat mice is a hypomorphic mutation. A null mutant of *mzpl3* has not been described in mammalians, and based on the results of *mpzl3* knock-down in zebrafish might be embryonic lethal. Although the zebrafish study did not provide strong support for our previous hypothesis that *mzpl3* may have an immune function (Racz et al, 2009), a link with the immune system was suggested by the lack of *rag1* expression in *mplz3* morphants. Furthermore, the motility defects in *mplz3* morphants might be related to defects in the formation or maintenance of myelin sheaths, which also requires the function of the closely related *mpz* gene. Our microarray analysis of *mpzl3* morphants suggested alterations in Wnt and Notch signaling processes, which might underlie the observed developmental phenotypes. As Wnt and Notch signaling are also important for skin and nervous system development and immunological processes, the altered regulation of these pathways provides a useful lead for further investigations in the zebrafish and rough coat mouse models

Materials and Methods

Characterization of the zebrafish Mpzl3 protein:

The NCBI (http://www.ncbi.nlm.nih.gov/) and Ensembl (http://www.ensembl.org/index.html) databases were used for gene structure and sequence analyses. For deriving the protein sequence the translate tool accessible on the ExPASy proteomics server was used. Mpzl3 domain structure was identified with EBI-InterProScan

(http://www.ebi.ac.uk/Tools/InterProScan/) software.

Phylogenetic analysis:

By means of MART export using the Ensembl release 54 - May 2009 database (http://www.ensembl.org/biomart/index.html) all the PR00213 - PRINTS fingerprints database records (Myelin_Po domain) in zebrafish (Ensembl54 Danio rerio Zv8-dataset) were listed. The list was manually complemented with the Mpz, Mpzl1, and Mpzl3 protein sequences. The alignment and the phylogenetic tree were made using the ClustalW multiple sequence alignment program (http://www.ebi.ac.uk/Tools/kalign/index.html) and the neighbor joining method.

Zebrafish strains and husbandry:

Zebrafish were handled in compliance with the local animal welfare regulations and maintained according to standard protocols (zfin.org). Experiments were performed with ABxTL zebrafish and the fli:EGFP transgenic line was used to investigate the cardiovasculatory system of the morphant fish. Embryos were grown at 28.5–30°C in egg water (60 µg/ml Instant Ocean sea salts). Embryos used for whole mount *in situ* staining were kept in egg water containing 0.003% 1-phenyl-2-thiourea (Sigma-Aldrich) to prevent melanization.

RNA isolation:

Embryos for RNA isolation were snap-frozen in liquid nitrogen and subsequently stored at -80°C. Embryos were homogenized in 1 ml of TRIzol reagent (Invitrogen), and subsequently total RNA was extracted according to the manufacturer's instructions. The RNA samples were incubated for 20 min at 37°C with 10 U of DNaseI (Roche Applied Science) to remove residual genomic DNA before purification using the RNeasy MinElute Cleanup kit (Qiagen) according to the RNA clean-up protocol. Total RNA concentrations were determined spectrophotometrically using a Nanodrop ND-1000 (Isogen Life science). Optical density A260/A280 ratios of all samples ranged from 1.8– 1.9, indicating high purity.

Whole-mount *in situ* hybridization:

Embryos were fixed overnight in 4% paraformaldehyde in PBS at 4°C and whole-mount *in situ* hybridization using alkaline phosphatase detection with BM purple substrate (Roche) was performed according to Thisse et al. (45). Total RNA was used to generate templates for riboprobes synthesis by PCR using *mpzl3* gene-specific primers sets including the binding site for T7 RNA polymerase in the reverse primer: FW primer: 5'TGGTCTCCAGCAGAGGTCAGT3', REV primer: 5'TAATACGACT CACTATAGGGTGGTGTGTTCATGCAGTTTG3'. As a marker for the thymus we used recombination activating gene-1 (*rag1*): The sequences of the primers for *rag1* probe synthesis were: FW primer: 5'ATGGCATCACCATCTTCCAGGAAC3', REV primer: 5'TAATACGACTCACTATAGGGTATTGACAGAGTTGGTCAGGGCAG

3'. Digoxigenin-labeled riboprobes were synthesized using the labeling mixes from Roche and Ambion MEGAscript reagents for in vitro transcription.

cDNA synthesis and quantitative real-time PCR:

cDNA synthesis reactions were performed in a 40µl mixture of 1000 µg of RNA, 8 µl of 5x iScript reaction mix (Bio-Rad Laboratories), and 2 µl of iScript reverse transcriptase (Bio-Rad Laboratories). The reaction mixtures were incubated at 25°C for 5 min, 42°C for 30 min, and 85°C for 5 min. Real-time PCR was performed using the Chromo4 Real-time PCR detection system (Bio-Rad Laboratories) according to the manufacturer's instructions. Each reaction was performed in a 25-µl volume comprised of 1 µl of cDNA, 12.5 µl of 2x iQ SYBR Green Supermix (Bio-Rad Laboratories), and 10 pmol of each primer. Cycling parameters were 95°C for 3 min to activate the polymerase, followed by 40 cycles of 95°C for 15 s and 60°C for 45 s. Fluorescence measurements were taken at the end of each cycle. Melting curve analysis was performed to verify that no primer dimers were amplified. All reactions were performed as technical duplicates. For normalization, peptidylprolyl isomerase A-like (*ppial*) was taken as reference (Stockhammer et al., 2009). Results were analyzed using the $\Delta\Delta Ct$ method. Sequence of *mpzl3* forward primer: 5'GCTGCTGCTACTTCAAGGACTC3' and *mpzl3* reverse primer: 5'TGTGACTCTGTGATGGTGTGTTC3'.

Overexpression experiments:

Mpzl3 cDNA was cloned by RT-PCR on RNA from zebrafish embryos using the Superscript III one tube PCR system with Platinum taq (Invitrogen). Primers were designed to contain EcoRI and BamH1 restriction sites (FW:5'-CGGATCCTCACC ATGTCGGTGTGGTCTCCAGCAGAGG-3'; REV: 5'-GGTGAATTCCTAACACT-GTGACTCTGTGATGG-3') for cloning into pCS2+ vector (http://sitemaker.umich.edu/dlturner.vectors/home). The pCS2+-mpzl3 construct was checked by sequencing performed by ServiceXS (Leiden, The Netherlands). To generate *in vitro* capped RNA for micro-injection the pCS2+-mpzl3 plasmid was digested with BamHI and EcoRI restriction endonuclease and used as a template for RNA synthesis using SP6 polymerase according to the mMessage mMachine kit protocol (Ambion). Embryos at the 1 to 2 cell stage were injected with 1 nl containing 5 -75 pg mRNA.

Morpholino knock-down experiments:

Morpholino oligonucleotides (Gene Tools) were diluted to desired concentrations in 1 Danieu's buffer (58 mM NaCl, 0.7 mM KCl, 0.4 mM $MgSO_4$, 0.6 mM $Ca(NO_3)_2$, 5.0 mM HEPES (pH 7.6)) containing 1% phenol red (Sigma-Aldrich). To block translation of the *mpzl3* mRNA, we injected between 0.1 mM (0.85 ng) and 1 mM (8.4 ng) per embryo at the 1 to 2 cell stage. Morpholino sequences were: 5'-CTGCTGGAGACCACACCGACATGC-3' (MO1) and 5'-AACCCGGAAGTGAA-GAAAACACACC-3' (MO2). To control for aspecific morpholino effects, we used the standard control morpholino from Gene Tools.

Microscopy:

Images were taken using Leica M165C stereo and MZ16FA stereo fluorescence microscopes equipped with a DFC420C camera. Images were processed using Leica application suite (LAS) software.

Microarray analysis:

For microarray analysis embryos were injected at the 1-2 cell stage with 0.25 mM of MO1, 0.125 mM of MO2 or 0.25 mM of the standard control morpholino and RNA was isolated at 8 hpf. RNA (cRNA) was synthesized in one amplification round from 500ng of total RNA using the Agilent Two color Quick Amp kit. The dual-color hybridization of the microarray chips was performed according to Agilent protocol G4140-90050 version 5.7 (www.Agilent.com) for two-color microarray-based gene expression analysis. Labeled RNA from embryos injected with MO1 or MO2 was hybridized against RNA from embryos injected with the standard control morpholino. The hybridizations were performed in duplicate with a dye swap. Microarray data were processed from raw data image files with Feature Extraction Software 9.5.3 (Agilent Technologies). Processed data were subsequently imported into Rosetta Resolver 7.0 (Rosetta Biosoftware) and subjected to default ratio error modeling. The data were analyzed at the level of the individual probe sequences. Gene ontology (GO) analysis was performed using the GeneTools eGOn v2.0 web-based gene ontology analysis software (www.genetools.microarray.ntnu.no).

Acknowledgments

This work was partially supported by the European Commission Sixth Framework Program ZF-TOOLS (LSHG-CT-2006-037220). We thank Oliver Stockhammer, Peter Schoonheim, and Chao Cui for helpful discussions and Ulrike Nehrdich, Karen Bosma, and Davy de Witt for zebrafish care.

Chapter 5

Summary and General discussion

The rough coat mutation spontaneously developed in the C57BL/6J mouse strain and was identified in 1966 (Dickie, 1966) and mapped in 1977 at the 9th chromosome close to the *Mpi-1* gene (Eicher and Reynolds, 1977). The next few decades the rough coat strain was not studied but in 2004 the laboratory of Dr. Csiszar focused on identifying the causative gene of the rough coat phenotype, as it was hypothesized that it might be allelic with Lysyl oxidase like gene (*loxl*), a matrix component. It turned out that rough coat is not allelic with *loxl* (Hayashi et al., 2004) but the interest in the mutation remained. The main aim of my study described in this thesis was to answer two questions about the rough coat mutation: where is the exact location of the mutation in the mouse genome, and what kinds of mechanisms underlie the complex rough coat phenotype? To answer these questions we used forward and reverse genetic approaches, and investigated the mutation both by *in vivo* and *in silico* approaches.

For identification of the mutation we first investigated in detail the phenotype of the rough coat mice and determined the phenotypic characteristics for the positional cloning analyses in Chapter 2. The mutated mice developed cyclic and progressive hair loss by the weaning age and ulcers appeared on the ventral skin of the neck (63%) over the first year. Histological examination of the skin showed enlargement of the glands that secrete a waxy substance called sebum that functions to lubricate the skin and hair, and also showed excessive proliferation of the cells (sebocytes) involved in sebum production. Histological dissection of the ulcers revealed typical signs of chronic wounds. Previously the linkage of the rough coat locus (*rc*) with two microsatellite markers *D9Mit162* at 49.954 Mb and *D9Mit104* at 65.953 Mb was described (Hayashi et al., 2004). Using two different mice strains and published as well as novel polymorphic microsatellites we identified the mapping interval of the *rc* locus and by sequence analyses we identified a point mutation in the open reading frame within a novel gene (ENSMUSG00000070305) located at 44.989~45.009 Mb. The mutation is a G→A transition in exon 3 of this gene, resulting in an Arg100→Gln (R100Q) substitution. EST analyses revealed that at least two different transcripts exist in mice. One longer transcript consists of 6 exons and encodes a 237 amino acid polypeptide and the shorter one consists of 2 exons and encodes a 96 amino acid polypeptide. The protein was predicted as a cell adhesion molecule with the highest homology to Myelin Protein Zero (MPZ), Myelin Protein Zero-like 1 (MPZL1), and Myelin Protein Zero-like 2 (MPZL2, also called Epithelial V-like Antigen, EVA1). We therefore named this gene *Mpzl3* (Myelin Protein Zero-like 3). All three proteins belong to a conserved protein family called Myelin Protein Zero. The major characteristic of this family is that all the members have immunoglobulin V type and myelin Po domains. We analyzed the expression pattern of *Mpzl3* both at the transcript level using Reverse transcriptase-PCR and at the protein level using Western blot analysis. We found that *Mpzl3* was expressed in all the investigated organs including brain, esophagus, heart, intestine, kidney, liver, lung, muscle, skin and spleen. Closer examination of the skin by immunofluorescence staining of skin sections using a

polyclonal antibody specific for extracellular domain of MPZL3 revealed that MPZL3 is expressed in the keratinocytes in the epidermis, hair follicles, and sebocytes in the sebaceous glands. By examining staining at high magnifications, it was clear that the staining was strong around the plasma membrane, consistent with the prediction of a transmembrane protein involved in cell adhesion. We also detected staining in the cytoplasm, but not in the nuclei.

To extend our knowledge of MPZL3, in Chapter 3 we addressed the question whether this protein exists only in mammals or is an older evolutionary conserved protein. We were also interested in its domain structure and its possible role in human. Therefore, we analyzed the MPZL3 orthologue proteins in the available public databases and we investigated the sequence and domain structure with web based bioinformatics tools. We identified orthologues of MPZL3 in other mammals with 79–99% identity at the protein level, and also found the protein to be conserved in other vertebrates, including chicken and zebrafish, with 30-55% amino acid identity. All the putative orthologue proteins possess the myelin Po protein signature and immunoglobulin V-Type domain. Based on EST counts in the UniGene database of NCBI, MPZL3 is expressed in wide variety of organs in human. Similar to our expression data in mouse, *MPZL3* expression was detected in human brain, esophagus, heart, kidney, liver, lung, muscle, spleen, and in addition in blood, colon, eye, lymph node, mammary gland, mouth, ovary, parathyroid, pharynx, pituitary gland, prostate, stomach, testis, uterus and vascular tissues. Furthermore, EMBL-EBI Array Express microarray database analysis showed *MPZL3* expression in dendritic cells, and in CD4 and CD8 central memory and effector T cells. The R100Q mutation we identified in rc mice is in the Ig-domain recognition loop that has known functions in T-cell receptors and cell adhesion. The homologous MPZ and MPZL2/EVA1 also play roles in cell adhesion and in the immune response. NCBI Entrez database analysis revealed multiple SNPs and mutations within the MPZL3 gene suggesting that humans with homozygous or compound heterozygous mutations may develop symptoms similar to the anomalies observed in rc mice. To investigate whether MPZL3 has a similar expression pattern in the skin as we observed in mice we performed Western blot analysis and detected a 54 kDa and a fainter 56 kDa band in cultured primary human dermal fibroblasts, which may result from dimerization and/or from posttranslational modifications of MPZL3 (predicted MW 25.98 kDa). Using indirect immunofluorescence we localized MPZL3 in similar regions of the human skin as in the mouse skin (Cao et al., 2007). It can be hypothesized that, based on our in silico data, MPZL3 might be involved in immune-mediated hereditary disorders presenting with hair loss, like alopecia area or alopecia universalis.

As the rough coat point mutation in *Mpzl3* already has strong effects, it is possible that the complete lack of *Mpzl3* function may lead to more drastic changes in the affected organ systems and result in a lethal phenotype in mice. Considering the time investment and the possible outcome of the mouse knock-out experiment, in Chapter 4 we decided first to investigate the *mpzl3* gene function in the zebrafish

embryo model, in which rapid knock-down studies are possible. First we investigated the zebrafish *mpzl3* sequence in the public databases, and analyzed the domain structure of the predicted protein with EBI-InterProScan web based software. We identified its evolutionary related counterparts by phylogenetic analysis using the neighbor joining method and found that closely related genes in zebrafish included *mpz*, *mpzl1*, *eva1*, and *scn4b*. By using quantitative reverse transcriptase PCR (qRT-PCR) we observed high *mpzl3* expression in the embryos within the first 5 hours post fertilization, likely derived from maternal RNA, but at later time points *mpzl3* expression became gradually reduced. We analyzed the localization of *mpzl3* expression by whole mount *in situ* hybridization and recognized specific expression in the head and in neuromasts of the lateral line of larvae at 5 days post fertilization. To investigate the role of *mpzl3* in zebrafish we synthesized *mpzl3* mRNA and injected this into embryos at the 1-2 cell stage. We observed a general retardation of development, bent and shortened tails or edema of the heart cavity in some embryos, but we also observed consistent anophthalmia. Some embryos showed aberrant development of both eyes and others showed asymmetric development of the two eyes, with one developing normally and the other being highly abnormal or completely undeveloped. Based on this unexpected phenotype, we decided to investigate the phenotype of the eye in rough coat mouse and we observed clear eye abnormalities in the mutant too (Figure1). Homozygous rough coat mice have been noted to be prone to develop an eye phenotype that could described in lay terms as "cloudy", or as a whitish haze. It may affect one eye, sometimes both eyes. It has not been investigated whether these mice are able to see with those affected eyes. The onset has not been seen before four months.

To analyze the effect of *mplz3* knock-down on development of zebrafish we used translation blocking morpholinos. The morphant fish obtained with two different morpholinos showed lower survival rates, immobility in response to touch stimuli, and cardiovascular system defects. They also showed a deficiency in the expression of recombination activating gene 1 (*rag1*) in the thymus, a gene essential for the development of the adaptive immune system. The morphant phenotypes could be rescued by co-injection of *mpzl3* mRNA. To identify the molecular pathways underlying the *mpzl3* morphant phenotype we performed a preliminary microarray analysis to analyze the gene expression pattern changes at 8 hours post fertilization, prior to the appearance of the phenotypic abnormalities. Based on gene ontology term analysis of the overlapping gene set showing altered expression with both morpholinos we identified several genes that play a role in developmental processes, including components of the Wnt and Notch signaling pathways. These microarray data provide useful leads for further investigation of *mpzl3* function in zebrafish and mouse models.

In conclusion, in this study the gene responsible for the rough coat phenotype in mouse was identified and shown to encode a member of the Myelin Protein Zero family that we named *Mpzl3*. The hypomorphic mutation in the rough coat mice was

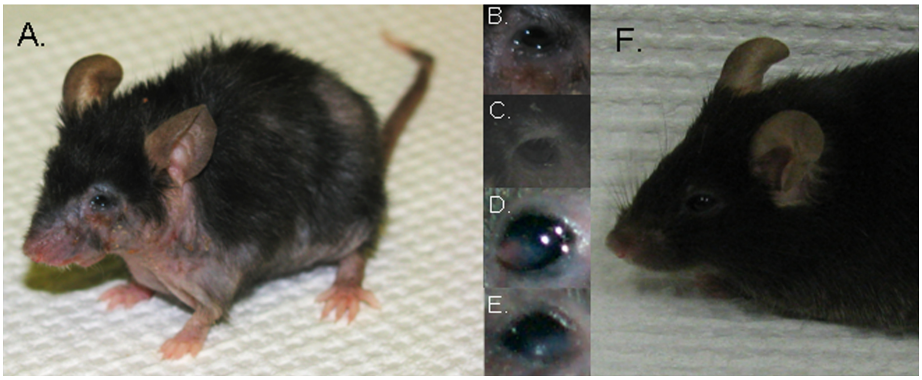


Figure 1. Eye phenotypes of rough coat mice. Figure **(A)** shows a 6 months old rc/rc male mouse with affected eyes. In Figure **(B)** and **(C)** it can be observed that both eyes are affected; however, the appearance of the abnormalities is different. Figure **(D)** and **(E)** shows the cloudiness of the eyes. Figure **(F)** shows a 6 months old rc/+ control male littermate.

shown to be due to an amino acid substitution in the conserved immunoglobulin domain of *Mpzl3* and resulted in severe skin abnormalities. We argue that mutations in the human orthologue of *Mpzl3* may be involved in immune-mediated heriditary hair loss diseases. Furthermore, we identified the *mpzl3* gene in zebrafish and we present here the first functional study of this gene. Our overexpression and loss-of-function experiments indicated a role for *mpzl3* in developmental processes during zebrafish embryogenesis, which based on microarray analysis might involve Wnt and Notch signaling. In future work, it will be of great interest to study the connection of *mpzl3* with these signaling pathways and the possible role of the gene in skin development, myelination and immune functions using zebrafish and mouse models

Bibliography

Al-Adhami MA K. Y. (1977) Ontogenesis of haematopoietic sites in Brachydanio rerio (hamilton-buchanan) teleostei. *Dev Growth Differ* **19**, 171–9.

Arnold I. and Watt F. M. (2001) c-Myc activation in transgenic mouse epidermis results in mobilization of stem cells and differentiation of their progeny. *Curr Biol* **11**, 558-68.

Barclay A. N. (2003) Membrane proteins with immunoglobulin-like domains--a master superfamily of interaction molecules. *Semin Immunol* **15**, 215-23.

Barreto V. M., Pan-Hammarstrom Q., Zhao Y., Hammarstrom L., Misulovin Z. and Nussenzweig M. C. (2005) AID from bony fish catalyzes class switch recombination. *J Exp Med* **202**, 733-8.

Berman J., Hsu K. and Look A. T. (2003) Zebrafish as a model organism for blood diseases. *Br J Haematol* **123**, 568-76.

Blanpain C., Lowry W. E., Pasolli H. A. and Fuchs E. (2006) Canonical notch signaling functions as a commitment switch in the epidermal lineage. *Genes Dev* **20**, 3022-35.

Blom N., Gammeltoft S. and Brunak S. (1999) Sequence and structure-based prediction of eukaryotic protein phosphorylation sites. *J Mol Biol* **294**, 1351-62.

Buljan M. and Bateman A. (2009) The evolution of protein domain families. *Biochem Soc Trans* **37**, 751-5.

Bushell K. M., Sollner C., Schuster-Boeckler B., Bateman A. and Wright G. J. (2008) Large-scale screening for novel low-affinity extracellular protein interactions. *Genome Res* **18**, 622-30.

Cagan R. L. and Ready D. F. (1989) Notch is required for successive cell decisions in the developing Drosophila retina. *Genes Dev* **3**, 1099-112.

Cao T., Racz P., Szauter K. M., Groma G., Nakamatsu G. Y., Fogelgren B., Pankotai E., He Q. P. and Csiszar K. (2007) Mutation in Mpzl3, a gene encoding a predicted the adhesion protein, in the rough coat (rc) mice with severe skin and hair abnormalities. *J Invest Dermatol* **127**, 1375-86.

Carenini S., Maurer M., Werner A., Blazyca H., Toyka K. V., Schmid C. D., Raivich G. and Martini R. (2001) The role of macrophages in demyelinating peripheral nervous system of mice heterozygously deficient in po. *J Cell Biol* **152**, 301-8.

Chapon F., Latour P., Diraison P., Schaeffer S. and Vandenberghe A. (1999) Axonal phenotype of Charcot-Marie-Tooth disease associated with a mutation in the myelin protein zero gene. *J Neurol Neurosurg Psychiatry* **66**, 779-82.

Chow R. L., Altmann C. R., Lang R. A. and Hemmati-Brivanlou A. (1999) Pax6 induces ectopic eyes in a vertebrate. *Development* **126**, 4213-22.

Corripio-Miyar Y., Bird S., Treasurer J. W. and Secombes C. J. (2007) RAG-1 and IgM genes, markers for early development of the immune system in the gadoid haddock, Melanogrammus aeglefinus, L. *Fish Shellfish Immunol* **23**, 71-85.

Crispin J. C. and Tsokos G. C. (2008) Novel molecular targets in the treatment of systemic lupus erythematosus. *Autoimmun Rev* **7**, 256-61.

Czerny T., Halder G., Kloter U., Souabni A., Gehring W. J. and Busslinger M. (1999) twin of eyeless, a second Pax-6 gene of Drosophila, acts upstream of eyeless in the control of eye development. *Mol Cell* **3**, 297-307.

Davies D. R., Sarma R., Labaw L. W., Silverton E., Segal D. and Terry W. D. (1971) X-ray diffraction and electron microscope studies on a crystalline human immunoglobulin. *Ann N Y Acad Sci* **190**, 122-9.

De Jonghe P., Timmerman V., Ceuterick C., Nelis E., De Vriendt E., Lofgren A., Vercruyssen A., Verellen C., Van Maldergem L., Martin J. J. and Van Broeckhoven C. (1999) The Thr124Met mutation in the peripheral myelin protein zero (MPZ) gene is associated with a clinically distinct Charcot-Marie-Tooth phenotype. *Brain* **122 (Pt 2)**, 281-90.

Demehri S. and Kopan R. (2009) Notch signaling in bulge stem cells is not required for selection of hair follicle fate. *Development* **136**, 891-6.

DeMonte L., Porcellini S., Tafi E., Sheridan J., Gordon J., Depreter M., Blair N., Panigada M., Sanvito F., Merati B., Albientz A., Barthlott T., Ozmen L., Blackburn C. C. and Guttinger M. (2007) EVA regulates thymic stromal organisation and early thymocyte development. *Biochem Biophys Res Commun* **356**, 334-40.

Dickie M. (1966) Rough coat. *Mouse News Letter* **34**.

Eicher EM F., S., Reynolds, S. (1977) Rough coat on Chromosome 9. *Mouse News Letter* **56**.

Fernandez-Gonzalez A., La Spada A. R., Treadaway J., Higdon J. C., Harris B. S., Sidman R. L., Morgan J. I. and Zuo J. (2002) Purkinje cell degeneration (pcd) phenotypes caused by mutations in the axotomy-induced gene, Nna1. *Science* **295**, 1904-6.

Fraser J. S., Yu Z., Maxwell K. L. and Davidson A. R. (2006) Ig-like domains on bacteriophages: a tale of promiscuity and deceit. *J Mol Biol* **359**, 496-507.

Freyschmidt-Paul P., Hoffmann R., Levine E., Sundberg J. P., Happle R. and McElwee K. J. (2001) Current and potential agents for the treatment of alopecia areata. *Curr Pharm Des* **7**, 213-30.

Frye M., Gardner C., Li E. R., Arnold I. and Watt F. M. (2003) Evidence that Myc activation depletes the epidermal stem cell compartment by modulating adhesive interactions with the local microenvironment. *Development* **130**, 2793-808.

Gage P. J. and Zacharias A. L. (2009) Signaling "cross-talk" is integrated by transcription factors in the development of the anterior segment in the eye. *Dev Dyn* **238**, 2149-62.
Gaiano N. and Fishell G. (2002) The role of notch in promoting glial and neural stem cell fates. *Annu Rev Neurosci* **25**, 471-90.
Gilhar A. and Kalish R. S. (2006) Alopecia areata: a tissue specific autoimmune disease of the hair follicle. *Autoimmun Rev* **5**, 64-9.
Gilhar A., Kam Y., Assy B. and Kalish R. S. (2005) Alopecia areata induced in C3H/HeJ mice by interferon-gamma: evidence for loss of immune privilege. *J Invest Dermatol* **124**, 288-9.
Ginalski K., Elofsson A., Fischer D. and Rychlewski L. (2003) 3D-Jury: a simple approach to improve protein structure predictions. *Bioinformatics* **19**, 1015-8.
Gompel N., Cubedo N., Thisse C., Thisse B., Dambly-Chaudiere C. and Ghysen A. (2001) Pattern formation in the lateral line of zebrafish. *Mech Dev* **105**, 69-77.
Grillitsch S., Medgyesy N., Schwerte T. and Pelster B. (2005) The influence of environmental P(O(2)) on hemoglobin oxygen saturation in developing zebrafish Danio rerio. *J Exp Biol* **208**, 309-16.
Guex N. a. P., M.C. (1997) SM2 SWISS-MODEL and the Swiss-PdbViewer: An environment for comparative protein modeling. *Electrophoresis* **18, 2714-2723**.
Gupta R J. E., Brunak S. (2004) Prediction of N-glycosylation sites in human proteins. *In preparation*.
Guttinger M., Sutti F., Panigada M., Porcellini S., Merati B., Mariani M., Teesalu T., Consalez G. G. and Grassi F. (1998) Epithelial V-like antigen (EVA), a novel member of the immunoglobulin superfamily, expressed in embryonic epithelia with a potential role as homotypic adhesion molecule in thymus histogenesis. *J Cell Biol* **141**, 1061-71.
Halaby D. M. and Mornon J. P. (1998) The immunoglobulin superfamily: an insight on its tissular, species, and functional diversity. *J Mol Evol* **46**, 389-400.
Harpaz Y. and Chothia C. (1994) Many of the immunoglobulin superfamily domains in cell adhesion molecules and surface receptors belong to a new structural set which is close to that containing variable domains. *J Mol Biol* **238**, 528-39.
Hawkins R. D., Bashiardes S., Powder K. E., Sajan S. A., Bhonagiri V., Alvarado D. M., Speck J., Warchol M. E. and Lovett M. (2007) Large scale gene expression profiles of regenerating inner ear sensory epithelia. *PLoS One* **2**, e525.
Hayashi K., Cao T., Passmore H., Jourdan-Le Saux C., Fogelgren B., Khan S., Hornstra I., Kim Y., Hayashi M. and Csiszar K. (2004) Progressive hair loss and myocardial degeneration in rough coat mice: reduced lysyl oxidase-like (LOXL) in the skin and heart. *J Invest Dermatol* **123**, 864-71.
Horiguchi M., Inoue T., Ohbayashi T., Hirai M., Noda K., Marmorstein L. Y., Yabe D., Takagi K., Akama T. O., Kita T., Kimura T. and Nakamura T. (2009) Fibulin-4 conducts proper elastogenesis via interaction with cross-linking enzyme lysyl oxidase. *Proc Natl Acad Sci U S A* **106**, 19029-34.
Hutchinson E. G. and Thornton J. M. (1993) The Greek key motif: extraction, classification and analysis. *Protein Eng* **6**, 233-45.
Jiang Y. J., Brand M., Heisenberg C. P., Beuchle D., Furutani-Seiki M., Kelsh R. N., Warga R. M., Granato M., Haffter P., Hammerschmidt M., Kane D. A., Mullins M. C., Odenthal J., van Eeden F. J. and Nusslein-Volhard C. (1996) Mutations affecting neurogenesis and brain morphology in the zebrafish, Danio rerio. *Development* **123**, 205-16.
Julenius K., Molgaard A., Gupta R. and Brunak S. (2005) Prediction, conservation analysis, and structural characterization of mammalian mucin-type O-glycosylation sites. *Glycobiology* **15**, 153-64.
Katoh M. (2008) WNT signaling in stem cell biology and regenerative medicine. *Curr Drug Targets* **9**, 565-70.
Kazakova N., Li H., Mora A., Jessen K. R., Mirsky R., Richardson W. D. and Smith H. K. (2006) A screen for mutations in zebrafish that affect myelin gene expression in Schwann cells and oligodendrocytes. *Dev Biol* **297**, 1-13.
Kerstetter A. E., Azodi E., Marrs J. A. and Liu Q. (2004) Cadherin-2 function in the cranial ganglia and lateral line system of developing zebrafish. *Dev Dyn* **230**, 137-43.
Korhonen J., Partanen J., Armstrong E., Vaahtokari A., Elenius K., Jalkanen M. and Alitalo K. (1992) Enhanced expression of the tie receptor tyrosine kinase in endothelial cells during neovascularization. *Blood* **80**, 2548-55.
Krogh A., Larsson B., von Heijne G. and Sonnhammer E. L. (2001) Predicting transmembrane protein topology with a hidden Markov model: application to complete genomes. *J Mol Biol* **305**, 567-80.
Kuchler A. M., Gjini E., Peterson-Maduro J., Cancilla B., Wolburg H. and Schulte-Merker S. (2006) Development of the zebrafish lymphatic system requires VEGFC signaling. *Curr Biol* **16**, 1244-8.
Lathia J. D., Mattson M. P. and Cheng A. (2008) Notch: from neural development to neurological disorders. *J Neurochem* **107**, 1471-81.
Lee J., Basak J. M., Demehri S. and Kopan R. (2007) Bi-compartmental communication contributes to the opposite proliferative behavior of Notch1-deficient hair follicle and epidermal keratinocytes. *Development* **134**, 2795-806.
Letunic I., Goodstadt L., Dickens N. J., Doerks T., Schultz J., Mott R., Ciccarelli F., Copley R. R., Ponting C. P. and Bork P. (2002) Recent improvements to the SMART domain-based sequence annotation resource. *Nucleic Acids Res* **30**, 242-4.

Leyns L., Bouwmeester T., Kim S. H., Piccolo S. and De Robertis E. M. (1997) Frzb-1 is a secreted antagonist of Wnt signaling expressed in the Spemann organizer. *Cell* **88**, 747-56.

Loosli F., Winkler S. and Wittbrodt J. (1999) Six3 overexpression initiates the formation of ectopic retina. *Genes Dev* **13**, 649-54.

Ma A., Koka R. and Burkett P. (2006) Diverse functions of IL-2, IL-15, and IL-7 in lymphoid homeostasis. *Annu Rev Immunol* **24**, 657-79.

Ma E. Y. and Raible D. W. (2009) Signaling pathways regulating zebrafish lateral line development. *Curr Biol* **19**, R381-6.

Manly K. F., Cudmore R. H., Jr. and Meer J. M. (2001) Map Manager QTX, cross-platform software for genetic mapping. *Mamm Genome* **12**, 930-2.

Martinez-Mir A., Zlotogorski A., Gordon D., Petukhova L., Mo J., Gilliam T. C., Londono D., Haynes C., Ott J., Hordinsky M., Nanova K., Norris D., Price V., Duvic M. and Christiano A. M. (2007) Genomewide scan for linkage reveals evidence of several susceptibility loci for alopecia areata. *Am J Hum Genet* **80**, 316-28.

Maurer M., Kobsar I., Berghoff M., Schmid C. D., Carenini S. and Martini R. (2002) Role of immune cells in animal models for inherited neuropathies: facts and visions. *J Anat* **200**, 405-14.

McDonagh A. J. and Tazi-Ahnini R. (2002) Epidemiology and genetics of alopecia areata. *Clin Exp Dermatol* **27**, 405-9.

McMillan J. R. and Shimizu H. (2001) Desmosomes: structure and function in normal and diseased epidermis. *J Dermatol* **28**, 291-8.

Meeker N. D. and Trede N. S. (2008) Immunology and zebrafish: spawning new models of human disease. *Dev Comp Immunol* **32**, 745-57.

Metaserver1. http://bioinfo.pl/meta/.

Miller J. R. (2002) The Wnts. *Genome Biol* **3**, REVIEWS3001.

Misu K., Yoshihara T., Shikama Y., Awaki E., Yamamoto M., Hattori N., Hirayama M., Takegami T., Nakashima K. and Sobue G. (2000) An axonal form of Charcot-Marie-Tooth disease showing distinctive features in association with mutations in the peripheral myelin protein zero gene (Thr124Met or Asp75Val). *J Neurol Neurosurg Psychiatry* **69**, 806-11.

Moog-Lutz C., Cave-Riant F., Guibal F. C., Breau M. A., Di Gioia Y., Couraud P. O., Cayre Y. E., Bourdoulous S. and Lutz P. G. (2003) JAML, a novel protein with characteristics of a junctional adhesion molecule, is induced during differentiation of myeloid leukemia cells. *Blood* **102**, 3371-8.

Mulroy T., McMahon J. A., Burakoff S. J., McMahon A. P. and Sen J. (2002) Wnt-1 and Wnt-4 regulate thymic cellularity. *Eur J Immunol* **32**, 967-71.

Niehrs C. (1999) Head in the WNT: the molecular nature of Spemann's head organizer. *Trends Genet* **15**, 314-9.

Park Y. G., Hayasaka S., Takagishi Y., Inouye M., Okumoto M. and Oda S. (2001) Histological characteristics of the pelage skin of rough fur mice (C3H/HeJ- ruf/ruf). *Exp Anim* **50**, 179-82.

Pelster B. and Burggren W. W. (1996) Disruption of hemoglobin oxygen transport does not impact oxygen-dependent physiological processes in developing embryos of zebra fish (Danio rerio). *Circ Res* **79**, 358-62.

Peri S. e. a. (2003) Development of human protein reference database as an initial platform for approaching systems biology in humans. *Genome Research* **13**, 2363-2371.

Poljak R. J., Amzel L. M., Avey H. P., Chen B. L., Phizackerley R. P. and Saul F. (1973) Three-dimensional structure of the Fab' fragment of a human immunoglobulin at 2,8-A resolution. *Proc Natl Acad Sci U S A* **70**, 3305-10.

Racz P., Mink M., Ordas A., Cao T., Szalma S., Szauter K. M. and Csiszar K. (2009) The human orthologue of murine Mpzl3 with predicted adhesive and immune functions is a potential candidate gene for immune-related hereditary hair loss. *Exp Dermatol* **18**, 261-3.

Rebagliati M. R., Toyama R., Haffter P. and Dawid I. B. (1998) cyclops encodes a nodal-related factor involved in midline signaling. *Proc Natl Acad Sci U S A* **95**, 9932-7.

Richardson J. S. (1981) The anatomy and taxonomy of protein structure. *Adv Protein Chem* **34**, 167-339.

Ruvinsky I., Chertkov O., Borue X. V., Agulnik S. I., Gibson-Brown J. J., Lyle S. R. and Silver L. M. (2002) Genetics analysis of mouse mutations Abnormal feet and tail and rough coat, which cause developmental abnormalities and alopecia. *Mamm Genome* **13**, 675-9.

Schmid C. D., Stienekemeier M., Oehen S., Bootz F., Zielasek J., Gold R., Toyka K. V., Schachner M. and Martini R. (2000) Immune deficiency in mouse models for inherited peripheral neuropathies leads to improved myelin maintenance. *J Neurosci* **20**, 729-35.

Searle AG S. R. (1957) "Matted", a new hair mutant in the house mouse: genetics and morphology. *J Embryol Exp Morphol* **5**.

Setoguchi R., Hori S., Takahashi T. and Sakaguchi S. (2005) Homeostatic maintenance of natural Foxp3(+) CD25(+) CD4(+) regulatory T cells by interleukin (IL)-2 and induction of autoimmune disease by IL-2 neutralization. *J Exp Med* **201**, 723-35.

Shy M. E., Arroyo E., Sladky J., Menichella D., Jiang H., Xu W., Kamholz J. and Scherer S. S. (1997) Heterozygous Po knockout mice develop a peripheral neuropathy that resembles chronic inflammatory demyelinating polyneuropathy (CIDP). *J Neuropathol Exp Neurol* **56**, 811-21.

Silver S. J. and Rebay I. (2005) Signaling circuitries in development: insights from the retinal determination gene

network. *Development* **132**, 3-13.
Smith D. K. and Xue H. (1997) Sequence profiles of immunoglobulin and immunoglobulin-like domains. *J Mol Biol* **274**, 530-45.
Stevens R., Goble C. A. and Bechhofer S. (2000) Ontology-based knowledge representation for bioinformatics. *Brief Bioinform* **1**, 398-414.
Suzuki K., Hu D., Bustos T., Zlotogora J., Richieri-Costa A., Helms J. A. and Spritz R. A. (2000) Mutations of PVRL1, encoding a cell-cell adhesion molecule/herpesvirus receptor, in cleft lip/palate-ectodermal dysplasia. *Nat Genet* **25**, 427-30.
Sweet HO O. S., Taylor BA, Rowe L, Davisson MT, Cook S et al. (1990) Rough fur (ruf). *Mouse Genome* **86**, 236-237.
Talora C., Campese A. F., Bellavia D., Felli M. P., Vacca A., Gulino A. and Screpanti I. (2008) Notch signaling and diseases: an evolutionary journey from a simple beginning to complex outcomes. *Biochim Biophys Acta* **1782**, 489-97.
Teichmann S. A. and Chothia C. (2000) Immunoglobulin superfamily proteins in Caenorhabditis elegans. *J Mol Biol* **296**, 1367-83.
TMHMM. http://www.cbs.dtu.dk/services/TMHMM/.
Traver D., Herbomel P., Patton E. E., Murphey R. D., Yoder J. A., Litman G. W., Catic A., Amemiya C. T., Zon L. I. and Trede N. S. (2003) The zebrafish as a model organism to study development of the immune system. *Adv Immunol* **81**, 253-330.
Tydell C. C., David-Fung E. S., Moore J. E., Rowen L., Taghon T. and Rothenberg E. V. (2007) Molecular dissection of prethymic progenitor entry into the T lymphocyte developmental pathway. *J Immunol* **179**, 421-38.
Varas A., Hager-Theodorides A. L., Sacedon R., Vicente A., Zapata A. G. and Crompton T. (2003) The role of morphogens in T-cell development. *Trends Immunol* **24**, 197-206.
Waikel R. L., Kawachi Y., Waikel P. A., Wang X. J. and Roop D. R. (2001) Deregulated expression of c-Myc depletes epidermal stem cells. *Nat Genet* **28**, 165-8.
Wakae K., Magor B. G., Saunders H., Nagaoka H., Kawamura A., Kinoshita K., Honjo T. and Muramatsu M. (2006) Evolution of class switch recombination function in fish activation-induced cytidine deaminase, AID. *Int Immunol* **18**, 41-7.
Wang S., Krinks M., Lin K., Luyten F. P. and Moos M., Jr. (1997) Frzb, a secreted protein expressed in the Spemann organizer, binds and inhibits Wnt-8. *Cell* **88**, 757-66.
Wehrli M. and Tomlinson A. (1998) Independent regulation of anterior/posterior and equatorial/polar polarity in the Drosophila eye; evidence for the involvement of Wnt signaling in the equatorial/polar axis. *Development* **125**, 1421-32.
Willett C. E., Cherry J. J. and Steiner L. A. (1997) Characterization and expression of the recombination activating genes (rag1 and rag2) of zebrafish. *Immunogenetics* **45**, 394-404.
Willett C. E., Cortes A., Zuasti A. and Zapata A. G. (1999) Early hematopoiesis and developing lymphoid organs in the zebrafish. *Dev Dyn* **214**, 323-36.
Wilson A. L., Shen Y. C., Babb-Clendenon S. G., Rostedt J., Liu B., Barald K. F., Marrs J. A. and Liu Q. (2007) Cadherin-4 plays a role in the development of zebrafish cranial ganglia and lateral line system. *Dev Dyn* **236**, 893-902.
Xue Y., Zhou F., Fu C., Xu Y. and Yao X. (2006) SUMOsp: a web server for sumoylation site prediction. *Nucleic Acids Res* **34**, W254-7.
Yaniv K., Isogai S., Castranova D., Dye L., Hitomi J. and Weinstein B. M. (2006) Live imaging of lymphatic development in the zebrafish. *Nat Med* **12**, 711-6.
Yoshinari N., Ishida T., Kudo A. and Kawakami A. (2009) Gene expression and functional analysis of zebrafish larval fin fold regeneration. *Dev Biol* **325**, 71-81.
Yu M., Kissling S., Freyschmidt-Paul P., Hoffmann R., Shapiro J. and McElwee K. J. (2008) Interleukin-6 cytokine family member oncostatin M is a hair-follicle-expressed factor with hair growth inhibitory properties. *Exp Dermatol* **17**, 12-9.

Samenvatting

Het zogenoemde "*rough coat*"-fenotype (*rc*) van de muis is ontstaan door een spontane mutatie in de veelgebruikte laboratoriumstam C57BL/6J. De mutatie werd in 1966 ontdekt (Dickie, 1966) en in 1977 gelokaliseerd op chromosoom 9 (Eicher and Reynolds, 1977). In 2004 richtte de groep van Dr. Csiszar zich op de identificatie van het gen dat verantwoordelijk is voor het *rc*-fenotype. Aanvankelijk hadden zij de hypothese dat het gemuteerde gen een allel zou zijn van het *loxl*-gen (*Lysyl oxidase like*), dat codeert voor een component van de extracellulaire matrix (Hayashi et al., 2004). Het bleek echter dat *rc* onafhankelijk was van *loxl*. Hierna bleef de interesse in de identificatie van de *rc*-mutatie bestaan. Het belangrijkste doel van het onderzoek beschreven in dit proefschrift was het beantwoorden van twee vragen rond the *rc*-mutatie: wat is de exacte locatie van de mutatie in het genoom van de muis en welke mechanismen liggen ten grondslag aan het complexe *rc*-fenotype? Om deze vragen te beantwoorden hebben wij verschillende genetische strategieën gebruikt om het gemuteerde gen te identificeren en de functie ervan te onderzoeken. Hierbij hebben gebruik gemaakt van twee modelorganismen, de muis en de zebravis. Naast de "*in vivo*"-experimenten in deze modelorganismen werden tevens "*in silico*"-studies uitgevoerd om de functie van het overeenkomstige gen in de mens te voorspellen.

Om de *rc*-mutatie te identificeren hebben wij eerst in detail het fenotype van de "rough coat"-muizen onderzocht en de kenmerken vastgesteld op grond waarvan de positionele klonering van het gemuteerde gen kon worden uitgevoerd. Dit onderzoek is beschreven in hoofdstuk 2. Jonge muizen met de *rc*-mutatie ontwikkelden een cyclische en progressieve haaruitval en gedurende het eerste jaar ontstonden er bij 63% van de dieren zweren op de huid aan de onderzijde van de nek. Histologisch onderzoek van de huid liet zien dat er een vergroting was van de klieren die een vettige substantie (sebum) uitscheiden dat dient om de huid en het haar te smeren. Tevens was het aantal cellen dat betrokken is bij de sebum-productie (sebocyten) sterk verhoogd. De zweren in de huid vertoonden typische kenmerken van chronische wonden. Eerder was beschreven dat het *rc*-locus genetisch is gekoppeld met twee microsatelliet-markers, *D9Mit162* op 49.954 Mb en *D9Mit104* op 65.953 Mb (Hayashi et al., 2004). Door gebruik te maken van twee verschillende muizenstammen en gepubliceerde zowel als nieuwe microsatelliet-polymorfismen konden we de chromosomale positie van het *rc*-locus in kaart brengen. Vervolgens werd door sequentieanalyse een puntmutatie gevonden in de coderende regio van een nieuw gen (ENSMUSG00000070305) gelegen op 44.989~45.009 Mb. De mutatie is een G→A-transitie in exon 3 van dit gen, resulterend in een Arg100→Gln-substitutie (R100Q). Uit databaseanalyses bleek dat er in de muis minstens twee verschillende transcripten bestaan van dit gen. Het langste transcript bestaat uit 6 exonen en codeert voor een polypeptide van 237 aminozuren, terwijl het kortere transcript uit 2 exonen bestaat en codeert voor een polypeptide van 96 aminozuren. De voorspelde functie van het eiwit is dat het een celadhesiemolecuul betreft, homoloog met Myelin

Protein Zero (MPZ), Myelin Protein Zero-like 1 (MPZL1) en Myelin Protein Zero-like 2 (MPZL2, ook bekend als EVA1 voor Epithelial V-like Antigen 1). Wij hebben het nieuwe gen daarom *Mpzl3* (Myelin Protein Zero-like 3) genoemd. MPZ, MPZL1, MPZL2 en MPZL3 behoren allevier tot een geconserveerde eiwitfamilie, genaamd Myelin Protein Zero. Het belangrijkste kenmerk van deze eiwitfamilie is dat alle leden V-type-immunoglobulinedomeinen en myeline-P0-domeinen bevatten. Wij hebben het expressiepatroon van *Mpzl3* geanalyseerd zowel op transcriptniveau door middel van reverse-transcriptase-PCR als op eiwitniveau door middel van Western-blot-analyse. Hieruit bleek dat *Mpzl3* tot expressie komt in alle onderzochte weefsels en organen, waaronder de hersenen, de slokdarm, de darm, de nier, de lever, de milt, het hart, de longen, het spierweefsel en de huid. Coupes van huidweefsel werden nader onderzocht door middel van immunofluorescentie-analyse met een polyclonaal antilichaam specifiek voor het extracellulaire domein van het MPZL3-eiwit. Hiermee kon het MPZL3-eiwit aangetoond worden in de keratinocyten van de huidepidermis, in de haarwortels en in de sebocyten van de sebum-producerende klieren. Bij hoge vergroting was te zien dat de kleuring het sterkste was rond de plasmamembraan van de cellen. Dit is in overeenstemming met de voorspelde functie van het eiwit als een transmembraaneiwit betrokken bij celadhesie. Er was ook kleuring in het cytoplasma aantoonbaar, maar niet in de celkern.

Om meer kennis te vergaren over MPZL3 hebben wij in hoofdstuk 3 de vraag onderzocht of het eiwit alleen in zoogdieren bestaat of dat het een ouder, evolutionair geconserveerd eiwit betreft. Ook waren wij geïnteresseerd in de domeinstructuur van het eiwit en de mogelijke functie in de mens. Daarom hebben wij de beschikbare publieke databasen doorzocht om homologe eiwitten te identificeren en hebben webgebaseerde bioinformaticasoftware toegepast om de domeinstructuur te analyseren. In andere zoogdieren vonden wij eiwitten die op aminozuurniveau 89-96% identiek waren aan MPZL3 van de muis. Ook vonden wij het eiwit in andere gewervelde diersoorten, waaronder de zebravis en de kip, met 30 % identiteit op aminozuurniveau. Alle voorspelde orthologe eiwitten van MPZL3 bevatten de myeline-P0-signatuur en de V-type-immunoglobulinedomeinen. Gebaseerd op transcriptsequenties in de UniGene-database van het NCBI komt het humane *MPZL3*-gen tot expressie in diverse organen van de mens. In overeenstemming met onze expressiedata van de muis, zijn humane *MPZL3*-transcripten aantoonbaar in hersenen, slokdarm, hart, nier, lever, long, spier en milt. Tevens is er expressie gedetecteerd in bloed en vaatweefsel, in oog, mond en keelholte en het maagdarmkanaal, in lymfeklieren, melkklieren, bijschildklier en hypofyse, en in prostaat en testis, alsmede uterus en ovarium. Uit analyse van de microarray-databank van het EMBL-EBI bleek tevens dat *MPZL3* tot expressie komt in dendritische cellen van het humane immuunsysteem, evenals in CD4- en CD8-positieve geheugen- en effector-T-cellen. De R100Q-mutatie die wij geïdentificeerd hadden in de "*rough coat*"-muizen is gelokaliseerd in een regio ("recognition loop") van het immunoglobulinedomein met bekende functies in T-cell receptoren en bij celadhesie. De homologe MPZ- en MPZL2/EVA1-eiwitten

spelen ook een rol in celadhesie en in de immuunrespons. Bij analyse van de NCBI-database werden verschillende nucleotide-polymorfismen en mutaties in het humane *MPZL3*-gen gevonden, wat erop zou kunnen wijzen dat mensen met homozygote of samengestelde heterozygote mutaties symptomen zouden kunnen ontwikkelen die lijken op de afwijkingen in muizen met de *rc*-mutatie. Om te onderzoeken of het humane *MPZL3*-gen een vergelijkbaar expressiepatroon vertoont in de huid als het overeenkomstige gen in de muis hebben wij een Western-blot-analyse uitgevoerd. In extracten van gekweekte humane huidcellen (een cultuur van primaire fibroblasten) kon een eiwitband met een grootte van 54 kDa aangetoond worden en een zwakkere band van 56 kDa. Deze banden kunnen het resultaat zijn van dimeervorming en/of van post-translationele modificatie van MPZL3, dat een molecuulgewicht heeft van 25.98 kDa. Met behulp van indirecte immunofluorescentie konden wij het MPZL3-eiwit lokaliseren in vergelijkbare regionen van de humane huid als in de huid van de muis (Cao et al., 2007). Op grond van onze *in silico*-studie kan de hypothese gemaakt worden dat MPZL3 betrokken zou kunnen zijn bij immuun-gemedieerde erfelijke afwijkingen die gepaard gaan met haaruitval, zoals de ziekten alopecia area of alopecia universalis.

Omdat de *rc*-puntmutatie in *Mpzl3* al ernstige effecten heeft, is het waarschijnlijk dat een volledig verlies van de functie van dit gen (knock-out) zou kunnen leiden tot nog ernstiger afwijkingen en tot een letaal fenotype in de muis. Gezien de tijdsinvestering en de mogelijke uitkomst van een knock-out-experiment in de muis, hebben wij in hoofdstuk 4 besloten om eerst de functie van het *mpzl3*-gen te bestuderen in het zebravisembryomodel, waarin snelle knock-down-studies mogelijk zijn. Eerst hebben wij de sequentie van het *mpzl3*-gen van de zebravis onderzocht in de publieke databases en de domeinstructuur van het gecodeerde eiwit geanalyseerd met het webgebaseerde programma EBI-InterProScan. Door middel van fylogenetische analyse met de "neighbor joining"-methode hebben wij de evolutionaire verwantschappen van *mpzl3* met andere genen in het zebravisgenoom bepaald, waaruit bleek dat *mpz*, *mpzl1*, *eva1* en *scn4b* het meest nauw verwant zijn aan *mpzl3*. Met behulp van kwantitatieve reverse-transcriptase-PCR (qRT-PCR) kon een hoge expressie van *mpzl3* in embryo's worden aangetoond binnen de eerste 5 uur na fertilisatie (waarschijnlijk afkomstig van maternaal RNA), maar tijdens latere ontwikkelingsstadia nam het expressieniveau van *mpzl3* geleidelijk af. Vervolgens hebben wij het expressiepatroon van *mpzl3* verder geanalyseerd door middel van *in situ*-hybridisatie van zebravisembryo's en -larven. Hierbij werd specifieke expressie waargenomen in de kop en in de neuromastcellen van het zijlijnorgaan van zebravislarven op de leeftijd van 5 dagen. Om de rol van *mpzl3* tijdens de zebravisontwikkeling te onderzoeken hebben wij *mpzl3*-mRNA gesynthetiseerd en dit geïnjecteerd in embryo's van het 1- tot 2-celstadium. Wij observeerden een algemene vertraging van de ontwikkeling en een gebogen en verkorte staart of hartoedeem in sommige embryo's. Echter, het meest opvallende en consistente fenotype was de afwezigheid van ogen (anophthalmia). Sommige embryo's vertoonden een afwijkende ontwikkeling van beide ogen en

bij andere ondergingen de ogen een asymmetrische ontwikkeling, waarbij één oog zich normaal ontwikkelde terwijl het andere sterk misvormd of volledig onderontwikkeld was. Vanwege dit onverwachte fenotype besloten wij om het fenotype van de ogen van de muizen met de *rc*-mutatie te inspecteren en vonden hier ook duidelijke oogafwijkingen. Homozygote *rc*-muizen ontwikkelen vaak een oogfenotype dat in lekentermen omschreven zou kunnen worden als troebel of als een witachtige waas over het oog. Soms is één oog aangedaan en soms beide. Het is nog niet onderzocht of de muizen zicht hebben in deze ogen. De aandoening treedt niet eerder op dan na vier maanden.

Om het effect van uitschakeling van de *mpzl3*-genfunctie op de ontwikkeling van zebravisembryo's te onderzoeken hebben wij gebruikt gemaakt van morfolino's, waarmee specifiek de translatie van het *mpzl3*-mRNA geblokkeerd kan worden (knock-down-techniek). De knock-down-embryo's verkregen met twee verschillende morfolino's vertoonden een verminderde overleving, waren immobiel in reactie op een aanrakingsstimulus en vertoonden afwijkingen in het hart- en vaatstelsel. Tevens vertoonden deze embryo's een deficiëntie in de expressie van het *rag1*-gen (recombination activating gene 1, een essentieel gen voor het immuunsysteem) in de thymus. Als controle-experiment kon het knock-down-fenotype opgeheven worden door *mpzl3*-mRNA te injecteren samen met de morfolino. Om inzicht te krijgen in de moleculaire processen die ten grondslag liggen aan het knock-down-fenotype van *mpzl3* hebben wij een preliminaire microarrayanalyse uitgevoerd om de veranderingen in het genexpressiepatroon te onderzoeken op 8 uur na fertilisatie, een tijdspunt vóór de zichtbaarheid van de fenotypische afwijkingen. De set van genen die veranderde expressie vertoonde bij beide morfolino's bevatte verschillende genen die een rol spelen bij ontwikkelingsprocessen, waaronder componenten van de Wnt- en Notch-signaalroutes. Deze microarraydata hebben bruikbare aanknopingspunten opgeleverd voor verder onderzoek naar de functie van *mpzl3* in de zebravis- en muismodelsystemen.

Samenvattend heeft deze studie geleid tot de identificatie van het gen dat verantwoordelijk is voor het "*rough coat*"-fenotype in de muis en heeft aangetoond dat dit gen codeert voor een eiwit van de Myelin Protein Zero-familie, dat wij MPZL3 genoemd hebben. De hypomorfe mutatie in de "*rough coat*"-muizen bleek veroorzaakt te zijn door een aminozuursubstitutie in het geconserveerde immunoglobulinedomein van MPZL3 en resulteerde in verschillende huidafwijkingen. Wij betogen dat mutaties in de humane ortholoog van MPZL3 betrokken kunnen zijn bij immuungemedieerde erfelijke ziekten die gepaard gaan met haaruitval. Daarnaast hebben wij het *mpzl3*-gen in zebravis aangetoond en beschrijven hier de eerste functionele studie van dit gen. Onze overexpressie- en knock-down-experimenten wijzen op een rol voor *mpzl3* bij ontwikkelingsprocessen tijdens de zebravisembryogenese, waarbij, gebaseerd op microarrayanalyse, de Wnt- en Notch signaalroutes mogelijk betrokken zijn. In toekomstige studies zal het zeer interessant zijn om het verband tussen *mpzl3* en deze signaalroutes verder te onderzoeken en om de rol van het gen

bij huidontwikkeling, bij de vorming van myelinescheden en bij het immuunsysteem verder te ontrafelen met gebruik van zebravis- en muis-modellen.

Összefoglalás

A C57BL/6J egértörzsben spontán mutációval keletkezett, ún. rough coat (*rc*) egereket 1966- ban a Main állambeli JAX laboratóriumban azonosították, majd a mutációt 1977-ben a 9-es kromoszómára térképezték közel az *Mpi1*-es génhez. Az ezt követő évtizedekben a mutáns törzs tudományos érdeklődés perifériájára került egészen 2004-ig, amikor is Prof. Dr. Csiszár Katalin a lysyl oxidase (*lox*) vizsgálata során célul tűzte ki, hogy azonosítja a rough coat fenotípus kóroki génjét, ami allélikus lehet a *lox*-al. Bár a két gén között allélizmus nem volt kimutatható, a tudományos kíváncsiság a rough coat törzzsel kapcsolatban továbbra is fennmaradt. E disszertációban olvasható tanulmánynak a célja, hogy azonosítsa a rough coat egerek megjelenésének genotipikus hátterét, valamint, hogy a mutáción keresztül ment gén molekuláris funkciójára fényt derítsen.

A tanulmány 2. fejezetének az elején azokat a fenotipikus jegyeket határoztuk meg, melyeket a pozícionális klónozás során követni kívántunk, majd a fejezet további részében a mutáció azonosításának lépéseit tárgyaltuk. A mutáns egerekre autoszómális recesszív öröklésmenet jellemző. Születéskor a mutáns egyedeket alomtársaiktól megkülönböztetni nem lehet, de az elválasztási korban már jól megmutatkozik a nevet is adó, borzolt szőrzettel jellemzhető szőrhullásos fenotípus, mely az idő múlásával progresszivitást mutat. Ultrastruktúrális vizsgálatok megmutatták, hogy a szőrhullás hátterében nem a szőrszáll megváltozott struktúrája áll, hanem feltételezhetően a szőr növekedési ciklusában bekövetkezett molekuláris változás. A bőr szerkezetének hisztopatológás analízise során hypertrophikus faggyúmirigy sejteket azonosítottunk, melyekre a vad típusú alomtársaikkal összehasonlítva erőteljes faggyútermelés volt a jellemző. Mindemellett az egerek szignifikáns hányadánál (63%) egy éves kor után spontán seb megjelenését tapasztaltuk a ventrális nyaki oldalon. A seb szövettani metszetén epidermális hiperpláziát, alatta a dermiszben pedig krónikus aktív inflaminációt figyelhetünk meg. Előzetes vizsgálatok az *rc* lókusz pozícióját a *D9Mit162* marker (49.954 Mb) és a *D9Mit104* (65.953 Mb) között azonosították. Két különböző egértörzs, már leírt és újonan felfedezett mikroszatelita markerek, valamint szekvencia analízis segítségével egy pontmutációt azonosítottunk egy eddig ismeretlen génen belül (ENSMUSG00000070305) 44.989~45.009 Mb között, mely feltételezhetően felelőssé tehető a mutáns fenotípus kialakításáért. A mutáció a gén 3- as exonjában egy G→A tranzíciót okoz, mely fehérjeszinten egy Arg100→Gln cserét eredményez. A gén EST analízise rávilágított, hogy a gén legalább 2 db transzkripttel rendelkezik egérben. Egy 6 exonból álló hosszabb transzkripttel, ami mintegy 237 aminosav hosszúságú polipeptid láncot kódol, valamint egy rövidebb, 2 exonból álló transzkripttel, ami 96 aminosavból álló láncolatot kódol. A fehérje aminosav sorrendje alapján a Myelin Po fehérje család Myelin Protein Zero (MPZ) és Myelin Protein Zero-like 2 (MPZL2, Epithelial V-like Antigen) fehérjéivel mutatott nagyfokú homológiát, ezért mi a rough coat egerekben azonosított új, mindidáig ismeretlen gént *Mpzl3* (Myelin Protein Zero-like 3) génnek neveztük el. A

gén expressziós vizsgálata kimutatta, hogy a géntermék számos helyen kifejeződik az egérben, úgymint az agyban, a belekben, a bőrben, az izomban, a lépben, a májban, a nyelőcsőben, a szívben, a tüdőben és a vesében. A bőr és függelékeinek közelebbi tanulmányozása poliklonális antitesttel kimutatta, hogy az MPZL3 a keratinociták, a szőrtüsző, és a faggyúmirigy sejtjeinek a palzmamembránjában lokalizálható.

Azért, hogy az *Mpzl3* természetét és funkcióját minél jobban megismerjük a 3. fejezetben *in silico* vizsgálatokat végeztünk el az *Mpzl3* nukleotid és fehérje szekvenciáját alapul véve. Kíváncsiak voltunk, vajon a fehérje csak az emlősökben található-e meg, vagy már az evolúció korábban megjelent szervezeti formáiban is kifejeződik. Mindemellett vizsgálni kívántuk az MPZL3 domain szerkezetét a fehérje humán ortológjának az esetében, azzal a céllal, hogy esetlegesen a szekvencia, valamint szerkezeti vizsgálatok az egér fenotipikus megjelenésével kiegészítve választ nyújthatnak a gén mutációjának humán patológiás kondíciójának a kifejeződésére is. Vizsgálataink kimutatták, hogy a fehérje először a gerinces szervezetekben jelent meg. A fehérje szekvenciája emlősökben 79–99% azonosságot mutat. Mindegyik vizsgált ortológ fehérje a Myelin Po fehérjecsaládba tartozott, és rendelkezett Immunoglobulin V típusú domainnel. Az USA Biotechnológia Információs Központjának (NCBI) UniGene adatbázisának EST analízise alapján humán szervezetben a gén - egér szervezetben tapasztaltakhoz hasonlóan - számtalan helyen mutat kifejeződést. Ezenfelül munkánk során vizsgáltuk a gén expresszivitását EMBL-EBI Array Express microarray adatbázis alapján. Eredményeink azt mutatták, hogy a gén az immunrendszer felépítésében is szerepet játszó dentrikus sejtekben, valamint a CD4 és CD8 sejtekben is kifejeződik. A fehérje 3D homológián alapuló analízise kimutatta, hogy az egérben tapasztalható Arg100→Gln mutáció az immunoglobulin V típusú domén extracelluláris oldalán található, és mint ilyen a prediktált adhéziós funkciót könnyen befolyásolhatja. A homológ fehérjék vizsgálata megmutatta, hogy *Mpzl3* homológ fehérjéi a Myelin Po (*Mpz*), valamint a Myelin Protein Like 2 (*Mpzl2*), vagy más néven az Epithelial-V-like antigen (*Eva1*) fehérjék szintén rendelkeznek adhéziós funkcióval, valamint jelentős szerepük van az immunrendszer működésében is. Azért, hogy megvizsgáljuk vajon a humán szervezetben a fehérje hasonló megjelenést mutat-e, mint az egérben, embrionális humán fibroblaszt sejttenyészet felhasználásával Western blot analízist végeztünk, valamint az egér poliklonális antitestjének felhasználásával humán metszeten immunhisztokémiai szövetfestést csináltunk. Az emberi bőrből származó szöveti vizsgálataink kimutatták, hogy *MPZL3* egy 54 kDa és egy 56 kDa nagyságú fehérjét kódol humánban, ami egy dimerizációnak, vagy posztranszlációs módosításnak lehet az eredménye. Immunhisztokémiai vizsgálatainkban egérhez hasonlóan a keratinociták és a szőrtüszők plazmamembránjában lévő kifejeződését tapasztaltuk. Az eddigi eredményeket figyelembe véve a 3. fejezetben leírt eredmények alapján azt feltételeztük, hogy a fehérje szerepet játszhat emberben az immunrendszernek hibás működésének következtében kialakuló szőrhullásos folyamatokban, mint amilyen az Alopecia számtalan formája.

Bár az *Mpzl3 in silico* analízise a gén funkcióját olyan adhéziós fehérjeként predik-

tálta, aminek szerepe lehet immunmediált szőrhullásos folyamatokban, mint amilyen az alopecia, a gén funkcionális annotációja nem történt meg. A disszertáció 4. fejezetében funkcióvesztéses és antiszensz morpholino knock down technikát alkalmazva kísérletet tettünk az *mpzl3* okozta komplex fenotípus hátterének a felderítésére zebrahalban. Mindenekelőtt bioinformatikai adatbázisokban szereplő adatok alapján vizsgáltuk az *mpzl3* genom szekvenciáját, majd EBI InterProScan software segítségével meghatároztuk annak doménstruktúráját, és a legközelebbi szomszéd módszerével (neighbour joining method) azonosítottuk a Myelin Po fehérjecsaládhoz tartozó többi fehérjéhez fűződő evolúciós kapcsolatait. Evolúciós értelemben vett legközelebbi fehérjék a *mpz*, a *mpzl1*, az *eva1* és a *scn4b.* Annak érdekében, hogy az *in silico* adatokat megerősítsük, qRT-PCR és *in situ* hibridizáció segítségével meghatároztuk az *mpzl3* expresszióját a fejlődő zebrahal embriókban. Vizsgáltaink magas *mpzl3* expressziós szintet mutattak már a megtermékenyítést követően, ami a génexpresszió anyai hatásának lehetséges következménye. Későbbi időpontba vett mintákon az *mpzl3* RNS szintjének a csökkkenését tapasztaltuk. *In situ* hibridizáció során a gén korai expresszióját figyeltük meg a halak oldalvonalának az érzékelősejteiben (neuromast-ban), a kloákában, a kopoltyúívekben, valamint az úszóhólyagban. Azért, hogy meghatározhassuk az *mpzl3* funkcióját, szintetikus *mpzl3* RNS-t készítettünk és 1-2 sejtes állapotban bejuttattuk a fejlődő zebrahal embriókba. A megnövekedett *mpzl3* szint hatására a halakra általános retardáció, a faroknyúlvány megrövidült mivolta, a szívburok hypertrophiája és veleszületett, anophthalmia volt a jellemző. Az embriók egy részénél mindkét szem teljes vagy részleges hiányát figyelhettük meg, míg másoknál csak az egyik szem fejlődése volt rendellenes, míg a másik normális fejlődést mutatott. Annak érdekébe, hogy az *mpzl3* funkciójáról teljes képet kaphassunk, antiszensz morfolino knockdown technika segítségével vizsgáltuk a lecsökkent *mpzl3* szint hatását a fejlődő zebrahal embriókra. A morfolinóval kezelt halakra megnövekedett letalitás, általános retardáció, az esetek 30 %-ban teljes mozgásképtelenség, valamint kardio-vaszkuláris elváltozások, úgymint hypertrophikus szívburok, és az érfal szerkezeti változásai voltak a jellemzőek. *In silico* adatok alapján feltételeztük, hogy az *mpzl3* által kódolt fehérje szerepet játszik a csecsemőmirigy és a T sejtek érésében, ezért a morphant halak csecsemőmirigy specifikus génjének, a recombination activating gene-*1*-nek (*rag1*) a kifejeződését vizsgáltuk. Megállapítottuk, hogy a morphant halakban nem fejeződik ki a *rag1* gén, ami a csecsemőmirigy fejlődési és funkcionális működésének a hiányosságára utal. Annak érdekében, hogy meghatározzuk a morphant halakban megjelenő transzkriptómikai változásokat, microarray analízist végeztünk el egyedi tervezésű 4x44 k mikrochipen. Mikrochip vizsgálataink a knockdown *mpzl3* morfolino embriókban az egyedfejlődésben fontos jelátviteli útvonalak olyan elemeinek megváltozott expresszióját azonosították, mint a Notch vagy a Wnt.

Összefoglalásképpen elmondhatjuk, hogy ebben a tanulmányban mikroszatelita markerek segítségével azonosítottuk a rough coat (*rc*) egértörzsben előforduló genetikai mutációt egy eddig ismeretlen génben, amit mi a Myelin Po fehérjecsaládhoz,

és legfőképpen a Myelin Protein Zero Like 2 (*Mpzl2*) fűződő nagyfokú szekvencia homológia miatt, Myelin Protein Zero Like 3 (*Mpzl3*)-nak neveztünk el. Az okozott fenotípus egy Arg-Glu szubsztitúció következménye a fehérje konzervált funkcionális régiójában. *In silico* technikák alkalmazásával vizsgáltuk eme fehérjének a meglétét, és expressziós mintázatát ember esetében is. Vizsgálataink alapján azt feltételeztük, hogy az említett fehérje szerepet játszhat az immunrendszer működésének rendelleneségeivel összefüggő szőrhullásos folyamatokban is, mint amilyen az alopécia. Hogy a gén funkcionális hátterét *in vivio* módon is tanulmányozni tudjuk, azonosítottuk az egér *mpzl3* ortológját zebrahalban, és a génre specifikus szintetikus RNS molekula és antiszensz morpholino oligonukleotid felhasználásával funkciónyeréses és funkcióvesztéses kísérletet végeztünk el. Vizsgálataink megmutatták, hogy az Mpzl3 számtalan fejlődési folyamatban szerepet játszik, aminek a hátterében mikrochip vizsgálat alapján a Wnt és a Notch szignalizációs útvonalak megváltozott működése állhat. Úgy gondoljuk, hogy a jövőben az Mpzl3 kapcsolata a fent említett szignalizációs útvonalakkal hozzájárulhat a bőr, az immunrendszer, valamint a demyelinizációs folyamatok a pontosabb megértéséhez.

Curriculum Vitae

Peter Imre Racz was born on 5 June in 1979 in Budapest, Hungary. He studied biology at the University of Szeged, Faculty of Science, Szeged, Hungary (formerly named as Jozsef Attila University). In 2003 as an undergraduate student he won the Scholarship of the Hungarian Republic and the Scholarship of the City of Szeged, and he took the opportunity to visit Prof. Dr. Katalin Csiszar's laboratory in the Cardiovascular Research Center at the University of Hawaii, USA for a semester. Here he started to work on a novel gene mutation in the rough coat (*rc*) mice that resulted in cyclic hair loss. After the graduation in 2004 he went back to the Cardiovascular Research Center and continued his work on the rough coat strain under the mentorship of Dr. Tongyu Cao. From 2007 he worked in the group of Dr. Matyas Mink in the Department of Genetics of University of Szeged, Hungary and in the company Zenon Bio Ltd. on the EU-funded project 'High-throughput Tools for Biomedical Screens in Zebrafish' project (ZF-TOOLS), carried out in collaboration with Dr. Annemarie Meijer and Prof Dr. Herman Spaink in the Institute of Biology, University of Leiden, where he enrolled as a PhD student. During this period he spent several months at the Institute of Biology, University of Leiden to extend his work on the rough coat mutation by studying the homologous gene in zebrafish. In addition, he graduated as an economist with a major in management studies in 2009 at the University of Szeged, Faculty of Economics and Business Administration.

List of publications

Cao T, **Racz P**, Szauter KM, Groma G, Nakamatsu GY, Fogelgren B, Pankotai E, He QP, Csiszar K. (2007) *Mutation in Mpzl3, a novel gene encoding a predicted adhesion protein, in the rough coat (rc) mice with severe skin and hair abnormalities.* J Invest Dermatol. 127:1375-86.

Racz P., Mink M., Ordas A., Cao T, Szalma S., Szauter KM, Csiszar K. (2009) *The human orthologue of murine Mpzl3 with predicted adhesive and immune functions is a potential candidate gene for immune-related hereditary hair loss.* Exp Dermatol. 18:261-3.

Z. Hegedűs, A. Zakrzewska, V. C. Ágoston, A. Ordas, **P. Racz**, M. Mink, H. P. Spaink and A. H. Meijer (2009) *Deep sequencing of the zebrafish transcriptome response to mycobacterium infection.* Mol Immunol. 46:2918-30.

Hegedus Z, Ordas A, **Racz P**, Spaink HP, Mink M, Meijer AH
Deep sequencing of the innate immune response of zebrafish embryos to Salmonella infection. (in preparation)

Racz P, Zakrzewska A, Csukonyi E, Ordas A, Spaink HP, Mink M, Meijer AH.
Functional analysis of the mpzl3 gene in zebrafish. (in preparation)

Supplementary tables

Supplementary table 1.
Results of the GO term based microarray analyses of the up-regulated genes in mpzl3 morphant fish.

GO-term	Name	Number of reporters associated	Gene Symbols
GO:0050789	**regulation of biological process**		
GO:0045449	regulation of transcription	32	pea3, erm, eve1, flh, foxd5, gbx1, her1, her6, hmgb1, ilf2, irx7, smad1, mespa, msgn1, msxe, nfil3, nrf1, otx1l, purb, LOC793089, sp5l, tbx6, tfap2a, trfp, tp73l, mycn, wu:fi38b05, wu:fk63e10, zgc:110825, zgc:136520, zgc:158360, zhx3
GO:0006306	DNA methylation	1	dnmt4
GO:0045786	negative regulation of cell cycle	1	tp73l
GO:0042664	negative regulation of cell growth	1	tp73l
GO:0030334	regulation of cell migration	1	bik
GO:0042127	regulation of cell proliferation	1	zic2a
GO:0042664	negative regulation of endodermal cell fate specification	1	bmp2b
GO:0030514	negative regulation of BMP signaling pathway	1	szl
GO:0030178	negative regulation of Wnt receptor signaling pathway	1	dkk1
GO:0040036	regulation of fibroblast growth factor receptor signaling pathway	3	dusp6, spry4, spry2
GO:0035023	regulation of Rho protein signal transduction	1	dzip1, dkk1, dusp6, szl, spry4, spry2, zgc:103517
GO:0042325	regulation of phosphorylation	1	zgc:73377
GO:0042981	regulation of apoptosis	3	bik, birc2, heatr1
GO:0043280	positive regulation of caspase activity	1	bik
GO:0006417	regulation of translation	2	eif4e1a, zgc:64152
GO:0043487	regulation of RNA stability	1	heatr1
GO:0050767	regulation of neurogenesis	1	gli2a
GO:0065008	**regulation of biological quality**		
GO:0006879	cellular iron ion homeostasis	1	tfa
GO:0007596	blood coagulation	1	crygm4/fbln4
GO:0050821	protein stabilization	1	szl
GO:0007154	**cell communication**		
GO:0045168	cell-cell signaling during cell fate commitment	2	bmp2b, dld
GO:0046331	lateral inhibition	1	dld
GO:0007186	G-protein coupled receptor protein signaling pathway	5	cxcr4a, fzd3, fzd8a, fzd8b, zgc:103757
GO:0007219	Notch signaling pathway	4	dld, her6, lfng, zgc:136520

GO-term	Name	Number of reporters associated	Gene Symbols
GO:0016055	Wnt receptor signaling pathway	9	ck2b, dact1, dkk1, fzd3, fzd8a, fzd8b, frzb, szl, sp5l,
GO:0007229	integrin-mediated signaling pathway	1	mibp2
GO:0007243	protein kinase cascade	2	mapk14a
GO:0007264	small GTPase mediated signal transduction	2	rab34, zgc:103517
GO:0009401	phosphoenolpyruvate-dependent sugar phosphotransferase system	1	kifc1
GO:0007049	**cell cycle GO:0007049**		
GO:0007067	mitosis	2	rad21, wu:fc04c01
GO:0007064	mitotic sister chromatid cohesion	1	rad21
GO:0048468	**cell development**		
GO:0055015	ventricular cardiac muscle cell development	1	bmp2b
GO:0006915	apoptosis	4	bik, birc2, heatr1, tp73l
GO:0030239	myofibril assembly	1	cxcr4a
GO:0014032	neural crest cell development	1	tfap2a
GO:0055002	striated muscle cell development	2	cxcr4a, gli2a
GO:0021953	central nervous system neuron differentiation	2	gli2a, wu:fc04c01
GO:0021954	central nervous system neuron development	1	wu:fc04c01
GO:0021523	somatic motor neuron differentiation	2	dld, gli2a
GO:0045165	**cell fate commitment**		
GO:0045165	cell fate commitment	4	bmp2b, dld, dusp6, ndr2
GO:0001709	cell fate determination	1	ndr2
GO:0042663	regulation of endodermal cell fate specification	2	bmp2b, dusp6
GO:0006928	**cell motility**		
GO:0042074	cell migration involved in gastrulation	3	bmp2b, dkk1, lbr
GO:0060030	dorsal convergence	1	bmp2b
GO:0008283	**cell proliferation**		
GO:0021846	cell proliferation in forebrain	1	zic2a
GO:0033278	cell proliferation in midbrain	1	zic2a
GO:0016043	**cellular component organization and biogenesis**		
GO:0006334	nucleosome assembly	1	zgc:65861
GO:0007018	microtubule-based movement	2	kifc1, wu:fb37a10
GO:0015031	protein transport	6	pcf11, dzip1, mrpl45, wu:fb61d08, zgc:76878
GO:0006607	NLS-bearing substrate import into nucleus	1	dzip1
GO:0000059	protein import into nucleus, docking	1	zgc:76878
GO:0006839	mitochondrial transport	1	ucp4

GO-term	Name	Number of reporters associated	Gene Symbols
GO:0007010	cytoskeleton organization and biogenesis	4	cxcr4a, kifc1, wu:fb37a10, zgc:63783
GO:0042254	ribosome biogenesis and assembly	4	ctsl1b, heatr1, nola1, tsr1
GO:0048869	**cellular developmental process**		
GO:0030154	cell differentiation	16	bik, birc2, bmp2b, cxcr4a, dld, dusp6, gli2a, heatr1, lfng, msgn1, ndr2, nono, tfap2a, tp73l, wu:fc04c01
GO:0001710	mesodermal cell fate commitment	1	bmp2b
GO:0050935	iridophore differentiation	1	tfap2a
GO:0030318	melanocyte differentiation	1	tfap2a
GO:0044237	**cellular metabolic process**		
GO:0006098	pentose-phosphate shunt	1	taldo1
GO:0006425	glutaminyl-tRNA aminoacylation	1	qars
GO:0006424	glutamyl-tRNA aminoacylation	1	qars
GO:0006432	phenylalanyl-tRNA aminoacylation	1	farsa
GO:0009117	nucleotide metabolic process	2	taldo1, zgc:66117
GO:0006412	translation	18	eif2s1l, eif4e1a, eif5a, qars, farsa, rpl10a, rpl3, rpl4, rpl5a, rpl7l1, rps15, rps2, rps4x, rps7, rpsa, zgc:153404, zgc:64152, zgc:92872
GO:0005975	carbohydrate metabolic process	2	taldo1, wu:fc20b11
GO:0042574	retinal metabolic process	1	rdh1l
GO:0006457	protein folding	4	cct5, ppial, pin1, si:ch211-288g17.3
GO:0043687	post-translational protein modification	10	dusp6, hdac8, mapk14a, plk4, parp1, si:dkey-14d8.5, ube2v2, zgc:103757
GO:0030163	protein catabolic process	5	psmc2, psmc1b, psmb1, usp5
GO:0006511	ubiquitin-dependent protein catabolic process	2	psmb1, usp5
GO:0051246	regulation of protein metabolic process	3	eif4e1a, ube2v2, zgc:64152
GO:0051258	protein polymerization	1	wu:fb37a10
GO:0006508	proteolysis	4	ctsl1b, psmb1, usp5, zgc:110307
GO:0042572	retinol metabolic process	2	rdh1l
GO:0008380	RNA splicing	1	rbm22
GO:0006397	mRNA processing	2	rbm22, zgc:110689
GO:0016071	mRNA metabolic process	3	rbm22, snrpd1, zgc:110689
GO:0006364	rRNA processing	3	ctsl1b, heatr1, nola1
GO:0000462	maturation of SSU-rRNA from tricistronic rRNA transcript (SSU-rRNA, 5.8S rRNA, LSU-rRNA)	1	heatr1
GO:0032502	developmental process		

GO-term	Name	Number of reporters associated	Gene Symbols
GO:0021984	adenohypophysis development	1	gli2a
GO:0021508	floor plate formation	2	gli2a, ndr2
GO:0001707	mesoderm formation	3	bmp2b, mespa, sp5l
GO:0014028	notochord formation	1	ndr2
GO:0043049	otic placode formation	1	msxe
GO:0035138	pectoral fin morphogenesis	1	rdh1l
GO:0048048	embryonic eye morphogenesis	1	ndr2
GO:0060059	embryonic retina morphogenesis in camera-type eye	1	zic2a
GO:0048547	gut morphogenesis	3	dld, gli2a, rdh1l
GO:0048618	post-embryonic foregut morphogenesis	1	gli2a
GO:0001702	gastrulation with mouth forming second	1	mespa
GO:0021575	hindbrain morphogenesis	1	irx7
GO:0002009	morphogenesis of an epithelium	4	blf, bmp2b, gli2a, ndr2
GO:0009887	organ morphogenesis	7	bmp2b, dld, gli2a, msxe, ndr2, rdh1l, zic2a
GO:0001889	liver development	1	bmp2b
GO:0035121	tail morphogenesis	1	sp5l
GO:0021536	diencephalon development	2	gli2a, zic2a
GO:0030900	forebrain development	3	dkk1, gli2a, zic2a
GO:0032835	glomerulus development	2	flh, gli2a
GO:0030902	hindbrain development	5	fzd3, irx7, otx1, sp5l, tfap2a
GO:0021754	facial nucleus development	1	fzd3
GO:0030901	midbrain development	2	otx1l, zic2a
GO:0030917	midbrain-hindbrain boundary development	1	otx1l
GO:0007420	brain development	10	dkk1, gli2a, fzd3, irx7, otx1l, sp5l, sfpq, tfap2a, zgc:136520
GO:0055016	hypochord development	1	lfng
GO:0030903	notochord development	4	bmp2b, dkk1, ndr2, sp5l
GO:0030325	adrenal gland development	1	flh
GO:0035050	embryonic heart tube development	3	dzip1, flh, ndr2
GO:0030097	hemopoiesis	1	spry4
GO:0001822	kidney development	3	flh, gli2a, zgc:101674
GO:0048793	pronephros development	1	zgc:101674
GO:0007517	muscle development	3	bmp2b, cxcr4a, gli2a
GO:0031018	endocrine pancreas development	1	gli2a
GO:0031017	exocrine pancreas development	1	rdh1l
GO:0001654	eye development	6	mcm2, mcm3, ndr2, nrf1, zgc:136520, zic2a
GO:0060041	retina development in camera-type eye	4	mcm2, mcm3, nrf1, zic2a
GO:0001501	skeletal development	2	rdh1l, tfap2a

GO-term	Name	Number of reporters associated	Gene Symbols
GO:0051216	cartilage development	1	tfap2a
GO:0007398	ectoderm development	2	ctnnb1, dkk1
GO:0007498	mesoderm development	4	bmp2b, mespa, msgn1, sp5l
GO:0009790	**embryonic development**		
GO:0001756	somitogenesis	5	dld, gli2a, her1, her6, zgc:136520
GO:0001757	somite specification	1	her6
GO:0009880	embryonic pattern specification	3	ctnnb1, her6, smad1
GO:0040016	**embryonic cleavage**	**2**	
GO:0000578	embryonic axis specification	1	ctnnb1
GO:0007275	**multicellular organismal development**		
GO:0007389	pattern specification process	18	bmp2b, ctnnb1, dzip1, dld, dusp6, eve1, flh, gli2a, her1, her6, smad1, ndr2, otx1l, szl, sp5l, spry2, zgc:136520, zic2a
GO:0048263	determination of dorsal identity	1	szl
GO:0048264	determination of ventral identity	1	bmp2b
GO:0007368	determination of left/right symmetry	5	bmp2b, dzip1, dld, flh, ndr2
GO:0009952	anterior/posterior pattern formation	7	dld, gli2a, her1, her6, otx1l, sp5l, zgc:136520
GO:0009953	dorsal/ventral pattern formation	6	bmp2b, dusp6, gli2a, szl, spry2, zic2a
GO:0006810	**transport**		
GO:0006820	anion transport	2	tomm40l, vdac2
GO:0006826	iron ion transport	1	tfa
GO:0006813	potassium ion transport	2	atp1b3a, zgc:77244
GO:0006814	sodium ion transport	1	atp1b3a
GO:0016192	vesicle-mediated transport	1	wu:fb61d08
GO:0002376	**immune system process**		
GO:0006955	immune response	1	ilf2
GO:0009617	response to bacterium	2	im:7144703, tfa
GO:0055114	**oxidation reduction**		
GO:0055114	oxidation reduction	4	adh5, rdh1l, zgc:100900, zgc:109991
GO:0003008	**system process**		
GO:0008015	blood circulation	1	gli2a
GO:0007601	visual perception	1	zgc:103757
GO:0050896	**response to stimulus**		
GO:0009409	response to cold	1	nrf1
GO:0002347	response to tumor cell	1	tp73l
GO:0032526	response to retinoic acid	1	mespa
GO:0006950	response to stress	5	crygm4, cox4i1, mapk14a, nrf1, ppial
GO:0001666	response to hypoxia	2	cox4i1, ppial
GO:0009611	response to wounding	2	crygm4 / fbln4
GO:0048511	**rhythmic process**		
GO:0048511	rhythmic process	1	nfil3

Supplementary table 2.
Results of the GO term based microarray analyses of the down-regulated genes in the mpzl3 morphant fish.

GO-term	Name	Number of reporters associated	Gene symbol
GO:0050789	**regulation of biological process**		
GO:0006417	regulation of translational	1	zgc:56330
GO:0042661	regulation of mesodermal cell fate specification	1	churc1
GO:0045449	regulation of transcription	17	arntl1a, bmi1, bmi1b, bzw1l, cebpg, cdc5l, churc1, eml2, foxa, smad2, , xtx2, nr2f1l, rab35, sox11b, mycl1a, zgc:153348, zgc:86635
GO:0006306	DNA methylation	1	dnmt1
GO:0030334	regulation of cell migration	1	churc1
GO:0042981	regulation of apoptosis	2	bokb, ripk2
GO:0032313	regulation of Rab GTPase activity	1	rutbc3
GO:0045449	regulation of transcription	19	arntl1a, bmi1, bmi1b, bzw1l, cebpg, eml2, foxa, , mad2, mxtx2, nr2f1l, , ab35, sox11b, mycl1a, zgc:86635
GO:0051246	regulation of protein metabolic process	5	ube2d2, zgc:100959, zgc:112077, zgc:55512, zgc:56330
GO:0065008	**regulation of biological quality**		
GO:0006879	cellular iron ion homeostasis	1	hd
GO:0042391	regulation of membrane potential	1	slc26a5
GO:0006914	**autophagy**		
GO:0006914	autophagy	3	atg5, zgc:73097
GO:0007154	**cell communication**		
GO:0007219	Notch signaling pathway	1	dab2
GO:0007179	transforming growth factor beta receptor signaling pathway	1	smad2
GO:0007169	transmembrane receptor protein tyrosine kinase signaling pathway	1	ptk2.1
GO:0007264	small GTPase mediated signal transduction	6	rab20, rab35, rutbc3, rhogc, zgc:77650, zgc:86635
GO:0007049	**cell cycle**		
GO:0007067	mitosis	2	zgc:64116, zgc:92321
GO:0048468	**cell development**		
GO:0006915	apoptosis	2	bokb, ripk2
GO:0051301	**cell division**		
GO:0000910	cytokinesis	1	kif23
GO:0006928	**cell motility**		
GO:0042074	cell migration involved in gastrulation	2	churc1, mxtx2

GO-term	Name	Number of reporters associated	Gene symbol
GO:0016043	**cellular component organization and biogenesis**		
GO:0006334	nucleosome assembly	1	h1m
GO:0007018	microtubule based movement	2	kif23, zgc:56231
GO:0015031	protein transport	14	arcn1l, chmp7, cog2, gosr2, rab35, snupn, tom1, zgc:100959, zgc:103537, zgc:55877, zgc:73136, zgc:77002, zgc:86635, zgc:92676
GO:0007034	vacuolar transport	1	zgc:92676
GO:0006909	phagocytosis	1	jmjd6
GO:0006898	receptormediated endocytosis	1	dab2
GO:0007030	Golgi organization and biogenesis	1	cog2
GO:0051276	chromosome organization and biogenesis	4	bmi1, bmi1b, dnmt1, h1m
GO:0007010	cytoskeleton organization and biogenesis	4	LOC559333, kif23, , xtx2, zgc:56231
GO:0044237	cellular metabolic process		
GO:0005975	carbohydrate metabolic process	9	aldoc, ldhb, pgm1, pgk1, pkm2, tpi1a, usp20, zgc:100959, zgc:63792
GO:0019642	anaerobic glycolysis	1	ldhb
GO:0006098	pentosephosphate shunt	1	tpi1a
GO:0006071	glycerol metabolic process	1	zgc:56068
GO:0006081	aldehyde metabolic process	1	aldh3a2
GO:0006542	glutamine biosynthetic process	1	glulb
GO:0006534	cysteine metabolic process	1	nfs1
GO:0006744	ubiquinone biosynthetic process	1	coq3
GO:0009117	nucleotide metabolic process	4	cmpk, rrm2b, rrm2, tpi1a
GO:0046114	guanosine biosynthetic process	1	zgc:66378
GO:0006633	fatty acid biosynthetic process	1	tpi1a
GO:0006511	ubiquitindependent protein catabolic process	2	uchl1, usp20
GO:0042744	hydrogen peroxide catabolic process	1	cat
GO:0008299	isoprenoid biosynthetic process	2	hmgcs1 zgc:103473
GO:0046839	phospholipid dephosphorylation	1	mtmr6
GO:0006644	phospholipid metabolic process	1	zgc:162119
GO:0008202	steroid metabolic process	1	osbpl2

GO-term	Name	Number of reporters associated	Gene symbol
GO:0043687	post-translational protein modification	15	dnmt1, prkcb1, ptk2.1, ptk2.1, ripk2, sgk, si:ch211-238n5.5,ube2d2, raf1, zgc:100959, zgc:112077, zgc:136697, zgc:55512, zgc:55587, zgc:56558
GO:0006508	proteolysis	4	ctsl1b, psmb1, usp5, zgc:110307
GO:0006457	protein folding	4	calrl, hspd1, LOC100002614, zgc:56703
GO:0006486	protein amino acid glycosylation	1	zgc:76904
GO:0006412	translation	3	mrpl3, rpl12, zgc:56330
GO:0006259	DNA metabolic process	10	cry1b, dnmt1, ,LOC791836, mcm3l, orc6l, rrm2, zgc:101596, zgc:103553, zgc:56122, zgc:66475
GO:0006281	DNA repair	3	cry1b, zgc:103553, zgc:66475
GO:0006270	DNA replication initiation	1	mcm3l
GO:0006367	transcription initiation from RNA polymerase II promoter	1	LOC799735
GO:0006400	tRNA modification	1	zgc:66378
GO:0008380	RNA splicing	1	zgc:123015
GO:0016071	mRNA metabolic process	2	dbr1, zgc:123015
GO:0006801	superoxide metabolic process	1	sod1
GO:0022610	**biological adhesion**		
GO:0007155	cell adhesion	1	cd36
GO:0032502	**developmental process**		
GO:0031101	fin regeneration	1	hspd1
GO:0001840	neural plate development	1	sinup
GO:0007369	gastrulation	3	churc1,mxtx2, mylip
GO:0002009	morphogenesis of an epithelium	2	mxtx2, sinup
GO:0060041	retina development in camera-type eye	1	dnmt1
GO:0007507	heart development	1	raf1
GO:0031017	exocrine pancreas development	1	dnmt1
GO:0007399	nervous system development	1	zgc:55580
GO:0009790	embryonic development		
GO:0040016	embryonic cleavage	1	kif23
GO:0001756	somitogenesis	1	nat13
GO:0009880	embryonic pattern specification	1	smad2
GO:0006810	**transport**		
GO:0006865	amino acid transport	1	zgc:110611
GO:0015904	tetracycline transport	2	hiat1a, slc46a1
GO:0015992	proton transport	1	zgc:55891
GO:0006821	chloride transport	1	slc26a5
GO:0008272	sulfate transport	1	slc26a5
GO:0015711	organic anion transport	1	slc16a3
GO:0006814	sodium ion transport	1	zgc:110611
GO:0006869	lipid transport	1	osbpl2
GO:0019532	oxalate transport	1	slc26a5

akkor	Name	Number of reporters associated	Gene symbol
GO:0016192	vesicle mediated transport	6	arcn1l, dab2, jmjd6, vamp4, zgc:103537, zgc:73136
GO:0009056	**catabolic process**		
GO:0016042	lipid catabolic process	2	si:dkey-174c12.2, zgc:162119
GO:0055114	**oxidation reduction**		
GO:0055114	oxidation reduction	7	aldh2l, aldh3a2, cat, jmjd6, ldhb, rrm2, sod1
GO:0050896	**response to stimulus**		
GO:0009416	response to light stimulus	1	arntl1a
GO:0046677	response to antibiotic	2	hiat1a, slc46a1
GO:0010038	response to metal ion	2	cat, sod1
GO:0051597	response to methylmercury	1	sod1
GO:0001666	response to hypoxia	1	pgk1
GO:0009611	response to wounding	1	hspd1
GO:0006950	response to stress	7	cat, cry1b, hspd1, hspa5, pgk1, zgc:103553, zgc:66475
GO:0048511	**rhythmic process**		
GO:0007623	circadian rhythm	1	arntl1a